Predicting Human Fetal Drug Exposure to Placental P-glycoprotein Substrates by PBPK Modeling and Simulation

Olena Anoshchenko

A dissertation

submitted in partial fulfillment of the

requirements for the degree of

Doctor of Philosophy

University of Washington

2021

Reading Committee:

Jashvant D. Unadkat, Chair

Yvonne S. Lin

Qingcheng Mao

Program Authorized to Offer Degree:

Pharmaceutics

University of Washington

ABSTRACT

Predicting Human Fetal Drug Exposure to Placental P-glycoprotein Substrates by PBPK Modeling and Simulation

Olena Anoshchenko

Chair of the Supervisory Committee:

Dr. Jashvant D. Unadkat

Pharmaceutics

More than 80% of pregnant women take at least one drug during pregnancy and about 50% during the first trimester when the fetus is the most vulnerable to drug toxicity (Scaffidi, Mol, & Keelan, 2017). To inform fetal risk and to optimize maternal-fetal drug therapy, it is important to measure or predict fetal drug exposure throughout pregnancy. Estimating fetal drug exposure by repeated sampling of fetal blood is not ethical or feasible. Obtaining a single plasma (blood) sample from the fetus is possible at term (e.g., from the umbilical vein). However, these sparse data are not sufficient to determine fetal drug exposure and hence alternative methodologies like physiologically-based pharmacokinetic (PBPK) modeling can be employed to **predict** (rather than measure) fetal drug exposure throughout pregnancy.

We previously developed and verified a maternal-fetal (m-f) PBPK model that can successfully predict maternal and fetal exposure at term to drugs that passively diffuse across the placenta (Zhang et al., 2017; Zhang & Unadkat, 2017). Here, for the first time, we extended this model to predict fetal drug exposure to drugs that are effluxed by P-glycoprotein, a drug transporter highly abundant in the human placentae (Anoshchenko et al., 2020; Han, Gao, & Mao, 2018; Mathias, Hitti, & Unadkat, 2005). To do so, we used the efflux ratio-relative expression factor (ER-REF) approach to predict fetal drug exposure, $K_{p,uu}$, at term (i.e., the ratio of fetal and maternal unbound drug plasma AUC), of four placental P-gp substrates: dexamethasone, betamethasone, darunavir and lopinavir. The ER-REF approach relies on scaling the *in vitro* drug efflux ratio (ER) in a transporter-overexpressing cell monolayer (e.g., hMDR1-MDCK$^{cP\text{-}gpKO}$ cells where human P-gp was overexpressed and the endogenous canine P-gp was knocked-out) to *in vivo* $K_{p,uu}$ using the relative expression factor (REF), the ratio of transporter abundances in placental tissue (**Chapter 2**) and in hMDR1-MDCK$^{cP\text{-}gpKO}$ cells (**Chapter 3**). To verify our predictions, we compared the ER-REF predicted fetal $K_{p,uu}$ with the *in vivo* fetal $K_{p,uu,}$ estimated from the observed UV/MP ratio data (in multiple maternal-fetal dyads) using our m-f PBPK model (**Chapter 3**). The predicted fetal $K_{p,uu}$ for dexamethasone, betamethasone, darunavir and lopinavir were 0.63, 0.59, 0.17 and 0.08, respectively, and fell within the 90% confidence interval ($CI_{90\%}$) of their estimated observed fetal $K_{p,uu}$ (0.30 – 0.66, 0.29 – 0.71, 0.11 – 0.22, 0.04 – 0.19, respectively), indicating success of our ER-REF approach.

Using the above fetal $K_{p,uu}$ data and our m-f PBPK model, we designed alternative dosing regimens for dexamethasone and betamethasone (**Chapter 4**) to address concerns regarding their maternal-fetal safety and efficacy (Vogel et al., 2017). To retain fetal efficacy, we propose maintaining dexamethasone total dose (24 mg) administered to the mother IM over 48 h. For

betamethasone, we found that its dose (24 mg over 48 h) could be potentially decreased by up to 80%. These regimens illustrate the utility of our ER-REF approach and m-f PBPK model to dynamically predict fetal exposure to drugs and therefore alternative dosing regimens of drugs administered to pregnant women. Any proposed alternative dosing regimens should be rigorously tested in the clinic for efficacy and toxicity prior to implementation.

The success of our ER-REF approach supports further utility of this approach together with our m-f PBPK model to estimate 1) fetal $K_{p,uu}$ at term of other placental P-gp substrates; 2) fetal $K_{p,uu}$ at term for substrates of other placental transporters or multiple transporters (e.g., BCRP or BCRP/P-gp), provided their placental abundance at term has been quantified (see **Chapter 2** for such quantification); 3) fetal $K_{p,uu}$ at earlier gestational ages for substrates of various/multiple transporters (provided placental transporter abundance at various gestational ages is quantified; see **Chapter 2** for such quantification). This work emphasizes the need to predict fetal drug exposure to inform fetal drug efficacy and safety and to optimize drug dosing regimens for the maternal-fetal dyad.

TABLE OF CONTENTS

LIST OF FIGURES

LIST OF TABLES

ACKNOWLEDGEMENTS

I would like to thank my mentor Jash Unadkat for raising me as a scientist, engaging my curiosity, supporting my ideas, encouraging during the tough times, and fostering the strength of character it takes to achieve this accomplishment. Great thanks to my dissertation committee for challenging my knowledge and encouraging my growth. I am endlessly grateful for my lab mates who taught me and learned from me, who have always stood by my side and with whom I am hopeful to be colleagues again in future.

I would like to thank Dr. Artursson (University of Uppsala, Sweden) and Dr. Mao (University of Washington) for generously providing hMDR1-MDCK$^{cP\text{-}gpKO}$ and hABCG2-MDCKII cells, respectively; Dr. Maharao and Dr. Sachar for help with establishing the Transwell® assay, Dale Wittington and Scott Edgar for help with mass spectrometry analysis, and the University of Washington Pharmacokinetics of Drug Abuse during Pregnancy (UWPKDAP) program for informative discussions. I additionally thank Dr. Ping Zhao at the Bill & Melinda Gates Foundation and Alice Ban Ke at Certara for their valuable input.

I would like to acknowledge the generous funding support of Bill & Melinda Gates Foundation Grant [INV-006678] and NIH grant [P01 DA032507].

Chapter 1. INTRODUCTION

1.1 BRIEF SUMMARY, OBJECTIVES AND SPECIFIC AIMS

Pregnant women often take medications to treat a variety of conditions such as infections, depression, gestational diabetes, and many others. Most often drugs are administered in pregnancy "off-label", yielding the fetus vulnerable to the risks of compromised safety or lack of efficacy associated with maternal drug administration. Since fetal safety and/or efficacy are linked to fetal plasma drug exposure (AUC), determining fetal drug exposure at any gestational age is critical to optimizing drug therapy. Determining fetal drug exposure in clinic is impossible due to the inability to perform repeated fetal sampling, and hence alternative methodologies like physiologically based pharmacokinetic (PBPK) modeling can be employed to **predict** fetal drug exposure *in silico*, rather than to **measure** it in the clinic.

We previously developed a m-f PBPK model to predict fetal exposure to drugs that passively cross the placenta (Zhang et al., 2017; Zhang & Unadkat, 2017). This m-f PBPK model was successfully verified for drugs that passively cross the placenta and are not actively transported or metabolized in that tissue (i.e., midazolam, theophylline, and zidovudine). However, since pregnant women take drugs that are effluxed by transporters (e.g., P-glycoprotein), to make our m-f PBK model comprehensive, we aim to extend the m-f PBPK model to predict fetal drug exposure of effluxed drugs. We will study four drugs as our model P-gp substrates: two HIV protease inhibitors (PIs), darunavir (DRV) and lopinavir (LPV), and two antenatal corticosteroids (ACS), dexamethasone (DEX) and betamethasone (BET). These drugs are confirmed *in vitro* to be P-gp substrates and their umbilical vein/maternal plasma (UV/MP) ratio data are available in the literature for verification of our model. Once our *in vitro* to *in vivo*

extrapolation (IVIVE) approach to predict fetal drug exposure has been verified (**Chapters 2 and 3**), we will use this approach, in combination with our extended m-f PBPK model, to propose alternative DEX and BET dosing regimens in pregnancy to address concerns associated with DEX and BET safety and efficacy (**Chapter 4**).

The major **goal** of this work is to predict *in vivo* human fetal plasma drug exposure to placental transporter drug substrates using an *in vitro* to *in vivo* extrapolation (IVIVE) approach and verify our predictions by comparing them with corresponding *in vivo* data. The magnitude of fetal drug exposure can be described by fetal $K_{p,uu}$ (the ratio of fetal-to-maternal unbound plasma AUCs, or, alternatively, the ratio of fetal-to-maternal unbound steady-state plasma concentrations). Here we chose to predict fetal $K_{p,uu}$ of drugs effluxed by placental P-glycoprotein (P-gp), as P-gp is arguably the most important drug efflux transporter in the human placenta. We **hypothesize** that: *In vivo* human fetal $K_{p,uu}$ (reflective of fetal drug exposure) of DEX, BET, DRV and LPV can be accurately predicted by determining their efflux ratio (ER) in a P-gp-overexpressing cell line (*in vitro* system) and scaling this ER by a relative expression factor (REF). REF will be used to scale *in vitro* drug P-gp clearance (as reflected by ER) to its *in vivo* equivalent by correcting for the difference in transporter protein abundance between transporter abundance in human placentae (*in vivo*) and P-gp-overexpressing cell line (*in vitro*) using quantitative targeted proteomics. The ER-REF approach will permit the incorporation of P-gp efflux activity into the m-f PBPK model(**Chapter 2 and Chapter 3)**. To verify the predicted *in vivo* $K_{p,uu}$ from *in vitro* studies, we will compare predicted $K_{p,uu}$ with the observed *in vivo* $K_{p,uu}$ estimated by our m-f PBPK model and the observed UV/MP drug concentration ratios.

To achieve our goal, our specific aims are:

Aim 1. To determine the absolute abundance of transporters in human placentae (*ex vivo*) of different gestational ages by targeted quantitative proteomics (LC-MS/MS) (**Chapter 2)**.

Aim 2.

2A) To predict the *in vivo* $K_{p,uu}$ of DRV, LPV, DEX, and BET based on their ER determined in P-gp overexpressing MDCKII cells in the Transwell® assay and the ER-REF scaling approach (**Chapter 3)**

2B) To verify the predicted $K_{p,uu}$ (from Aim 2A) by comparing these predicted values with those estimated from *in vivo* $K_{p,uu}$ (here and from Aim 3A) using our m-f PBPK model (**Chapter 3**)

Aim 3.

3A) To estimate the *in vivo* $K_{p,uu}$ of DEX and BET using the observed UV/MP data and our m-f PBPK model (**Chapter 4**)

3B) Using the estimated *in vivo* $K_{p,uu}$ (Aim 3A), devise alternative dosing regimens for DEX and BET to improve their efficacy and safety (**Chapter 4**).

1.2 Clinical Relevance: The Pregnant Woman and Her Fetus Are Drug Orphans

1.2.1 *Challenges in determining fetal safety and efficacy.*

Medication (henceforth referred to as drugs) use in pregnancy is strikingly prevalent, despite the general belief that pregnant women do not take prescription or over-the-counter medication. Medication can be prescribed to pregnant women to treat a multitude of preexisting conditions (e.g., HIV infection, depression, epilepsy), acute conditions (e.g., influenza, infections) or pregnancy-related conditions (e.g., hypertension, nausea, gestational diabetes). As

a result, as many as 80% of pregnant women self-report medication use throughout pregnancy, and at least 50% of these women reported taking medication during the first trimester (Mitchell et al., 2011; Scaffidi et al., 2017).

Despite a high prevalence of drug use in pregnancy, 98% of clinical trials in the United States actively exclude pregnant population due to ethical, legal, and practical considerations (Scaffidi et al., 2017). The enthusiasm of scientific community to include pregnant population in drug trials has not yet been addressed by the industry, and hence, 90% of approved drugs lack information for use during pregnancy (Shields & Lyerly, 2013). Therefore, many of these drugs are administered to pregnant women off-label, that is without pharmacokinetic (PK), efficacy or safety assessment in this population. Such assessments are necessary to inform dosing in the pregnant population due to the physiological and PK changes that occur during pregnancy (Anderson, 2005). These changes include an increase in weight, cardiac output, and blood flows, and changes in hepatic and renal drug elimination (Abduljalil & Badhan, 2020; Abduljalil, Furness, Johnson, Rostami-Hodjegan, & Soltani, 2012). For example, a 2-fold induction of hepatic cytochrome P450 3A4 (CYP3A4) in pregnancy compared to non-pregnant individuals resulted in a 2-fold decrease in maternal exposure to hepatic CYP3A substrates (Hebert et al., 2008; Zhang, Farooq, Prasad, Grepper, & Unadkat, 2015). When pregnancy-induced physiological and PK changes are not accounted for when designing drug dosing, they can significantly affect both maternal and fetal drug disposition. This can lead to under- or overdosing of a drug when administered as a standard adult dosing regimen.

Off-label use of drugs in pregnancy can result in adverse drug effects to the mother and her fetus (Carey et al., 2017). For example, diethylstilbestrol (DES) was a non-steroidal hormone drug used in 1940s to 1970s to treat vaginitis and was prescribed to pregnant women to prevent

miscarriage. Epidemiological studies revealed that DES-exposed mothers developed higher risk of breast cancer and their offspring developed genital tract abnormalities, and had an increased risk of breast cancer and melanoma (Carey et al., 2017). Another example is an anti-epileptic drug, valproic acid, which is a known teratogen, and causes increased rates of lumbosacral spina bifida in children when their mothers take valproic acid during pregnancy (Ornoy, 2009). These and many other examples demonstrate that medication use in pregnancy, especially during the first trimester (a key period of fetal organogenesis), may present great risks, not only for the mother, but also for the fetus, since the fetus is *de facto* exposed to the drugs taken by the mother (Thorpe et al., 2013).

Not all the drugs administered to the mother are intended to treat the mother. Some drugs are administered to the mother to treat her fetus and for such agents, fetal efficacy and safety are critical to consider. Human immunodeficiency virus (HIV) protease inhibitors (PIs) to prevent vertical HIV transfer, antenatal corticosteroids (ACS) to promote fetal lung maturation, digoxin to treat fetal tachyarrhythmia and many others are used for fetal therapy. Therefore, dose adjustment in pregnancy should be informed by assessing **fetal** exposure, risk and efficacy, as well as maternal benefits and risks.

1.2.2 *Challenges in determining fetal drug exposure in the clinic.*

Since direct assessment of human fetal safety and efficacy is not usually possible, a surrogate marker can be used. Fetal drug exposure or area under the fetal plasma drug concentration-time profile (AUC) is often linked to fetal efficacy or toxicity. Fetal drug plasma AUC determination requires obtaining multiple fetal blood samples at various time points after the mother receives the drug. Such sampling is not ethical prior to delivery and, therefore, not

practical. A fetal blood sample can only be obtained immediately after delivery from the fetal umbilical vein (UV) or umbilical artery (UA). The sample is often obtained simultaneously with the maternal blood sample to assess the ratio of umbilical vein-to-maternal plasma (UV/MP) drug concentrations. This single UV/MP ratio is not indicative of fetal drug exposure (i.e., entire AUC) because it can vary depending on the time post-last drug dose administered to the mother (**Figure 1.1**). Therefore, a naïve pooled analysis of maternal-fetal samples taken at different times post-last dose from multiple maternal-fetal dyads would be a better surrogate of maternal and fetal drug exposure. Unfortunately, such studies are not done routinely and only available for few drugs. These studies may not record the time post-last dose or cover insufficient time range to determine the full extent of fetal drug exposure (AUC). Moreover, these studies are opportunistic in nature, have small sample sizes and are conducted only at term, leaving fetal drug concentrations at any other gestational age unknown.

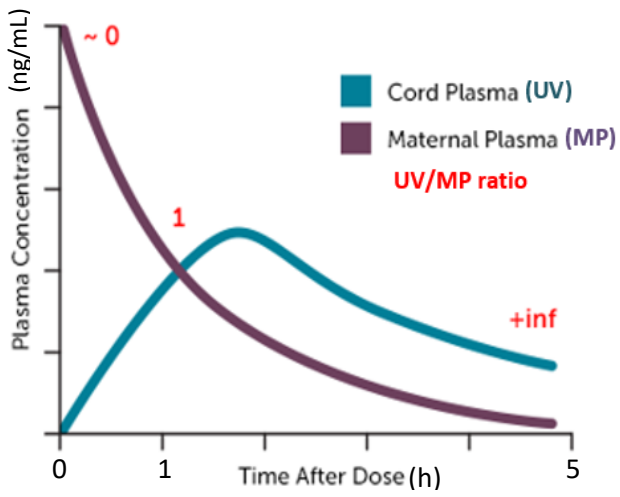

Figure 1.1. Pictorial demonstration of UV/MP concentration ratio dependence on time after last dose. Expected theoretical drug concentrations in maternal plasma (purple line) and fetal plasma (blue line) after intravenous (IV) drug administration to the mother. UV/MP ratios at three representative time points 0, 1.2 h and 5 h are 0, 1 and infinity, respectively and hence, when used individually, do not accurately estimate fetal drug exposure.

While determining maternal drug blood AUC is possible both at term and throughout pregnancy, it is a poor predictor of fetal AUC. Although maternal drug plasma concentrations drive the fetal concentrations, they do not always go in parallel with fetal drug plasma

concentrations. Fetal dug exposure can be influenced by transplacental and/or fetal pharmacokinetic parameters such as: **1)** placental passive diffusion clearance of the drug, **2)** active placental efflux, influx or metabolic drug clearance and **3)** fetal drug elimination clearance (e.g., fetal hepatic clearance) (Zhang et al., 2017). Changes in these clearances do not usually manifest in changes in maternal drug concentrations and exposure. The only instance when maternal AUC can approximate fetal AUC is when transplacental passive diffusion clearance is the sole determinant of fetal drug distribution (i.e., when active placental drug transport or placental/fetal elimination are absent or negligible) (Zhang & Unadkat, 2017). Therefore, the **ratio** of unbound fetal and maternal AUCs reflects the net magnitude of all three groups of clearances mentioned above and can be used as a measure of fetal drug exposure (i.e., fetal $K_{p,uu}$). In general, $K_{p,uu}$ is used to define unbound tissue drug exposure relative to the systemic exposure, particularly for the brain (Jeffrey & Summerfield, 2010). Fetal $K_{p,uu}$ is defined as the ratio of fetal-to-maternal unbound plasma AUCs, or, alternatively, as the ratio of fetal to maternal unbound plasma steady-state concentrations (**Eq 1.1**). $K_{p,uu}$, as a measure of fetal drug exposure, is a preferable parameter to the UV/MP ratio, as $K_{p,uu}$ (a) relies on the whole drug-plasma concentration time profile as opposed to single concentrations in the mother and the fetus; (b) is independent of drug binding in the mother and the fetus, while UV/MP is not; and (c) is reflective of placental processes governing fetal drug disposition. We assumed only unbound drug in plasma and tissue is pharmacologically active and available for passive and active clearance processes, thus $K_{p,uu}$ is more useful for reflecting fetal disposition compared to K_p, a partition coefficient uncorrected for protein binding.

Equation 1.1

$$K_{p,uu} = \frac{f_{u,f} \times AUC_f}{f_{u,m} \times AUC_m} = \frac{f_{u,f} \times C_{ss,f}}{f_{u,m} \times C_{ss,m}}$$

Additionally, $K_{p,uu}$ can be defined as the ratio of all clearances entering the fetus to the ones exiting the fetus, assuming no placental or fetal metabolic clearance of the drug (**Figure 1.2**). As mentioned above, if the sole determinant of fetal drug exposure is its transplacental passive diffusion clearance (if no active transport is present), $K_{p,uu}$ will equal to 1 (due to the assumption of equal magnitudes of intrinsic passive diffusion clearances in and out of the fetus). In)case of presence of active placental efflux processes or metabolism or fetal clearance, in addition to passive diffusion, $K_{p,uu}$ will be less than 1. If active placental influx is present (e.g., by uptake transporters), then $K_{p,uu}$ will be greater than 1. In cases when $K_{p,uu}$ deviates from unity fetal drug exposure cannot be estimated only from maternal drug unbound AUC.

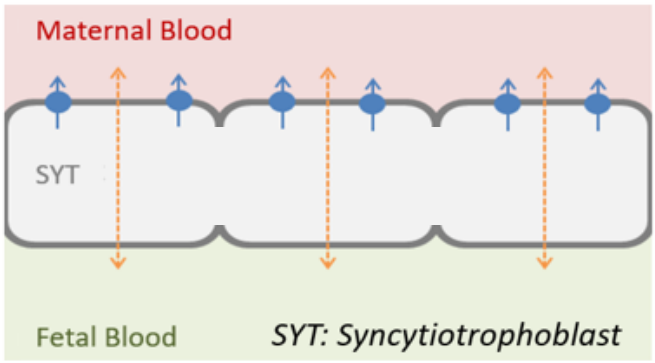

Figure 1.2. *In vivo* maternal and fetal blood compartments separated by syncytiotrophoblast (SYT) layer of placenta. Dashed arrows indicate bi-directional intrinsic passive diffusion clearance (CL_{PD}). Blue circles and blue arrows represent apically localized efflux transporters and the direction of active drug efflux (CL_{efflux}), respectively.

$$K_{p,uu} = \frac{CL_{PD}}{CL_{efflux} + CL_{PD}}$$

Nevertheless, **measuring** *in vivo* $K_{p,uu}$ at earlier gestational ages is not possible and difficult at delivery for the ethical and logistical reasons outlined above. **Predicting** this parameter is an

alternative and appealing approach. One such prediction tool is maternal-fetal PBPK (m-f PBPK) modeling and simulation.

1.3 In Silico Approach to Predicting Fetal Drug Exposure: Maternal-Fetal PBPK Modeling.

One tool to predict maternal and fetal drug disposition is PBPK modeling and simulation, a mechanistic multicompartmental approach to describe drug disposition in blood and tissues. Unlike other modeling platforms such as non-compartmental, semi-mechanistic or population PK, PBPK models incorporate a multitude of drug-specific and physiological parameters obtained *in vitro* or predicted *in silico*. By separating physiological framework from drug-specific parameters, PBPK models enable: (a) extrapolation of drug concentration-time predictions from one drug to another in a single population, (b) prediction of drug-drug interactions in a population, or (c) prediction of drug disposition characteristics in various populations (Jamei, Dickinson, & Rostami-Hodjegan, 2009; Rowland, Peck, & Tucker, 2011). These features make PBPK modeling informative for both industry and regulatory agencies and have resulted in multiple PBPK-informed drug approvals by FDA and EMA in recent years (Jamei, 2016; Sager, Yu, Ragueneau-Majlessi, & Isoherranen, 2015; Zhao, Rowland, & Huang, 2012). Due to the complexity of PBPK models, rich clinical data sets, preferably in multiple populations and via more than one route of drug administration, are necessary to verify PBPK model predictions.

The ability to incorporate of intrinsic and extrinsic subject characteristics to account for various physiological and pharmacokinetic changes that take place in both the mother and the fetus makes PBPK models particularly appealing to use for simulating drug disposition in

pregnancy. Conversely, the added complexity, the need for generalized assumptions and reliance on parameter prediction tools, require stringent verification procedures for m-f PBPK models. Rich *in vivo* verification data sets are required to assess model performance in both the non-pregnant and pregnant populations and after IV and extravascular drug administration. The orphan status of a pregnant woman and her fetus in regard to *in vivo* data greatly challenges such verification. While for some drugs, verification data such as UV/MP ratios obtained at term are available, for the majority of the drugs, they are lacking. Or when UV/MP ratios are available, the data are limited by sparse data of a small sample size, lacking clear maternal-fetal pairing, or time post-last dose for each sample. Moreover, predictions at gestational ages other than at term cannot be verified due to lack of fetal sampling pre-term. Nevertheless, multiple pregnancy PBPK models have emerged over the years and showed some success in predicting maternal drug disposition and more limited success in predicting fetal drug exposure (Abduljalil & Badhan, 2020; Dallmann, Pfister, van den Anker, & Eissing, 2018; Zhang et al., 2017; Zhang & Unadkat, 2017).

Predicting fetal drug exposure by m-f PBPK modeling has proven to be a formidable challenge for the following reasons. First, a majority of published models simplify feto-placental physiology by lumping these compartments together, limiting the physiological relevance and application of the models (Gaohua, Abduljalil, Jamei, Johnson, & Rostami-Hodjegan, 2012; Liu et al., 2020). One of the main reasons for this simplification was the limited data about gestational age-dependent fetal physiological parameters. Recently, we (Zhang et al., 2017) and other groups (SimCYP, version 19 and after) were able to expand the maternal-fetal PBPK models to include multiple fetal compartments, blood flows and placental clearances. Second, despite emerging knowledge about fetal organ composition and growth during pregnancy

(Abduljalil, Jamei, & Johnson, 2019), there remains a paucity of mechanistic and quantitative data on the major factors that affect fetal drug exposure namely, transplacental active transport clearance, passive diffusion clearances, placental metabolism, and fetal hepatic and/or renal elimination. Incorporation of such mechanistic data and emergence of well-designed clinical studies addressing placental drug transfer are prerequisites for successful m-f PBPK model verification. Third, the aforementioned fetal physiological parameters are often only available at later gestational weeks (>GW13 or later). Measurements are difficult due to small organ sizes and blood flows, and challenges in accurate measurement with current technologies (Abduljalil et al., 2019). Furthermore, the verification of the existing models is limited by lack of verification data sets (UV/MP drug plasma concentration ratios at term).

Initial efforts for m-f PBPK model development focused on a model that only accounted for passive diffusion across the placenta. We successfully developed and verified a m-f PBPK model that could dynamically predict maternal-fetal exposure to drugs that passively diffuse across the placenta (e.g., theophylline and zidovudine). Although the fetal $K_{p,uu}$ of these drugs was expected and observed to be 1, this value did not predict the dynamic exposure of the fetus to theophylline and zidovudine because $K_{p,uu}$ is a steady-state parameter. To predict the dynamic theophylline and zidovudine fetal exposure, we first estimated the placental passive diffusion clearance of midazolam. Then, we used this passive diffusion clearance as a “gold standard” to scale *in vitro* apparent permeability of theophylline and zidovudine to their respective *in vivo* placental passive diffusion clearances. Finally, we successfully verified the model for theophylline and zidovudine with the observed dynamic maternal and fetal plasma concentration-time data at term (Zhang & Unadkat, 2017). The verified m-f PBPK model can be

applied to predict maternal and fetal drug exposure to multiple drugs that passively diffuse through placenta, including ones for which observed *in vivo* data are not available.

While passive diffusion is a contributing process for all drugs to cross cell membranes, some drugs are also actively transferred across the placenta by various xenobiotic transporters present on the placental cell membranes. The placenta is richly endowed with drug transporters that are primarily localized to the syncytiotrophoblast layer separating maternal and fetal blood circulation (Burton & Fowden, 2015; Koren & Ornoy, 2018). Transporters are localized either on the apical (maternal blood-facing) or the basal (fetal blood-facing) membranes of syncytiotrophoblast and transfer a variety of xenobiotic and endogenous substrates in and out of the placenta (**Figure 1.3**) (Joshi et al., 2016; Vahakangas & Myllynen, 2009).

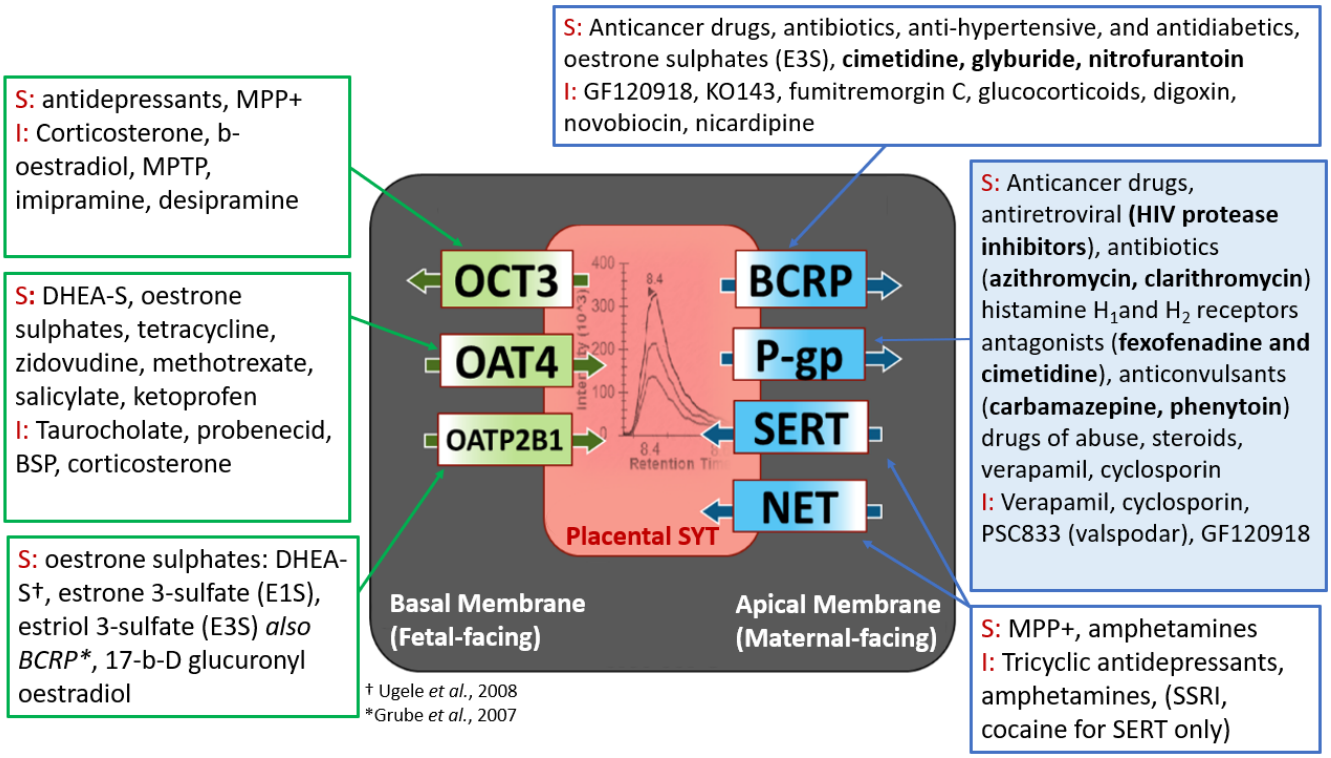

Figure 1.3. Visual representation of placental syncytiotrophoblast (SYT) layer and several apical and basal membrane transporters with their proposed direction of transport. Transporter substrates (S) and inhibitors (I) are listed in the corresponding boxes (not an exhaustive list).

Figure references:
BCRP: (Han et al., 2018; Joshi et al., 2016; Mao, 2008; Mao & Unadkat, 2015)
P-gp: (Gil, Saura, Forestier, & Farinotti, 2005; Mathias et al., 2005; Sun et al., 2006)
SERT/NET: (Bottalico et al., 2004; Vahakangas & Myllynen, 2009; Velasquez, Goeden, & Bonnin, 2013)
OCT3: (Hayer-Zillgen, Bruss, & Bonisch, 2002; N. Lee et al., 2013; Lee et al., 2018)
OAT4: (Cha et al., 2000; Kummu et al., 2015; Ugele, Bahn, & Rex-Haffner, 2008)
OATP2B1: (Grube et al., 2007; Ugele et al., 2008)

Placental drug efflux transporters, expressed on the apical membrane of the syncytiotrophoblast layer, transport move the drug from the placenta to the maternal circulation (Han et al., 2018; Joshi et al., 2016). These transporters include P-gp, BCRP, and MRP2 amongst others. Of these, BCRP and P-gp are highly abundant in the human placenta (Anoshchenko et al., 2020). BCRP and P-gp are promiscuous transporters with overlapping substrate selectivity and are hypothesized to protect the fetus from potentially harmful agents. BCRP and P-gp efflux drugs commonly administered to pregnant women such as HIV protease inhibitors, corticosteroids, antibiotics, anticonvulsants, anti-hypertensive and antidiabetic drugs and many others (**Figure 1.3**) (Han et al., 2018; Joshi et al., 2016). Significant placental efflux of drugs can be manifested in lower fetal unbound drug plasma concentration compared to maternal unbound drug plasma concentrations ($K_{p,uu} < 1$). Moreover, due to the change in placental abundance of transporters with gestational age, the magnitude of active placental drug efflux can vary as pregnancy progresses (Gil et al., 2005; Mao, 2008; Mao & Unadkat, 2015; Mathias et al., 2005; Meyer zu Schwabedissen et al., 2006; Sun et al., 2006). Failure to account for placental drug efflux can cause overestimation of fetal drug exposure ($K_{p,uu}$) and, hence, drug efficacy or toxicity to the fetus. Consideration of fetal efficacy is particularly important for the drugs where fetus is the therapeutic target (e.g., HIV protease inhibitors and corticosteroids), and failure to

address placental drug efflux may lead to under-dosing of the fetus and suboptimal treatment of the fetal condition. Therefore, determining the magnitude of active placental drug efflux throughout gestation is necessary to design optimal dosing regimens of drugs that are substrates of efflux transporters administered to pregnant women.

Typically, due to the limited number of *in vivo* studies in pregnancy, fetal exposure to placental efflux transporter substrate drugs on the market and in development cannot be **estimated directly** from *in vivo* data using m-f PBPK model. Therefore, it is important to be able to **predict** the magnitude of P-gp efflux and fetal $K_{p,uu}$ from *in vitro* studies with the aid of existing *in vitro* to *in vivo* extrapolation (IVIVE) techniques. The IVIVE scaling strategies need to account for the differences in transporter abundance between *in vitro* systems and *in vivo* tissue abundance by scaling with a REF. Three of the most time-tested approaches to estimate fetal drug transfer are: (1) perfused placenta studies, (2) vesicular transport assays, and (3) Transwell® assays. These approaches are discussed in the following section. Successful prediction of fetal $K_{p,uu}$ at term from *in vitro* models and successful verification with the observed $K_{p,uu}$ values, will present a proof-of-concept for our IVIVE approach that, in conjunction with m-f PBPK model, can be applied to predict fetal drug exposure for drug transporter substrates lacking available *in vivo* data. Additionally, this success will give us confidence in our predictions of fetal drug exposure at earlier gestational ages.

1.4 *IN VITRO* APPROACHES TO PREDICT FETAL DRUG EXPOSURE ($K_{P,UU}$)

1.4.1 *Perfused Placenta*

Perfused placenta has been considered a “gold standard” approach to study transplacental drug transfer *ex vivo* (Arumugasaamy, Rock, Kuo, Bale, & Fisher, 2020; Sastry, 1999). In the

perfused placenta setup, maternal and fetal vasculature are connected to catheters and bidirectional molecular transfer is studied by introducing the drug into the maternal compartment and analyzing the perfusate from the fetal compartment, or *vice versa* (**Figure 1.4**). Two types of perfusion, recirculating (closed) or single pass (open), can be performed depending on the questions asked in the study (Sastry, 1999). In the closed system, the perfusate is recirculated, and after an equilibration period, the drug and antipyrine, a freely diffusible marker are added to either maternal or fetal perfusate and sampled at regular intervals to assess drug content. Both systems can be used to estimate fetal $K_{p,uu}$ (based on the ratio of unbound fetal to maternal concentrations at steady-state or AUCs) and the magnitude of maternal-to-fetal or fetal-to-maternal clearances (e.g., using the compartmental modeling. The data obtained from the perfused placenta were comparable to the *in vivo* fetal $K_{p,uu}$ for several placental transporter substrates (Mandelbrot, Duro, Belissa, & Peytavin, 2014; Pinto et al., 2021). Additionally, percent of fetal transfer was used to populate a m-f PBPK model and successfully predicted fetal $K_{p,uu}$ of various drugs (De Sousa Mendes et al., 2015; De Sousa Mendes et al., 2017)

Figure 1.4. The perfused placenta setup (closed system), where the maternal and fetal vasculature of a cotyledon connected to the separate reservoirs by tubing (Arumugasaamy et al., 2020).

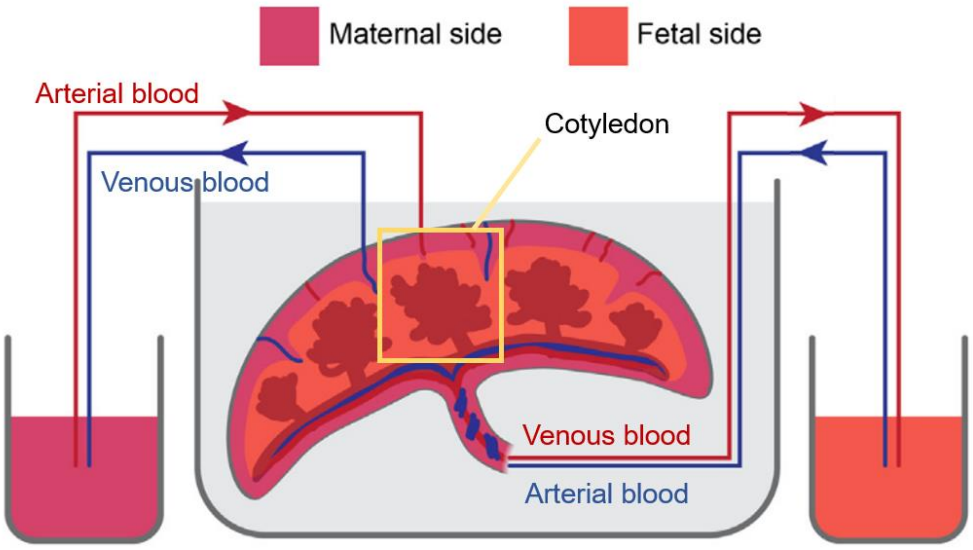

Figure 1.4. The perfused placenta setup (closed system), where the maternal and fetal vasculature of a cotyledon connected to the separate reservoirs by tubing.

The perfused placenta is the most physiologically relevant approach to describe bidirectional placental processes for any drug, regardless of the mechanisms of its transfer, but it has two practical limitations. First, this system is technically challenging and can take years to establish. Therefore, this system cannot be used routinely or in a high throughput fashion. Second, placentae for the perfusion experiments can only be obtained at term rendering extrapolation of drug transfer to other gestational ages impossible (without scaling using the REF approach). Therefore, we refrained from using this system to predict *in vivo* fetal $K_{p,uu}$.

1.4.2 *Membrane Vesicular Transport Assay*

The vesicular transport assay is the oldest membrane-based assay to detect efflux of drugs by ABC-transporters, such as P-gp, BCRP, MRP, etc. (Glavinas et al., 2008). Membrane vesicles used in this assay are in the "inside-out" orientation, where the ATP-binding site and substrate binding site face the buffer outside of the vesicle. Transporter substrates in the buffer are taken into these vesicles in an ATP-dependent manner. Upon uptake, the vesicles are

separated from the buffer by rapid filtration through a glass fiber filter, and the drug amount within the vesicles is measured by HPLC, LC-MS/MS, radioactivity or fluorescence readers depending on the structure of the drug or type of label, if present. The advantages of this assay are that it is a measure the transport of the drug substrate across the single membrane bilayer and the substrate concentrations in the buffer represent the ones at the transporter binding site. Additionally, this assay is rapid and has a high-throughput compared to perfused placenta or transporter-overexpressing cell lines. Nevertheless, there are considerable disadvantages to a vesicular transport assay. First, it exhibits high non-specific binding. The quantified compound is not only the drug inside the vesicle, but includes the drug attached to vesicular membrane, which is a major issue with the lipophilic compounds such as HIV protease inhibitors. This issue can lead to overestimation of transporter activity. Second, this assay is less useful for high passive permeability compounds due to the rapid drug diffusion out of the vesicles and results in underestimation of transporter activity. Third, the quantification of inside-out vs. right-side-out vesicles is necessary in each experiment to correct for the "inactive" right-side-out vesicles and can introduce additional technical variability. Due to these assay limitations, we opted to not use a vesicular transport assay. In addition, as for the Transwell® assays discussed in the next section, the transport and passive diffusion clearances determined in vesicles ultimately need to be scaled to *in vivo* values by quantifying the abundance of the transporter in the vesicles.

1.4.3 *Transwell® Assay with Efflux Ratio-Relative Expression Factor (ER-REF) Scaling Approach*

- Transwell Assay Overview

The Transwell® assay has recently gained popularity in determining and scaling the magnitude of active efflux (Storelli, Billington, Kumar, & Unadkat, 2021; Trapa et al., 2019;

Uchida, Ohtsuki, Kamiie, & Terasaki, 2011; Uchida, Ohtsuki, & Terasaki, 2014). In this approach, polarized cells with an overexpressed transporter of interest are seeded onto a Transwell® insert to create the apical compartment that corresponds to maternal blood and the basal compartment that corresponds to fetal blood within the well setup **(Figure 1.5)**. Drug is introduced to either of the compartments and sampled from the opposite side at various times post-dosing. The efflux ratio of apparent drug permeabilities, specifically the basal-apical vs. apical-basal flux is determined as the parameter describing the magnitude of *in vitro* transport through the cell monolayer (**Equation 1.2**; More detail can be found in **Chapter 3**).

Equation 1.2.

$$ER = \frac{P_{app(B\rightarrow A)}}{P_{app(A\rightarrow B)}} = \frac{CL_{int(B\rightarrow A)}}{CL_{int(A\rightarrow B)}} = \frac{cA_{A(R)} \cdot AUC_{A(D)}}{AUC_{B(D)} \cdot cA_{B(R)}}$$

where $P_{app(B\rightarrow A)}$ and $P_{app(A\rightarrow B)}$ are apparent permeabilities; $CL_{int(B\rightarrow A)}$ and $CL_{int(A\rightarrow B)}$ are apparent intrinsic clearances of a drug in corresponding directions (B-to-A or A-to-B); $cA_{A(R)}$ and $cA_{B(R)}$ are cumulative amounts of drug in corresponding receiver compartment; $AUC_{A(D)}$ and $AUC_{B(D)}$ are AUC of the drug in corresponding donor compartment.

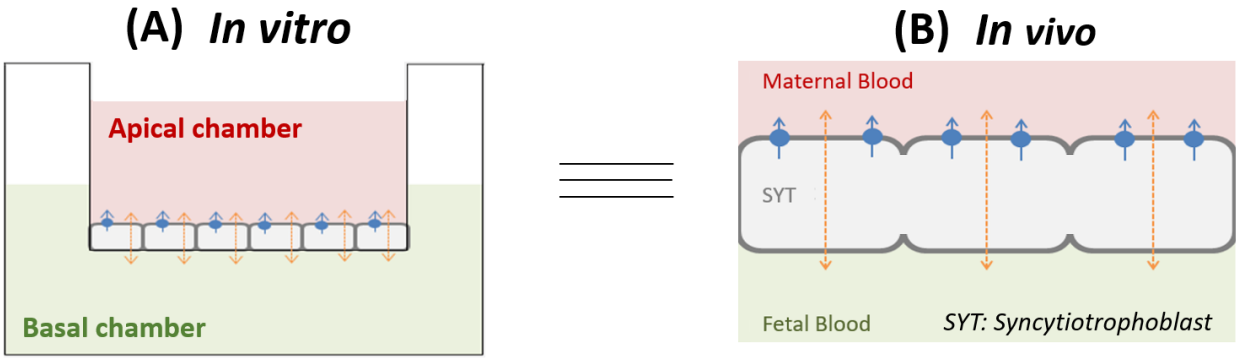

Figure 1.5. Representation of the cell monolayer in the *in vitro* Transwell® system used to predict fetal $K_{p,uu}$ (A) and in the syncytiotrophoblast (SYT) layer *in vivo* (B). Apical and basal chambers in the *in vitro* system mimic the *in vivo* maternal and fetal blood compartments, respectively. Dashed arrows indicate bidirectional intrinsic passive diffusion clearance. Blue circles and blue arrows represent apically localized efflux transporters and the direction of drug efflux, respectively.

- Cell Line for Transwell® Experiments

The primary consideration for the Transwell® assay is the choice of the cell line that would closely recapitulate passive drug transfer, active transport processes and accurately represent transporter abundance of the placenta. While human choriocarcinoma cell lines (e.g., BeWo, JAr and Jeg-3) are physiologically relevant and have been used to address transplacental transport (Ikeda et al., 2011; Poulsen, Rytting, Mose, & Knudsen, 2009), they often fail to form tight junctions (Egawa et al., 2008), a key property of blood-placental barrier and the major determinant of the magnitude of maternal-fetal drug transfer. Additionally, these cells fail to recapitulate syncytiotrophoblast phenotype, exhibit altered transporter abundance and metabolic activity (Rothbauer et al., 2017). To overcome limitations of trophoblast-derived cell lines, we chose to use a non-trophoblast-derived cell line. The Madin-Darby Canine Kidney (MDCK) cells possess two major properties essential to address placental transport questions: a) formation of tight junctions, and b) overexpression of human transporter of interest (e.g., P-gp) while its

endogenous canine transporter of interest (e.g., P-gp) is knocked-out. The latter was performed to eliminate the contribution of endogenous transporter activity and to avoid overestimation of drug efflux by the human transporter. Due to the extremely high transporter abundance in these cells, which is much greater than in placental tissue), the active transport by the cell monolayer must be scaled to correct for the overabundance. The advantages of using the MDCK cell line include: (1) its ability to recapitulate the major properties of blood-placental barrier relevant to maternal-fetal drug passage, including the formation of tight junctions and appropriate paracellular drug transfer, and (2) high abundance of the transporter of interest permitting easily detectable transporter activity *in vitro*.

The Transwell® assay with transporter-overexpressed cells has several limitations. The transporter-overexpressed cell monolayer does not represent the complex physiology of the placenta and lacks secondary cell populations (e.g., endothelial cells) where transport can occur (Joshi et al., 2016). However, P-gp abundance in secondary cell populations relative to the syncytiotrophoblast is minor and unlikely to significantly contribute to overall P-gp efflux (Joshi et al., 2016). Therefore, the MDCK system captures the transfer properties of syncytiotrophoblast and can be deemed fit for our scaling purposes. Another limitation of the Transwell® assay is that it requires mechanistic knowledge and identification of the specific transporter(s) involved in drug disposition in placenta, which are not always available. The MDCK cell systems have been shown to successfully express two transporters, though additional transporters could theoretically be expressed (Lopez Quinones, Wagner, & Wang, 2020; Muller, Konig, Hoier, Mandery, & Fromm, 2013). Unlike perfused placenta studies, the Transwell® assay is not constrained by a high degree of technical expertise, limited cell viability and throughput, hence, we chose to use this model for our *in vitro* to *in vivo* prediction of fetal $K_{p,uu}$.

- Efflux Ratio-Relative Expression Factor (ER-REF) Approach to Predict $K_{p,uu}$

In order to predict *in vivo* fetal $K_{p,uu}$ from the *in vitro* data available from the Transwell® studies, it is necessary to adopt an IVIVE scaling strategy that accounts for the differences in transport abundance between *in vitro* and *in vivo* systems. Recently, a novel and elegant approach to predict $K_{p,uu}$ has gained popularity (Trapa, Belova, Liras, Scott, & Steyn, 2016; Trapa et al., 2019). It scales efflux ratio (ER) of the drug in transporter-overexpressed cell line with proteomics-informed relative expression factor (REF) to predict *in vivo* $K_{p,uu}$ (**Equation 1.3, 1.4**).

Equation 1.3

$$K_{p,uu,IVIVE} = \frac{1}{\left(ER_{Inh(+)} - ER_{Inh(-)}\right) \cdot REF + 1}$$

Where Inh: transporter inhibitor; REF: relative expression factor measured by quantitative targeted proteomics.

Equation 1.4

$$REF = \frac{P-gp\ abundance\ in\ human\ placenta\ (pmol/mg\ MP)}{P-gp\ abundance\ in\ hMDR1-MDCKII^{cP-gp\ KO}\ cell\ line\ (pmol/mg\ protein)}$$

Where MP: total membrane protein in *ex vivo* human placental preparations, where P-gp abundance was quantified as described before

The strength of this approach is its independence from the **absolute** magnitude of passive diffusion clearances in the *in vitro* system (measured in clearance units, e.g L/h). This liberates us from the assumption that the *in vitro (scaled)* and *in vivo* passive diffusion clearances are equal. Instead, ER-REF approach relies on the magnitude of P-gp efflux clearance **relative** to the

passive diffusion clearance, which if scaled with REF (**Equation 1.4**), yields *in vivo* $K_{p,uu}$ value. The downside of this approach is that the *in vivo* $K_{p,uu}$ provides an estimate of the fetal:maternal unbound plasma AUC or the corresponding steady-state concentrations, while prediction of the dynamic plasma drug concentrations requires both passive and active clearances in maternal-fetal and fetal-maternal directions. In order to make dynamic predictions, we used our m-f PBPK model and previous data on transplacental clearance of passively diffused drug midazolam (Zhang & Unadkat, 2017) to estimate both passive diffusion and active transport clearances of P-gp substrates of interest (see **Chapters 3 and 4**).

Until recently, the ER-REF approach has been applied successfully to predict brain $K_{p,uu}$ for transporter substrates in preclinical species. Uchida *et al.* showed that ER-REF approach could predict mouse brain $K_{p,uu}$ within 3-fold of the estimated *in vivo* value for 11 P-gp substrates, such as quinidine and dexamethasone, using mouse P-gp-transfected LLC-PK1 (porcine kidney) cells (Uchida et al., 2011). The same group predicted non-human primate brain $K_{p,uu}$, using cynomolgus monkey P-gp-transfected LLC-PK1 cells (Uchida, Wakayama, et al., 2014). Trapa *et al.* extended this approach to substrates of two or more transporters (e.g., P-gp and BCRP) and predicted the brain $K_{p,uu}$ of 133 compounds in mouse, rat and non-human primates (Trapa et al., 2019). Finally, our group applied the ER-REF approach to successfully predict human brain $K_{p,uu}$ values of 3 P-gp substrates, verapamil, N-desmethyl loperamide and metoclopramide, using human P-gp transfected MDCK cell line where the endogenous canine P-gp was knocked out (Storelli, Anoshchenko, & Unadkat, 2021). By adopting this approach, we aimed to test its success in predicting **fetal** *in vivo* $K_{p,uu}$ at term for several actively transported drugs. We decided to focus on one model transporter, P-glycoprotein, and determine fetal drug exposure to its substrates. P-gp was chosen as it is highly expressed in the human placenta at all

gestational ages, many drugs are substrates of this transporters and are administered to pregnant women, and UV/MP data for selective P-gp substrates that are unlikely to be metabolized in placenta are available. *In vivo* studies determining UV/MP ratio of P-gp substrates at term were used for our model verification. Here, we used P-gp as a model transporter, but as shown in previously published studies, the ER-REF approach can be applied to substrates of other transporters (e.g., BCRP) or substrates of multiple transporters (e.g., both P-gp and BCRP).

- P-gp Substrates Used to Determine Fetal $K_{p,uu}$ at Term

Four sensitive P-gp substrates: dexamethasone (DEX), betamethasone (BET), darunavir (DRV) and lopinavir (LPV) were selected using UW Drug Interaction Database (UW DIDB) based on the following criteria. The drug has to: a) be an excellent *in vitro* substrate of P-gp as evidenced by average UV/MP value of much less than unity determined *in vivo* or in the perfused human placenta studies; b) not be a substrate of BCRP, the most abundant transporter in placenta (Joshi et al., 2016), or of other transporters or drug metabolizing enzymes present in the placenta; c) have published data that reports UV/MP ratio at term with corresponding time post-last dose administered to the mother; and d) have maternal drug plasma concentration-time profiles at known gestational ages.

Darunavir and Lopinavir (co-administered with Ritonavir)

Darunavir (DRV) and lopinavir (LPV) are two HIV protease inhibitors (PIs) that are co-administered with ritonavir (RTV) and other agents as a part of antiretroviral therapy to manage maternal HIV infection and to prevent vertical HIV transmission to the fetus (Andany & Loutfy, 2013). They have been extensively studied in pregnancy and, at the commonly administered doses, are efficacious as assessed by maternal viral suppression to < 50 copies/mL and reducing mother-to-child transfer of the virus (Andany & Loutfy, 2013; Salama, Eke, Best, Mirochnick, &

Momper, 2020). The general understanding is that the HIV virus cannot cross intact placenta and infect the fetus during pregnancy. The virus can infect the fetus when the placenta separates from the uterus at delivery or in case of placental damage during pregnancy due to infection or other reasons (Bawdon et al., 1994; Bawdon et al., 1995). Minimizing the chance of viral transfer makes the fetus as well as the mother therapeutic targets for HIV protease inhibitors. Therefore, it is paramount to maintain pregnant women on antiretroviral therapy to protect the maternal-fetal dyad from HIV infection.

Since maternal drug plasma concentrations and exposure are the major determinant of fetal drug plasma concentrations, it is important to accurately predict maternal drug concentration-time profiles in order to have confidence in fetal drug plasma concentration predictions. There are several key absorption, distribution, metabolism, excretion and transport (ADMET) processes that affect maternal and fetal drug disposition and fetal exposure ($K_{p,uu}$) to LPV and DRV ((Wagner et al., 2017), **Table 1.1**). First, both LPV and DRV are always co-administered with ritonavir as a booster. RTV is known to increase bioavailability of LPV and DRV by inhibiting CYP3A enzymes in the intestine and to a lesser degree in the liver (Kirby et al., 2011; Salama et al., 2020). RTV coadministration leads to the increased drug plasma concentrations of protease inhibitors when compared to their un-boosted profiles. In general, RTV has rather complex inhibition and induction profiles that can lead to various drug-drug interactions (**Table 1.1**). Second, both DRV and LPV are primarily eliminated hepatically, with CYP3A4 being major metabolizing enzyme (Salama et al., 2020). The combination of the 2-fold induction of hepatic CYP3A in pregnancy (Hebert et al., 2008; Zhang et al., 2015) that can decrease maternal plasma PI concentrations and concurrent inhibition of CYP3A by RTV that can increase maternal plasma PI concentrations, presents additional complexity to the maternal

disposition of these drugs. This complexity is possible to address within the framework of a m-f PBPK model by incorporating both inhibition and induction processes. Third, transplacental passage of DRV and LPV at term was shown to be relatively low (11-20%) (Andany & Loutfy, 2013), which was attributed to high placental P-gp efflux. The observed ER in Transwell® assays were 3.8 to 25 for DRV and 3.2 to 16 for LPV according to UW DIDB. Placental P-gp efflux can greatly affect fetal drug exposure and is the target for our *in vitro* and m-f PBPK predictions. Our m-f PBPK model accounts for the changes in drug protein binding in the mother and the fetus due to the difference in the concentration of albumin and alpha-1-acid glycoprotein in maternal and fetal blood (Zhang & Unadkat, 2017). The changes in *in vivo* maternal plasma protein binding of either PI are insignificant (Salama et al., 2020), while for the fetus such changes are not available, but can be predicted by our model.

Accounting for these and many other factors in our m-f PBPK model is necessary to predict fetal drug plasma concentrations and exposure. To do so, the above-mentioned and other relevant pharmacokinetic parameters were incorporated into the base model for DRV, LPV and RTV (non-pregnant PBPK model input parameters, **Table 1.1**). By adjusting for pregnancy changes, the m-f PBPK model was used to predict maternal and fetal drug plasma concentration-time profiles at term. These predictions were verified with the observed data (**Chapter 3**).

Dexamethasone and Betamethasone

Dexamethasone (DEX) and betamethasone (BET) were chosen as our model P-gp substrates. These two antenatal corticosteroids (ACS) are prescribed to pregnant women at risk (within 48 h) of preterm delivery (gestational weeks 24-34) to accelerate fetal lung maturation *in*

utero and prevent neonatal respiratory distress syndrome (RDS). These two epimers were first developed for rheumatoid arthritis (RA), and their use in human pregnancy was due to the accumulated evidence of their efficacy and survival of newborns delivered prematurely (Roberts, Brown, Medley, & Dalziel, 2017). The observed efficacy for the prevention of RDS in newborns is rather modest. The relative risk ratio of RDS comparing ACS treatment to placebo treatment was 0.6 - 1.16 (Oladapo et al., 2020) with increased incidences of maternal and fetal toxicities (e.g., infection, hypoglycemia) (Crowther et al., 2007; Crowther & Harding, 2007; Raikkonen, Gissler, & Kajantie, 2020; Roberts et al., 2017; Vogel et al., 2017). Nevertheless, despite many decades of their antenatal use, neither an optimal dosing strategy for ACS, nor exposure-response relationship for BET and DEX have been established in pregnancy. The drugs are most commonly administered to pregnant women as indicated for RA patients. DEX is given as an IM injection of 6 mg dexamethasone phosphate (DEX-P) every 12 h for 48 h and BET is given as an IM injection of 12 mg 1:1 betamethasone phosphate:acetate (BET-P:A) every 24 h for 48 h.

In addition to the lack of clarity on the efficacy and toxicity of clinically used doses, several other challenges exist for ACS dose optimization. One of them is non-overlapping socioeconomic settings of DEX and BET usage to prevent RDS. High-income countries predominantly use BET, while low-to-middle income countries primarily use DEX (Vogel et al., 2017). More than 20 clinical trials conducted in high-income countries report on the safety and efficacy of BET, while such data are lacking for DEX (Ke & Milad, 2019; Roberts et al., 2017). Moreover, the results from the antenatal corticosteroid trial (ACT) conducted in 6 low-to-middle income countries reported that the DEX intervention resulted in increased risk of neonatal mortality and maternal infection (Althabe et al., 2015). Several features of this trial (e.g., cluster-randomization, statistical analysis, etc.) were later criticized in secondary analyses (McClure et

al., 2016). In response, the WHO issued a set of prerequisites for ACS use in low-resource setting: ability to determine gestational age, lack of maternal infection, adequate childbirth care. Meeting such prerequisites in low-resource setting is often unrealistic, yet preterm births there account for 60% of live births, emphasizing the need for ACS use in these countries (Vogel, Oladapo, Manu, Gulmezoglu, & Bahl, 2015). The criticism of the ACT prompted further evaluation of clinical ACS dose efficacy study, which was recently conducted by WHO and that confirmed efficacy of DEX administered to pregnant women at standard dosing regimen in the low resource setting.

Nevertheless, the observed efficacy of ACS administered at their usual clinical doses does not inform us about the **optimal** dosing of these BET and DEX in pregnancy. The only data on exposure-response relationship exist in sheep and only for BET, where fetal drug plasma concentrations of 1 ng/mL promoted fetal lung maturation and improved various lung indices (Schmidt et al., 2018). The lack of corresponding data for DEX and the inability to obtain such data in human pregnancy further supports the use of modeling as an alternative to clinical studies to predict fetal drug exposure.

In addition to efficacy and safety considerations, there are several other pharmacokinetic considerations that challenge ACS dose optimization. DEX and BET are assumed to have similar biological activity despite the following differences in pharmacokinetics. First, the BET half-life after IV administration to non-pregnant individuals (5.6 h) is more than two-fold longer than for DEX (2.4 h) (Ke & Milad, 2019) (**Table 1.1**). Second, differences in IM dose formulation (DEX-P vs. BET-P:A) can further contribute to differences in drug exposure. Third, emerging evidence suggests differences in ACS clearance between Caucasian and Indian populations, which has been noted for CYP3A substrates (Ahsan et al., 1993). Population differences in CYP3A-

mediated clearance, if reproduced for ACS, may necessitate development of different PBPK modeling approaches for Caucasian and Indian ethnic population. Fourth, the induction of hepatic CYP3A4 in pregnancy (compared to non-pregnant women) adds another source of maternal variability that can affect BET and DEX disposition and should be accounted for in the m-f PBPK modeling approach. Of note, ACS are not expected to further induce CYP3A4 due to the acute nature of their administration (2-4 doses within 48 h). Fifth, DEX and BET are *in vitro* substrates of P-gp with variable reported efflux ratios of ~2-4 for DEX and ~2-7 for BET (Yates et al., 2003). The *in vivo* UV/MP ratios were slightly higher for BET than that for DEX (0.5-0.6 and 0.4-0.5, respectively) (Ballabh et al., 2002; Tsuei, Petersen, Ashley, McBride, & Moore, 1980). These factors and others (**Table1.1**) can cumulatively and differentially affect maternal and fetal drug exposure to DEX and BET. Due to the lack of established ACS exposure-response relationship, it is critical to accurately predict fetal exposure using a m-f PBPK model in conjunction with scaled *in vitro* $K_{p,uu}$ and verify the predictions with observed *in vivo* data at term. Once successfully verified, we will use the model to develop alternative dosing regimens of DEX and BET with different doses/schedules and at earlier gestational ages to inform the safe and efficacious administration of BET and DEX in pregnancy.

Overall, the four P-gp substrates (DEX, BET, DRV and LPV) were chosen as model verification drugs for our *in vitro* to *in vivo* scaling of fetal $K_{p,uu}$ at term (described in **1.4.3.3**). Due to the availability of observed UV/MP ratios only at delivery, these predictions can be verified using our m-f PBPK model only at term. After verification, the model can be used to predict fetal $K_{p,uu}$ at other gestational ages or devise alternative dosing regimens. To elucidate the magnitude of fetal drug exposure to placental transporter substrates, we present the following goal, hypothesis and specific aims to test this hypothesis.

Goal:

To predict in vivo human fetal plasma drug exposure to placental transporter drug substrates using an in vitro to in vivo extrapolation (IVIVE) approach and verify our predictions by comparing them with corresponding in vivo data.

Hypothesis:

In vivo human fetal $K_{p,uu}$ (reflective of fetal drug exposure) of DEX, BET, DRV and LPV can be accurately predicted by determining their efflux ratio (ER) in a P-gp-overexpressing cell line (*in vitro* system) and scaling this ER by a relative expression factor (REF).

Specific Aims:

Aim 1. To determine the absolute abundance of transporters in human placentae (*ex vivo*) of different gestational ages by targeted quantitative proteomics (LC-MS/MS) (**Chapter 2)**.

Aim 2.

2A) To predict the *in vivo* $K_{p,uu}$ of DRV, LPV, DEX, and BET based on their ER determined in P-gp overexpressing MDCKII cells in the Transwell® assay and the ER-REF scaling approach (**Chapter 3)**

2B) To verify the predicted $K_{p,uu}$ (from Aim 2A) by comparing these predicted values with those estimated from *in vivo* $K_{p,uu}$ (here and from Aim 3A) using our m-f PBPK model (**Chapter 3**)

Aim 3.

3A) To estimate the *in vivo* $K_{p,uu}$ of DEX and BET using the observed UV/MP data and our m-f PBPK model (**Chapter 4**)

3B) Using the estimated *in vivo* $K_{p,uu}$ (Aim 3A), devise alternative dosing regimens for DEX and BET to improve their efficacy and safety (**Chapter 4**).

Table 1.1. Non-pregnant PBPK model input parameters for LPV, DRV, RTV, DEX and BET

Parameter	LPV [1]	DRV [1]	RTV [1]	DEX [2]	BET [2]
Physico-chemical properties					
MW [g/mol]	628.81	547.7	721	392.5	392.5
Log P	4.2	2.5	3.9	1.83	1.83
Compound type	Neutral	Neutral	Neutral	Monoprotic Base	Monoprotic Base
pK_a	2.6 (basic) 13.4 (acidic)	2.4 (basic) 13.6 (acidic)	2.8 (basic) 13.6 (acidic)	-3.3 (basic) 12.4 (acidic)	-3.3 (basic) 12.4 (acidic)
f_u	0.01	0.05	0.02	0.319	0.36
B/P	0.75	0.65	0.58	0.93	1.12
Absorption					
f_a	1 (assumed)	1 (assumed)	1 (assumed)	1 (assumed)	1 (assumed)
k_a [1/h]	0.57 (pred)	1.04	0.22	2.0 (IM)	2.0 (IV) 0.2 (IM)
T_{lag} [h]	1.5	1.3		1 (IM)	1 (IM)
Distribution					
PBPK model	full	full	minimal	full	full
V_{ss} [L/kg]	0.82 (pred)	1.7	0.4	0.71 [3]	1.4
K_p scalar	0.098	1	0.048	0.22	0.25
Elimination					
CYP3A4	CL_{int}: 93.4	CL_{int}: 182	V_{max}: 1.37 K_m: 0.07	CL_{int}: 19	CL_{int}: 8.3
CYP3A5			V_{max}: 1 K_m: 0.05		
CYP2D6			V_{max}: 0.7 K_m: 1		
CL_R [L/h]	0.15	0.3	0.27	0.41	0.49
Additional CL		Systemic: 6.5 [L/h]	HLM: 50 [µL/min/pmol]	0.49 [µL/min/mg]	
Interaction - Inhibition					
CYP2B6		K_i: 500	K_i: 1.3		

CYP2C9		K_i: 52	K_i: 1.22		
CYP2C19		K_i: 25			
CYP2D6		K_i: 41	K_i: 0.06		
CYP3A4	K_{app}: 0.41 K_{inact}: 1	K_i: 0.4	K_{app}: 0.25 K_{inact}: 19.8		
CYP3A5	K_{app}: 1 K_{inact}: 1	K_i: 0.4	K_{app}: 0.25 K_{inact}: 19.8		
Interaction - Induction					
CYP3A4			Ind_{max}: 68.5 Ind_{C50}: 1		
CYP3A5			Ind_{max}: 68.5 Ind_{C50}: 2		

Table 1 references, abbreviations and units

[1] Wagner, C., Zhao, P., Arya, V., Mullick, C., Struble, K., & Au, S. (2017). Physiologically Based Pharmacokinetic Modeling for Predicting the Effect of Intrinsic and Extrinsic Factors on Darunavir or Lopinavir Exposure Coadministered With Ritonavir. J Clin Pharmacol, 57(10), 1295-1304. doi:10.1002/jcph.936

[2] Ke, A. B., & Milad, M. A. (2019). Evaluation of Maternal Drug Exposure Following the Administration of Antenatal Corticosteroids During Late Pregnancy Using Physiologically-Based Pharmacokinetic Modeling. Clin Pharmacol Ther, 106(1), 164-173. doi:10.1002/cpt.1438

[3] Tsuei, S. E., Moore, R. G., Ashley, J. J., & McBride, W. G. (1979). Disposition of synethetic glucocorticoids. I. Pharmacokinetics of dexamethasone in healthy adults. J Pharmacokinet Biopharm, 7(3), 249-264

B/P - blood:plasma partition ratio; CL_{int} - intrinsic clearance [µL/min/mg protein]; CL_R - renal clearance [L/h]; CYP - cytochrome P450; f_a - fraction absorbed; f_u - fraction of unbound drug in plasma; HLM - human liver microsomes; Ind_{C50} - inducer concentration that yields half-maximal induction [µmol/L]; Ind_{max} - inducer concentration that yields maximum induction [µmol/L]; k_a - absorption rate constant [h^{-1}]; K_{app} - concentration of mechanism-based inhibitor associated with half-maximal inactivation rate [µmol/L]; K_i - inhibitor concentration that yields half-maximal inhibition [µmol/L]; K_{inact} - inactivation rate of given enzyme [h^{-1}]; K_m - Michaelis-Menten constant [µmol/L]; K_p - partition coefficient; log P - logarithm of octanol-water partition coefficient; MW - molecular weight [g/mol]; pK_a - negative decadal logarithm of acid dissociation constant; T_{lag} - absorption lag time [h]; pred - predicted; V_{max} - maximum rate of metabolite formation [pmol/min/mg microsomal protein]; V_{ss} - volume of distribution at steady state [L/kg]

Chapter 2. GESTATIONAL AGE-DEPENDENT ABUNDANCE OF HUMAN PLACENTAL TRANSPORTERS AS DETERMINED BY QUANTITATIVE TARGETED PROTEOMICS

The work presented in this chapter was previously published in Drug Metabolism and Disposition 48:735-741(2020)

2.1 ABSTRACT

Some women take medication during pregnancy to address a variety of clinical conditions. Due to ethical and logistical concerns, it is impossible to determine fetal drug exposure, and therefore fetal risk during pregnancy. Hence alternative approaches need to be developed to predict maternal-fetal drug exposure throughout pregnancy. To do so, we previously developed and verified a maternal-fetal physiologically based pharmacokinetic (m-f-PBPK) model, which can predict fetal exposure to drugs that passively cross the placenta. However, many drugs are actively transported by the placenta (e.g., HIV protease inhibitors). In order to extend our m-f-PBPK model to these actively transported drugs, we determined the gestational-age dependent changes in the protein abundance of placental transporters. Total cellular membrane fractions from first trimester (T1, n=15), second trimester (T2, n=19) and term (n=15) human placentae, obtained from uncomplicated pregnancies, were isolated by ultracentrifugation. Transporter protein abundance was determined by targeted quantitative proteomics using LC-MS/MS. We observed that BCRP and P-gp abundance decreased from T1 to term by 55% and 69%, respectively (per gram of tissue). OATP2B1 abundance decreased from T1 to T2 by 32%. In contrast, OCT3 and OAT4 abundance increased with gestational age (2-fold from T1 to term, 1.6-fold from T2 to term). SERT and NET did not change with

gestational age. The abundance of BSEP, MRP1-5, NTCP, OATP1B1, OATP1B3, OCTN1-2, CNT1-3, ENT2, and MATE1 could not be quantified. These data can be incorporated into our m-f-PBPK to predict fetal exposure to drugs which are actively transported across the placenta.

2.2 INTRODUCTION

To date, approximately 40-80% of women take drugs during pregnancy and about 50% take at least one drug in the first trimester (Scaffidi et al., 2017). Pregnant women take drugs for a variety of reasons including to treat preexisting disease (e.g. depression, epilepsy), pregnancy-induced conditions (e.g. gestational diabetes and hypertension), prevent vertical transmission of infectious agents (e.g. HIV, malaria) or treat fetal conditions such as poorly developed lungs due to preterm birth (Sheffield et al., 2014).

Despite the striking prevalence of drug use during pregnancy, there is little information on the extent of maternal-fetal drug exposure throughout pregnancy. When a pregnant woman takes a drug, the fetus is de-facto exposed to the drug even if s/he is not the target for drug therapy. Fetal drug exposure, and therefore fetal risks, are driven by maternal drug exposure, placental transporters/metabolism and fetal metabolism (Zhang et al., 2017). Physiological and drug disposition changes throughout pregnancy result in time-dependent changes in maternal drug exposure (Anderson, 2005; Tasnif, Morado, & Hebert, 2016). In addition, the placenta is richly endowed with efflux transporters such as P-glycoprotein (P-gp, ABCB1)/Breast Cancer Resistance Protein (BCRP, ABCG2) (Han et al., 2018; Mathias et al., 2005) as well as influx transporters such as organic anion transporter 4 (OAT4)/norepinephrine transporter (NET) (**Figure 2.1**) (Vahakangas & Myllynen, 2009). The abundance of these placental transporters may change as pregnancy proceeds (Mathias et al., 2005). Consequently, pregnancy is a dynamic process whereby maternal-fetal drug exposure changes in a time-dependent manner. Thus, for optimum therapy of the pregnant woman and to minimize fetal risk, the challenge is to measure or predict maternal-fetal drug exposure throughout pregnancy.

While fetal drug exposure can be determined by sampling cord blood (umbilical vein, UV) only at the time of delivery, such sampling is not possible earlier in gestation (Scaffidi et al., 2017). Also, sampling UV blood at term provides only a snapshot of fetal blood drug concentration at a given time and does not provide information on fetal drug exposure (i.e., fetal plasma/blood AUC)(Zhang et al., 2017). Moreover, even though pharmacokinetic studies of a drug can theoretically be conducted in pregnant women throughout gestation, such studies pose considerable logistical and ethical challenges. Thus, alternative methods need to be developed to predict (rather than determine) maternal-fetal drug exposure throughout pregnancy. To do so, we have developed and verified a maternal-fetal **P**hysiologically **B**ased **P**harmaco**k**inetic (m-f-PBPK) model which can predict time-dependent changes in maternal-fetal exposure to drugs metabolized by CYP enzyme and cross the placenta by passive diffusion (Zhang & Unadkat, 2017). However, many drugs are transported at the blood-placental barrier which is made of the syncytiotrophoblast layer of the placental villi (Enders & Blankenship, 1999; Joshi et al., 2016; Myllynen, Pasanen, & Pelkonen, 2005). In order to extend our m-f-PBPK model to predict maternal-fetal exposure to drugs that are transported into or out of the placenta, we determined the gestational-age dependent changes in the abundance of placental transporters by targeted quantitative proteomics using LC-MS/MS.

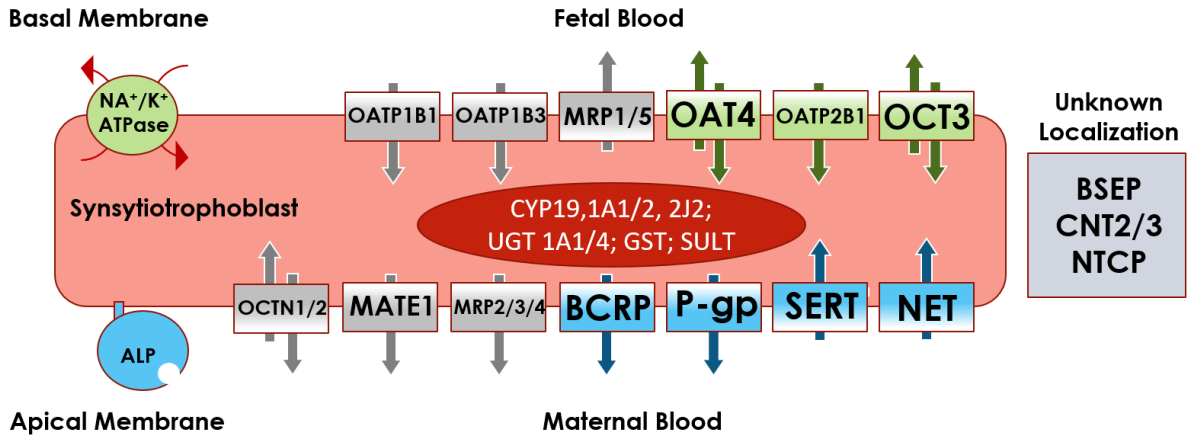

Figure 2.1. Transporters, their proposed localization and directionality of transport in the syncytiotrophoblast of the human placenta. Transporters and membrane markers that were successfully quantified are shown in green (basal membrane proteins) and blue (apical membrane proteins) (success criterion: LLOQ 5-fold signal-to-noise ratio) while the ones targeted, but not quantifiable (below LLOQ), are shown in grey. Most abundant drug metabolizing enzymes that are present in the placenta but were not attempted to quantify are indicated in the red oval (Blanco-Castaneda et al., 2020)**.** The key studies and review articles informing membrane localization of the transporters were: P-gp (Atkinson, Sibley, Fairbairn, & Greenwood, 2006; Sun et al., 2006); BCRP (Maliepaard et al., 2001); SERT (Balkovetz, Tiruppathi, Leibach, Mahesh, & Ganapathy, 1989; Bottalico et al., 2004); NET(Bottalico et al., 2004); OCT3 (Lee et al., 2018); OAT4 (Ugele et al., 2008) and OATP2B1 (Ugele et al., 2008); key review articles (Han et al., 2018; Joshi et al., 2016; Myllynen, Immonen, Kummu, & Vahakangas, 2009; Vahakangas & Myllynen, 2009)**.**

2.3 MATERIALS AND METHODS

2.3.1 *Chemicals and Reagents*

Homogenization buffer reagents and the protease inhibitor cocktail, Pefabloc SC, were purchased from Sigma-Aldrich (St. Louis, MO) and Roche (Basel, Switzerland). Omni Bead Ruptor Homogenizer, 7 mL soft tissue tubes and metal beads for homogenization were purchased from Omni International (Kennesaw, GA). Bicinchoninic acid (BCA) assay kit, dithiothreitol, iodoacetamide, sequencing grade trypsin were obtained from Pierce Biotechnology (Rockford, IL). Isotope-labeled heavy internal standard peptides were obtained from Thermo Fischer Scientific (Rockford, IL) and corresponding unlabeled surrogate peptides were purchased from New England Peptide (Gardner, MA) (**Table 2.S1**). High-performance liquid chromatography (HPLC)-grade acetonitrile, methanol, chloroform, formic acid and ammonium bicarbonate were obtained from Thermo Fischer Scientific (Fair Lawn, NJ). Sodium deoxycholate (98% purity) was purchased from MP Biomedicals (Santa Ana, CA).

2.3.2 *Procurement of human placental tissue samples*

Collection of placentae from uncomplicated pregnancies was approved and classified as nonhuman subject research by the Institutional Review Board of the University of Washington. Placentae were separated into three gestational age (GA) groups (mean ± SD): 1st trimester (T1: 63.1 ± 10.8 days, n=15), 2nd trimester (T2: 117 ± 19.6 days, n=19) and term (gestational age not available, n=15) (**Table 2.1** and **2.S3)**. To be consistent with the definition of gestational age used by the American College of Obstetricians and Gynecologists (ACOG), T1 and T2 gestational ages were expressed based on the last menstrual period. These ages were determined by adding 14 days to the age based on fetal foot size. T1 and T2 placentae were obtained from

University of Washington Birth Defect Research Laboratory (UWBDRL). Term placentae were obtained from the Labor and Delivery Unit of the University of Washington. After collection, tissues were immediately snap frozen and stored at -80°C.

Table 2.2. Gestational age grouping, protein yield and membrane marker enrichment of placentae. Data shown as means ± SD. Identical symbols next to the values denote significant differences between the respective values (Kruskal-Wallis test with Dunn's multiple comparisons, $p<0.05$, T1 – 1st trimester, T2 – 2nd trimester).

	T1 Day 1 - 98	**T2 Day 99 - 196**	**Term Day 273 - 287**
Gestational Age (days)	63.1 ± 10.8	117 ± 19.6	N/A
Number of Samples	15	19	15
Homogenate Total Protein yield (mg HP / g tissue)	26.6 ± 8.5 †	20.1 ± 3.0 †,‡	28.5 ± 7.4 ‡
Membrane Total Protein Yield (mg MP / g tissue)	0.8 ± 0.4 $	0.7 ± 0.3	0.5 ± 0.2 $
Membrane Marker Enrichment (fold)			
Alkaline Phosphatase	3.0 ± 1.7 &	2.7 ± 1.2 ^	4.2 ± 1.5 &, ^
Na^+/K^+-ATPase	3.1 ± 2.3	2.7 ± 1.0	2.2 ± 1.1

2.3.3 *Total membrane preparation and quantitative targeted proteomics*

Total membranes from human placentae were isolated by means of differential centrifugation (**Figure 2.S1)**. Briefly, frozen tissue was thawed, washed, blotted, weighed and approximately 1.5-2 g was homogenized in Omni Bead Ruptor Homogenizer. Aqueous buffer containing 250 mM sucrose, 100 mM KNO_3, 0.2 mM $CaCl_2$, 10 mM HEPES, 10 mM Tris, pH 7.4 was used for homogenization. Protease inhibitor cocktail Pefabloc SC was used to prevent protein degradation. The homogenates were centrifuged for 30 min at 10,000 g at 4°C in an

Optima L-90K Ultracentrifuge (Beckman Coulter, Brea, CA) to generate S9 fractions, which were immediately centrifuged for 1 h at 125,000 g at 4°C to generate cytosolic and total membrane fractions (i.e., combined microsomal, apical and basal plasma membranes). An aliquot of homogenate and membrane fractions were vesiculated through a 6-guage needle to resuspend the sample and diluted to a working concentration of 2 mg of total protein/mL as quantified by Pierce BCA assay.

To quantify the membrane proteins by targeted proteomics, total proteins in the homogenate and membrane fractions were reduced, denatured, alkylated and concentrated, and digested by trypsin as described previously (Vertommen, Panis, Swennen, & Carpentier, 2010; H. Wang et al., 2005). All samples were digested in triplicate after addition of Bovine Serum Albumin (BSA, 4 µg/mL). Digestion of BSA was used to correct for any variability in digestion efficiency. A heavy-labeled internal standard of each peptide was added at the end of the trypsin digestion process. Surrogate peptides were quantified on an AB Sciex Triple Quad 6500 tandem mass spectrometer coupled with Waters Acquity UPLC system (Waters, Hertfordshire, UK) (**Figure 2.S1, Tables 2.S1 and 2.S2).** Calibration curve for surrogate peptide quantification consisted of Buffer A spiked with known quantities of synthetic light peptides.

To assess inter-day variability in protein abundance, membrane fractions were prepared on three different days from site 1 of T2 placentae (n=3) (**Figure 2.S2**). To assess if protein abundance was site-dependent, membrane fractions from three different sites were prepared on the same day from these T2 placentae (n=3). Only second trimester placentae were used for these analyses as the umbilical cord placement and morphology were visible for only these placentae (**Figure 2.S2 (A)**).

2.3.4 *Data Analysis and Scaling*

Peak areas for two transitions and where possible, three transitions for each surrogate peptide of interest and heavy-labeled internal standard were integrated using the AB Sciex Analyst software 1.6.2. The average of these peak area ratios was computed, and protein abundance was calculated from calibration curves prepared in buffer A and analyzed as described previously (Prasad, Gaedigk, et al., 2016). Quality control (QC) samples were prepared in triplicate in a similar manner at the low (0.62 and 1.25 nmol/L), middle (10 nmol/L) and upper (40 nmol/L) range of the calibration curve. Each LC-MS/MS run was considered qualified if the means of the QC samples were within 20% of the nominal values.

To account for variability in digestion efficiency, protein abundance was normalized to the maximum observed BSA digestion efficiency. In addition, to account for inter-tissue variability in membrane isolation, the enrichment of the apical membrane marker (Alkaline Phosphatase, ALP) and basal membrane marker (Na^+/K^+-ATPase) was quantified. ALP and Na^+/K^+-ATPase were selected as these proteins are highly abundant in the apical membrane and basal membrane, respectively. Membrane marker enrichment was defined as the ratio of marker abundance in 1 mg of total membrane protein (MP) to marker abundance in 1 mg of homogenate protein (HP) (**Eq 2.1**). Transporters preferentially expressed in apical or basal membranes were corrected for the corresponding membrane marker enrichment by dividing by the marker enrichment value and scaled to abundance per g tissue as shown in **Eq 2.2**. Additionally, the protein abundance per g tissue was scaled to pmol analyte per predicted weight of the whole placenta. The weight of each placenta was estimated as a function of gestational age (GA) using a method described previously (**Eq 2.3**) (Abduljalil et al., 2012). Predicted placental weight values were used due to the lack of information on the exact weight of each placenta.

$$\boldsymbol{Marker\ Enrichment\ (fold)} = \frac{\frac{\boldsymbol{pmol\ Membrane\ \ marker}}{mg\ MP}}{\frac{\boldsymbol{pmol\ Membrane\ \ marker}}{mg\ HP}} \tag{2.1}$$

$$\boldsymbol{Protein\ abundance}\ \left(\frac{\boldsymbol{pmol\ protein}}{g\ tissue}\right) = \frac{\frac{\boldsymbol{pmol\ protein}}{mg\ MP}}{\boldsymbol{Marker\ Enrichment\ (fold)}} \times \frac{\boldsymbol{mg\ HP}}{g\ tissue} \tag{2.2}$$

$$\boldsymbol{Placental\ weight\ (g)} = \frac{-0.0122*\boldsymbol{GA}^3+0.9149*\boldsymbol{GA}^2-0.716*\boldsymbol{GA}}{1.048} \tag{2.3}$$

The lower limit of quantification (LLOQ) was defined by LC-MS/MS signal less than 5-times background noise. Abundance values for OATP2B1 in several T2 samples were below the LLOQ and were conservatively assigned the value of LLOQ for data analysis. Data were analyzed by non-parametric Kruskal-Wallis and Dunn's multiple comparison test in GraphPad Prism 7 with statistical significance set at $p<0.05$. Site-dependent and inter-day variability data was analyzed by Kruskal-Wallis test with Dunns's multiple comparisons. Continuous data were analyzed by Pearson correlation and the significance cut-off was defined as $R^2 \geq 0.5$.

Table 2.3. Protein-protein correlation of placental transporter abundance (N=49).
Black cells: Pearson coefficient R^2>0.5.

	BCRP	P-gp	SERT	NET	OAT4	OATP2B1	OCT3
BCRP							
P-gp	**0.78**						
SERT	**0.62**	**0.63**					
NET	0.10	0.11	0.34				
OAT4	0.10	0.11	0.22	0.28			
OATP2B1	0.10	0.19	0.26	0.15	**0.53**		
OCT3	0.00	0.00	0.05	0.16	0.42	0.43	

2.4 RESULTS

2.4.1 *Interday Variability and Site-dependent Variability in Transporter Abundance*

Transporter protein abundance in three T2 placentae was independent of the sampling site and day of preparation (**Figure 2.S2 B, C**) and hence site 1 was chosen as the sampling site for further analyses. Overall, placenta H27108 showed greater variability than other two placentae (data not shown) perhaps due to its earlier gestational age.

2.4.2 *Total Membrane Yield, Marker Enrichment and Scaling Approach*

As expected, membrane protein yield was about 3% of that in the homogenate. There was a modest difference in protein yields between the trimesters (**Table 2.1, Figure 2.2**). Na^+/K^+-ATPase enrichment did not change significantly between three gestational age groups. ALP enrichment was significantly different at term compared to T1 and T2 (**Table 2.1**). A strong correlation was observed between enrichment of ALP and Na^+/K^+-ATPase within each preparation ($R^2>0.63$, $p<0.05$, data not shown), confirming the utility of these markers in addressing membrane loss during preparation. Hence, we incorporated membrane marker enrichment values into our scaling approach (**Eq 2.1-2.3**) using ALP for transporters expressed on the apical membrane and Na^+/K^+-ATPase for transporters expressed on the basal membrane of the syncytiotrophoblast.

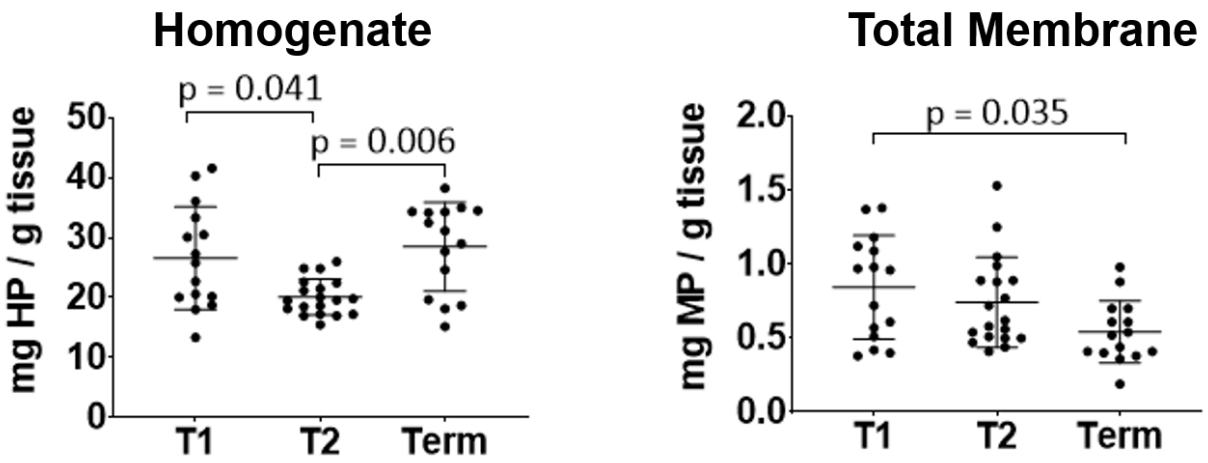

Figure 2.2. Total protein yield in homogenate (HP) and total membranes (MP) isolated from T1, T2 and Term placentae. Lines denote mean and standard deviations (T1 n=15; T2 n=19; Term n=15). Significant differences by Kruskal-Wallis Test (with Dunn's multiple comparisons) are indicated. Mean values are also presented in **Table 2.S4**. T1 – 1st trimester, T2 – 2nd trimester.

2.4.3 *Abundance of apical and basal membrane transporters in human placentae of various gestational ages*

Of the four apical membrane transporters, BCRP and P-gp showed gestational age-dependent decrease in protein abundance (pmol of analyte per gram of tissue) between T1 and term (55% and 69% respectively) and between T2 and term (42% and 52% respectively (**Figure 2.3, Table 2.S4**). Neither SERT nor NET showed significant change in protein abundance with gestation. Of the three basal membrane transporters, OCT3 showed a 2-fold increase between T1 and term) and OAT4 showed a 1.6-fold increase between T2 and term in protein abundance. OATP2B1 showed a decrease in protein abundance between T1 and T2 (32%; **Figure 2.3, Table 2.S4**). OATP2B1 was below LLOQ (0.46 nmol/L) in 5 of 19 T2 samples and hence these samples were assigned the value of LLOQ. When the values were scaled to the predicted size of the whole placenta, all proteins showed drastic increase in abundance with gestational age

(**Figure 2.S3 B**). In addition to the above proteins, the remaining transporters targeted for quantification were below the LLOQ (5-fold signal-to-noise ratio) (**Figure 2.1, Table 2.S1)**.

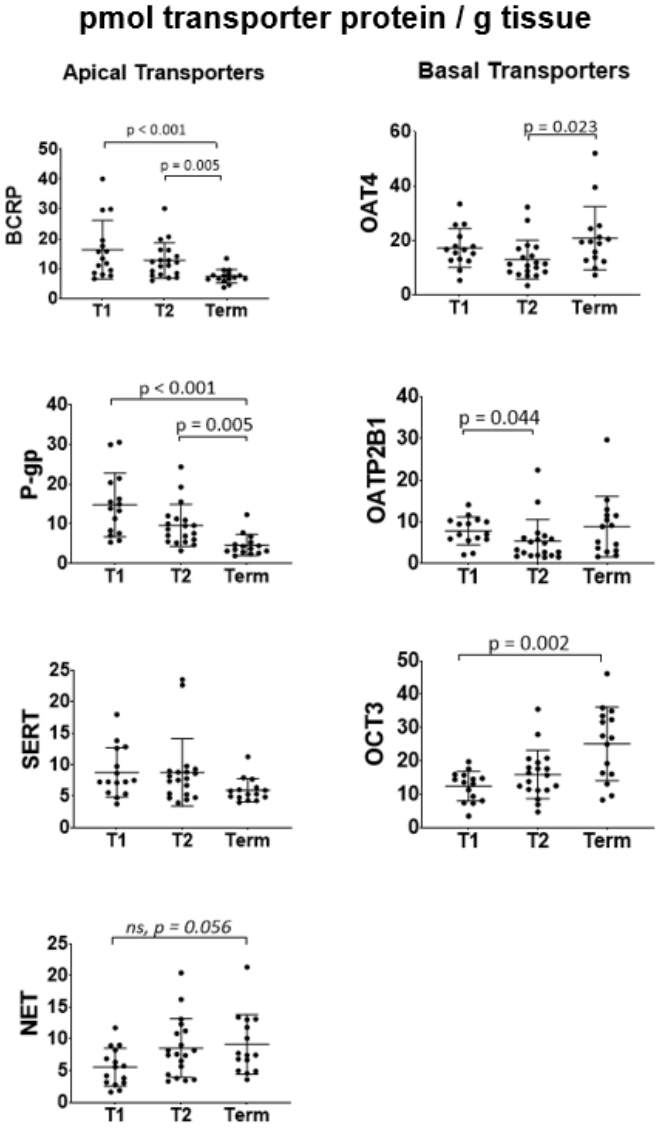

Figure 2.3. Protein abundance of apical and basal membrane transporters in human placentae of three gestational ages (pmol/g tissue). Abundance of BCRP was 55% lower at term than in T1 and 42% lower at term than in T2 ($p<0.05$). Abundance of P-gp was 69% lower at term than in T1 and 52% lower at term than in T2 ($p<0.05$). Abundance of OCT3 was 2-fold higher at Term than in T1. Abundance of OAT4 was 1.6-fold higher at term than in T2. Abundance of OATP2B1 was 32% lower in T2 than in T1. Neither SERT nor NET showed significant change in protein abundance with gestational age. Dots are measured values, lines are mean and standard deviations (T1, n=15; T2, n=19; Term, n=15); only significant differences (Kruskal-Wallis Test

with Dunn's multiple comparisons) are shown except for NET, where ns denotes marginally insignificant difference. T1 – 1st trimester, T2 – 2nd trimester.

2.4.4 *Transporters Abundance at Three Gestational Ages*

When abundances of all proteins across the three gestational age groups were compared, term placentae looked notably distinct from T1 and T2 (**Figure 2.4**). When relative transporter protein abundance was compared (**Figure 2.4**, pie charts), a decrease in apical membrane transporters (black bars: from 55% in T1 to 33% at term) and an increase in basal membrane transporters (grey bars: from 45% in T1 to 67% at term) were observed.

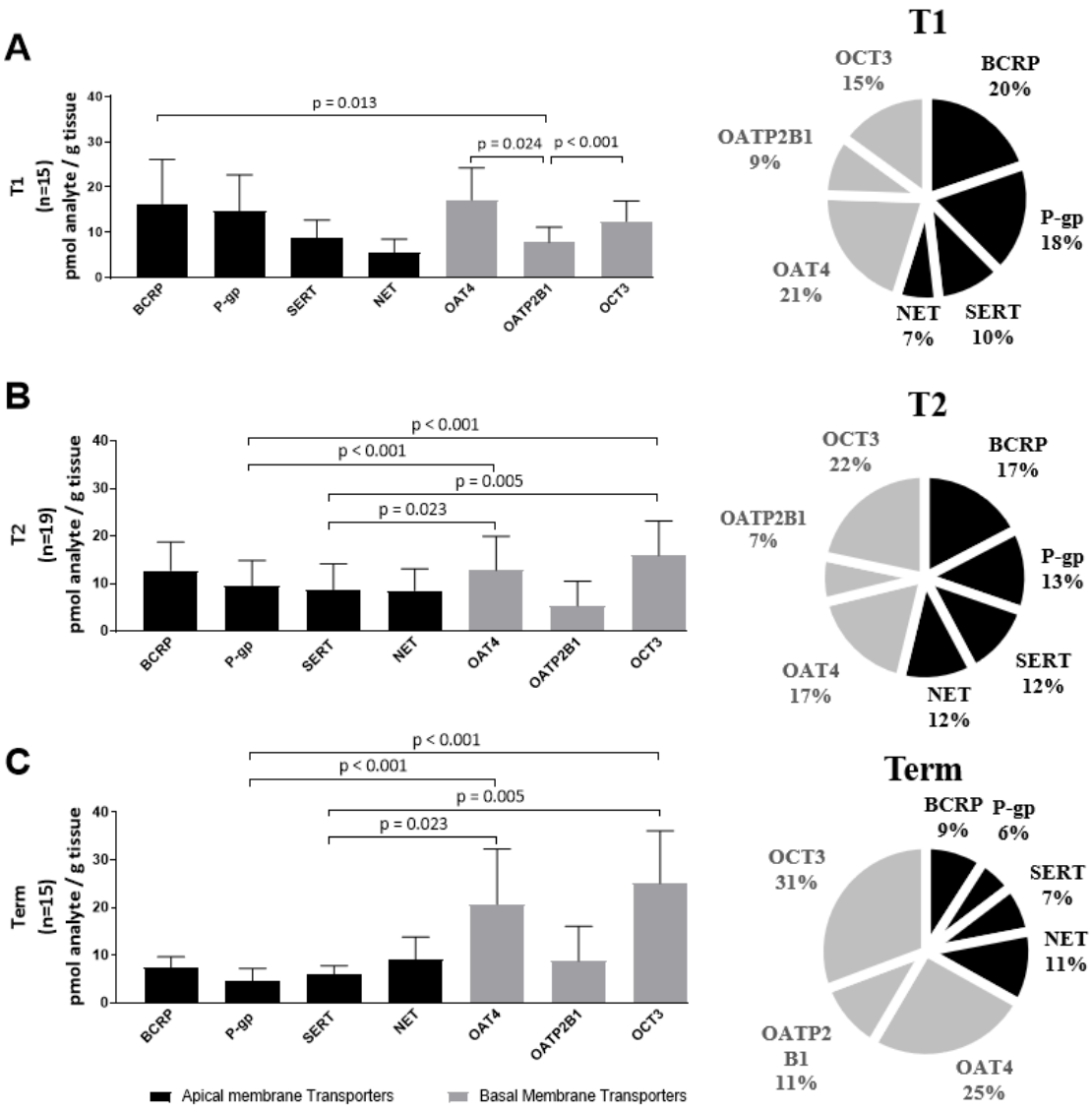

Figure 2.4. Protein abundance of transporters in human placentae per gram of tissue (A-C bar graphs) or as a percent of the total abundance of the quantified transporters (A-C pie charts) at three gestational ages. The data show the changes in pattern of expression as pregnancy proceeds. T1 and T2 placentae show similar pattern of transporter abundance while term placentae show a distinct pattern. The contribution of all basal membrane transporters increased from 45% and 46% in T1 and T2, respectively, to 67% at Term. Consequently, apical membrane transporter contribution decreased from 55% and 54% in T1 and T2, respectively, to 33% at Term. Data shown in bar graphs are means ± SD. Data were analyzed using the Kruskal-Wallis Test with Dunn's multiple comparisons. T1 – 1st trimester, T2 – 2nd trimester.

2.4.5 *Protein-Protein Correlations of Placental Transporters*

Multiple pairs of transporters showed a strong protein-protein correlation (Pearson correlation $R^2>0.5$ with $p<0.05$) (**Table 2.2, Figure 2.S5**). Strong correlations were observed between BCRP and P-gp ($R^2=0.78$), BCRP and SERT ($R^2=0.62$), P-gp and SERT ($R^2=0.63$), and OAT4 and OATP2B1 ($R^2=0.53$).

2.5 DISCUSSION

Although placental transporter abundance has been previously quantified by our group (Mathias et al., 2005) and others (Gil et al., 2005; Meyer zu Schwabedissen et al., 2006; Sun et al., 2006), these studies have used either Western Blotting or ELISA to quantify the transporter protein abundance or qPCR to quantify transporter mRNA expression (Nishimura & Naito, 2005). Western Blot is inherently semi-quantitative and cannot be used to compare the abundance of multiple transporters without the availability of protein standards. mRNA abundance does not always correspond to protein abundance and should not be used for PBPK modeling and simulation. To address the shortcomings of these previous studies, we incorporated several unique features in the study presented here. First, we utilized the state-of-the art targeted quantitative proteomics to quantify the abundance of multiple transporters, a method that does not depend on the availability of protein standards. These transporters were chosen based on previously published gene expression data (mRNA or protein) indicating that they are present in the human placenta (Mathias et al., 2005; Gil, Saura, Forestier, & Farinotti, 2005; Meyer zu Schwabedissen et al., 2006; Sun et al., 2006; Nishimura & Naito, 2005). Second, we quantified the abundance of transporters across multiple gestational ages from placentae obtained from uncomplicated pregnancies. Third, we extended the transporters quantified to those not previously studied (e.g., SERT, NET). Fourth, we utilized a greater number of placentae in each gestational age ($n>15$) than prior studies. Fifth, we determined if the abundance of the transporters in the placentae was sample-site dependent. Sixth, we corrected the inter-tissue variability in membrane isolation by utilizing enrichment of validated membrane markers, ALP and Na^+/K^+-ATPase.

We did not observe any differences when preparations were made on different days or sampled from different sites (**Figure 2.S2**). Lack of inter-day variability indicated our technical consistency in preparation methodology and lack of site-dependent variability implied homogeneous distribution of transporters throughout placenta. This homogenous distribution was reported previously in term placentae (Memon et al., 2014). Due to this lack of variability, we chose to prepare membrane fractions using tissue obtained from site 1 (**Figure 2.S2**) for all the placenta samples.

We observed a 3- to 4-fold enrichment of membrane markers in all the preparations. Membrane marker enrichment value was incorporated into the scaling strategy to control for the variability in membrane loss between preparations. ALP and Na^+/K^+-ATPase were chosen as highly abundant markers detectable in both homogenate and membrane fractions. Two separate markers were chosen due to possible differences in enrichment of apical or basal membranes. Overall, the fold-enrichment values for both markers were comparable for each gestational age, except for higher ALP enrichment values at term (**Table 2.1**). Both enrichment values were relatively low compared with those reported in the literature (separate isolation of apical and basal membranes) (Illsley, Wang, Gray, Sellers, & Jacobs, 1990; Jimenez, Henriquez, Llanos, & Riquelme, 2004; Kelley, Smith, & King, 1983). The reason for this difference is unknown but could be due to greater contamination from other membranes during our preparation. Nonetheless, the low enrichment values did not detract from our ability to quantify the most abundant and important xenobiotic transporters (i.e., P-gp, BCRP, and OCT3) though the abundances of some transporters were below limits of detection (i.e., MRP1-5, OATP1B1/3, MATE1, OCTN1/2, CNT2/3, BSEP, and NTCP) (**Figure 2.1, Table 2.S1**).

We found the most pronounced differences with gestational age in abundance of BCRP, P-gp and OCT3 while that of OAT4 and OATP2B1 proteins was less affected (**Figure 2.3)**. This differential gestational-age transporter abundance indicates that the observed changes are not an artifact of our method. The mechanistic basis of this differential effect remains to be elucidated. Teleologically, increased abundance of efflux transporters per gram of tissue could be a mechanism to protect the fetus from exposure to xenobiotics. In addition, these results are consistent with previous studies conducted by us and others on P-gp (Gil et al., 2005; Sun et al., 2006), BCRP (Meyer zu Schwabedissen et al., 2006) and OCT3 (N. Lee et al., 2013). More modest changes in protein abundance for OAT4 and OATP2B1 as well as the lack of significant changes in abundance of SERT and NET are described here for the first time. Additionally, the current findings agree with the previous conclusion that the placenta expresses BCRP at higher levels than the kidney and liver and show that placental P-gp protein abundance is similar to that in the liver (**Figure 2.S4**).

The impact of these transporter abundances on fetal distribution of drugs can now be predicted using PBPK modeling and simulation. To do so, the abundance of the transporters in the entire organ is needed. When scaled to the whole organ, a consistent gestational age-dependent increase in the abundance of all 7 proteins was observed (**Figure 2.S3 B**). This finding is due to the dramatic increase in placental weight (> hundred-fold) with gestation (**Eq 2.3**) in comparison to modest changes (2- to 3-fold) in protein abundance per gram of tissue. Hence, placental weight becomes the major determinant for the differences observed in the whole organ.

Our quantification results captured some elements of placentogenesis, a very dynamic and multifaceted process (Abduljalil et al., 2012; Burton & Fowden, 2015). The pattern of

placental transporter protein abundance was similar between T1 and T2 but less so between T1/T2 and term (**Figure 2.4**). Such observations can be explained by the T1 and T2 placentae being closer in gestational age than Term placentae (**Table 2.1**) and hence more similar in developmental processes. Additionally, induction of parturition-responsive genes can alter placental gene expression as the organ reaches term (Peng et al., 2011). Hence, at earlier gestational ages (T1 and T2), fetal drug exposure to transporter substrates may be more similar than at term.

The observed strong correlation between pairs of protein abundances (**Table 2.2, Figure 2.S5**) may indicate the involvement of common regulatory mechanisms (e.g., by the same nuclear receptor) or possibly protein-protein interactions as reported between OATP1B3 and OCT1 in human hepatocytes (Shoop, Ruggiero, Zhang, & Hagenbuch, 2015).

Our approach to transporter quantification has several limitations. We assumed that all measured transporter proteins are active and localized to the membrane indicated in Fig.1 rather than internalized or present in cells other than the syncytiotrophoblast layer (Joshi et al., 2016; Vahakangas & Myllynen, 2009). Since the enrichment values for both ALP and Na^+/K^+-ATPase were similar, misclassification of the membrane localization (apical vs. basal) will not have a large impact on the quantification of the transporters and eventual use of these values in IVIVE. Although methods are available to separate the apical from the basal membrane, such methods do not yield complete purification of each membrane (Jimenez et al., 2004). Therefore, we believe that our approach of using a membrane marker is superior to attempts to experimentally separate the apical from the basal membrane. The use of biotinylation assay can potentially address localization in *in vitro* systems (V. Kumar, Nguyen, Toth, Juhasz, & Unadkat, 2017), although such estimation in *ex vivo* tissue has not been evaluated. Further, in addition to

syncytiotrophoblast, some transporters (e.g., OCT3, BCRP) have been reported to be present on other placental cell types such as the endothelial cells (Joshi et al., 2016; Lee et al., 2018). Thus, our approach may lead to an overestimation of total transporter proteins at the plasma membrane of syncytiotrophoblast.

Collectively, these data can be used to populate a maternal-fetal PBPK model to predict fetal exposure to xenobiotic transporter substrates at various gestational ages. Failing to account for placental transporter abundance changes (e.g., P-gp) may lead to biased estimates of fetal exposure to transporter substrates and imprecision in fetal drug toxicity and efficacy for drugs where fetus is a therapeutic target (e.g., antenatal corticosteroids or HIV drugs). To predict fetal drug exposure, these data should be married with drug transport kinetics (i.e., K_m and V_{max}) determined *in vitro,* where the *in vitro* V_{max} can be extrapolated to that *in vivo* using the proteomics transporter expression data. Additionally, the transporter abundance can also help estimate the fraction transported (f_t), *in vivo*, by a given transporter. Estimate of f_t will also aid in prediction of placental drug-drug interactions that can modulate fetal drug exposure. This is especially important because when monitored from maternal plasma, perpetrator-driven inhibition of drug efflux (e.g., P-gp) can go undetected in maternal plasma while considerably modulating fetal drug exposure and therefore fetal toxicity or efficacy (Patilea-Vrana & Unadkat, 2016). Collectively, gestational age-dependent abundance of transporters in the placenta is valuable in predicting fetal drug exposure and therefore fetal efficacy and toxicity associated with drug administration during pregnancy (Zhang & Unadkat, 2017).

2.6 SUPPLEMENTARY INFORMATION

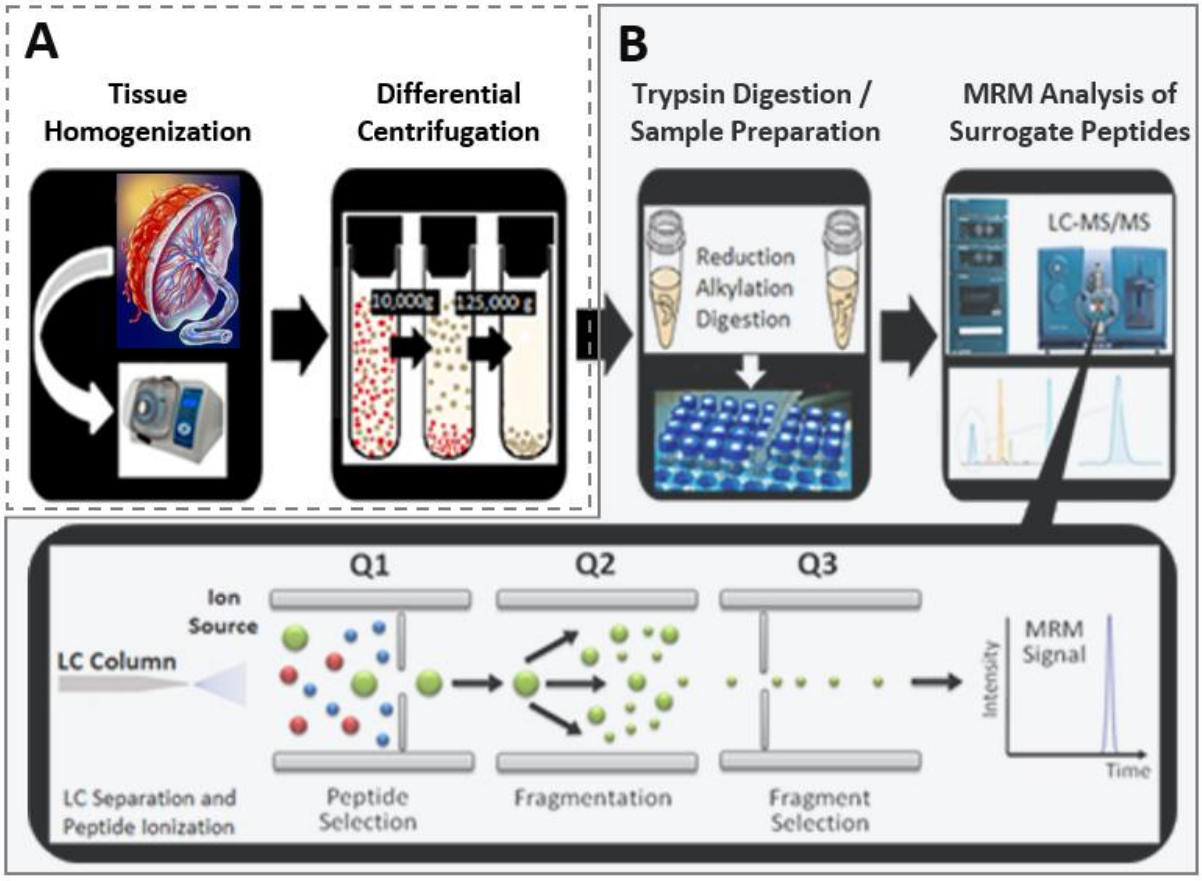

Figure 2.S1. Workflow for isolation of total membranes from the placental tissues (A) followed by quantitative targeted proteomics (B).

Table 2.S1. Surrogate peptides and LC-MS/MS parameters for quantification of placental drug transporters and membrane markers.

Protein Name	Surrogate Peptide	Peptide Type	Parent Ion	Fragment Ions	Declustering Potential	Collision energy
Apical Membrane Transporters						
BCRP	SSLLDVLAAR	Light	522.8	644.3, 757.4, 270.1	69	27, 25, 27
BCRP	SSLLDVLAA**R**	Heavy	527.8	654.3, 767.5, 270.1	69	28, 28, 27
P-gp	NTTGALTTR	Light	467.8	719.4, 618.4	70	23, 26
P-gp	NTTGALTT**R**	Heavy	472.8	729.4, 628.4	70	23, 26
SERT	LIITPGTFK	Light	495.3	227.18, 763.43, 549.3	80	27
SERT	LIITPGTF**K**	Heavy	499.3	227.2, 771.4, 557.3	80	27
NET	FTPAAEFYER	Light	615.8	814.4, 982.5, 885.4	80	30
NET	FTPAAEFYE**R**	Heavy	620.8	824.4, 992.5, 895.4	80	30
Alkaline Phosphatase	EAAEALGAAK	Light	465.8	201.1, 346.2, 530.3	80	24
Alkaline Phosphatase	EAAEALGAA**K**	Heavy	469.8	201.1, 354.2, 538.3	80	25
MATE1	GGPEATLEVR	Light	514.8	274.2, 457.8, 688.4	101	37, 25, 31
MATE1	GGPEATLEV**R**	Heavy	519.8	274.2, 457.8, 698.4		
MRP2	LTIIPQDPILFSGSLR	Light	885.8	1329.6, 989.6, 310.2	146	37, 57, 43
MRP2	LTIIPQDPILFSGSL**R**	Heavy	890.5	1339.6, 999.6, 310.3		
MRP3	ADGALTQEEK	Light	531.4	634.3, 747.4, 875.4	91	25
MRP3	ADGALTQEE**K**	Heavy	535.4	642.3, 755.4, 883.5		
MRP4	AEAAALTETAK	Light	538.4	875.4, 733.4, 201.0	76	25
MRP4	AEAAALTETA**K**	Heavy	542.4	883.4, 741.4, 201.0		
OCTN1	AFILDLFR	Light	497.8	776.5, 663.4, 550.3	67	27
OCTN1	AFILDLF**R**	Heavy	502.8	786.5,673.4, 560.3		
OCTN2	TWNIR	Light	345.2	588.3, 402.2	56	21

OCTN2	TWNI**R**	Heavy	350.2	598.3, 412.2		
			Basal Membrane Transporters			
OAT4	ATTALLLSFLGR	Light	636.9	579.3, 692.4, 805.5	90	25, 31, 33
OAT4	ATTALLLSFLG**R**	Heavy	636.9	589.3, 702.4, 815.5	96	25, 31, 33
OATP2B1	VLAVTDSPAR	Light	514.9	816.4, 646.3, 745.4	71	25, 25, 27
OATP2B1	VLAVTDSPA**R**	Heavy	519.8	826.4, 656.3, 755.4	71	25, 25, 27
OCT3	GIALPETVDDVEK	Light	693.4	242.2, 1031.5, 516.3	80	30
OCT3	GIALPETVDDVE**K**	Heavy	697.4	242.2, 1039.5, 520.3	80	30
Na^+/K^+-ATPase	AAVPDAVGK	Light	414.2	685.4, 586.3	61	19
Na^+/K^+-ATPase	AAVPDAVG**K**	Heavy	418.2	693.4, 594.3	61	19
MRP1	TPSGNLVNR	Light	479.3	759.4, 672.4, 428.8	81	29, 31, 27
MRP1	TPSGNLVN**R**	Heavy	484.3	769.4, 682.4, 428.8		
MRP5	SLSEASVAVDR	Light	567.3	717.4, 943.5	80	23
MRP5	SLSEASVAVD**R**	Heavy	572.3	727.4, 943.5		28, 29
OATP1B1	NVTGFFQSFK	Light	587.8	961.5, 860.4	60	26
OATP1B1	NVTGFFQSF**K**	Heavy	591.8	969.5, 868.4		
OATP1B3	NVTGFFQSLK	Light	570.8	927.49, 826.5, 622.3	60	26
OATP1B3	NVTGFFQSL**K**	Heavy	574.8	935.51, 834.5, 630.3		
			Transporters with Unknown Localization			
BSEP	STALQLIQR	Light	515.3	657.4, 529.3, 770.5	68	22
BSEP	STALQLIQ**R**	Heavy	520.3	667.4, 539.4, 780.5		
CNT2	LAYPEVEESK	Light	582.8	817.4, 980.5, 720.3	N/A	N/A
CNT2	LAYPEVEES**K**	Heavy	585.8	823.4, 986.5, 726.3	N/A	N/A
CNT3	DHFFAFK	Light	456.2	659.4, 365.2, 512.3	N/A	N/A
CNT3	DHFFAF**K**	Heavy	461.2	669.4, 375.2, 522.3	N/A	N/A
NTCP	GIYDGDLK	Light	440.7	710.3, 547.3	58	19
NTCP	GIYDGDL**K**	Heavy	444.7	718.4, 555.3		

Note: LLOQ for most quantified transporters was 3.1 fmol on-column (per 5 µL injection volume). LLOQ for OATP2B1 was 2.4 fmol on-column. R and K in bold in heavy peptides represent stable-labeled (^{13}C and ^{15}N) residues.

Table 2.S2. LC conditions for surrogate peptide quantification

Column	UPLC column (ACQUITY UPLC® HSS T3 column 1.8 µm, 2.1 mm x 100 mm, Waters)
Guard Column	Security Guard column (C18, 4 mm x 2.0 mm, Phenomenex)
Run Time	26 min
Injection Volume	5 µL
Column Oven Temperature	25°C
Autosampler Temperature	8°C

Gradient Table

Time (min)	Flow Rate (ml/min)	%A	%B	Curve
Initial	0.3	97	3	Initial
4	0.3	97	3	6
8	0.3	87	13	6
18	0.3	75	25	6
21	0.3	66.7	33.3	6
22	0.3	50	50	6
23	0.3	20	80	6
24	0.3	20	80	6
24.5	0.3	97	3	6
26	0.3	97	3	6

A = 0.1% formic acid in water; B = 0.1% formic acid in acetonitrile

Table 2.S3. Placentae donor demographics

Demographic Characteristic	n
Sex of the Fetus	
Male	15
Female	10
Not Available	24
Ethnicity/Race	
White	8
White/Native American	2
Hispanic	7
Asian	1
Black/African-American	3
Biracial	3
Not Available	25
Smoking history	
Yes	7
No	5
Not Available	37
Marijuana use	
Yes	9
No	0
Not Available	40
Yes	7
No	5
Not Available	37
Other medication use	
Prenatal Vitamins	3
Adderall, Albuterol, calcium carbonate, Divalproex, ferrous sulfate, Omeprazole, Propylthiouracil, Sumatriptan, Varex, Xanax , Zofran, Zyrtec	1 woman per medication
Not Available	34

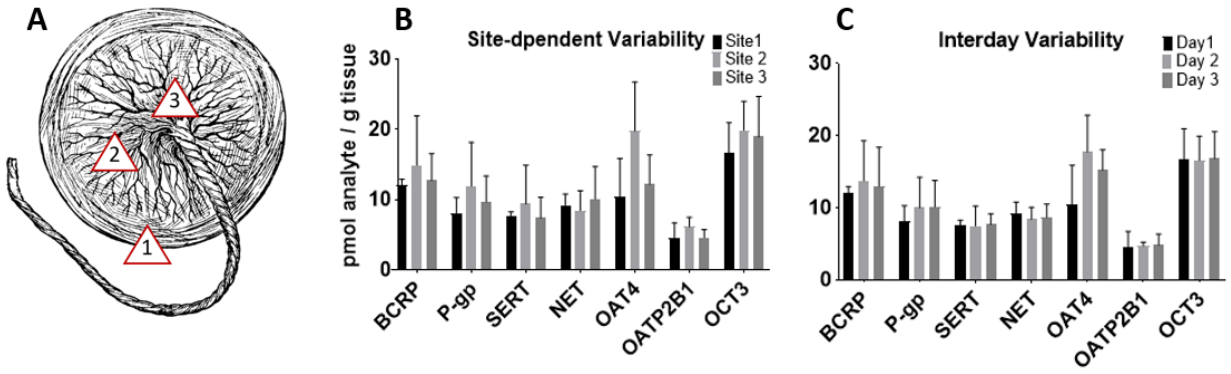

Figure 2.S2. Placental sites (A) used in the analyses of site-dependent (B) and inter-day variability (C) of transporter abundance in three T2 placentae. Protein abundance was independent of the site of of sampling or of the day of analyses when sampled from site 1 (C). Each bar represents mean ± SD of data from 3 placentae (each trypsin-digested twice). Placental ID: H26938 (152 gestational days), H27003 (137 gestational days) and H27108 (115 gestational days). Kruskal-Wallis test with Dunn's multiple comparisons was used for statistical analysis.

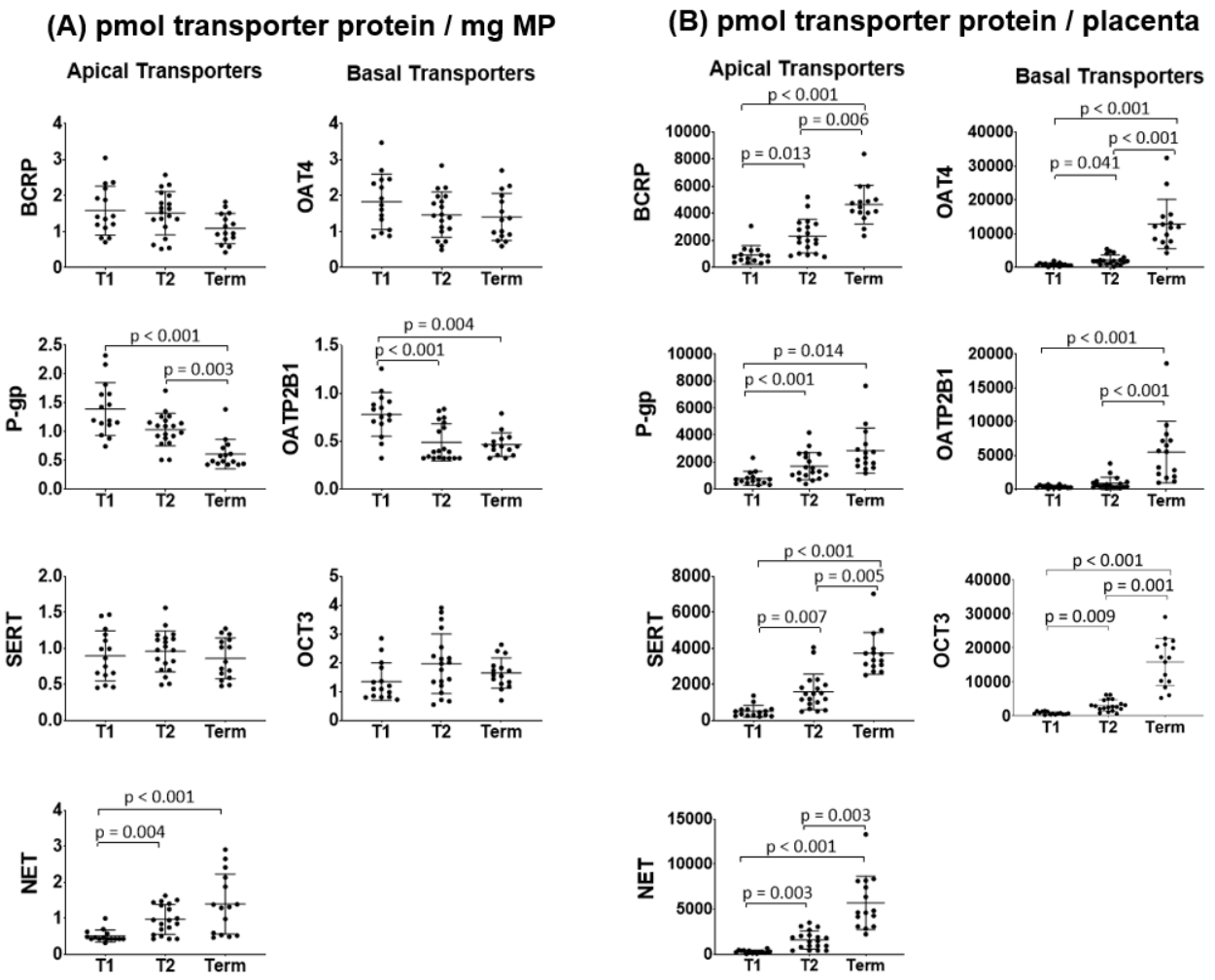

Figure 2.S3. Protein abundance of apical and basal membrane transporters in human placentae of three gestational ages. Panel (A) represents values expressed per mg of MP. Abundance of P-gp was 56% lower at term than in T1 and 41% lower at term than in T2. Abundance of NET was 1.9-fold higher in T2 than in T1 and 2.8-fold higher at term than in T1. Abundance of OATP2B1 was 37% lower at T2 than in T1 and 40% lower at term than in T1. Five measurements for OATP2B1 in T2 group were below LLOQ and were assigned the conservative value of LLOQ (2.3 fmol on column). Gestational age did not affect BCRP, SERT, OAT4 and OCT3 protein abundance. Panel (B) represents values expressed per placenta. All the transporters showed significant increase with gestational age. Dots are observed values, lines are mean and standard deviations (T1 n=15; T2 n=19; Term n=15); Only significant differences are shown; Kruskal-Wallis Test with Dunn's multiple comparisons, $p<0.05$.

Table 2.S4. Protein abundance of apical and basal membrane transporters in human placentae of three gestational ages. Values are given as mean ± SD and expressed in pmol/g tissue (N=49). T1 – 1st trimester, T2 – 2nd trimester.

	T1 (*n=15*)		T2 (*n=19*)		Term (*n=15*)	
Transporter	Protein Abundance	%CV	Protein Abundance	%CV	Protein Abundance	%CV
Apical						
BCRP	16.3 ± 9.79	60.1	12.8 ± 5.97	46.6	7.41 ± 2.28	30.8
P-gp	14.7 ± 8	54.4	9.57 ± 5.3	55.4	4.57 ± 2.67	58.4
SERT	8.78 ± 3.93	44.8	8.78 ± 5.36	61.0	5.95 ± 1.86	31.3
NET	5.52 ± 2.99	54.2	8.55 ± 4.61	53.9	9.12 ± 4.72	51.8
Basal						
OAT4	17.1 ± 7.11	41.6	12.8 ± 7.15	55.9	20.7 ± 11.6	56.0
OATP2B1	7.82 ± 3.34	42.7	5.31 ± 5.21	98.1	8.83 ± 7.25	82.1
OCT3	12.4 ± 4.47	36.0	16 ± 7.28	45.5	25.1 ± 11	43.8

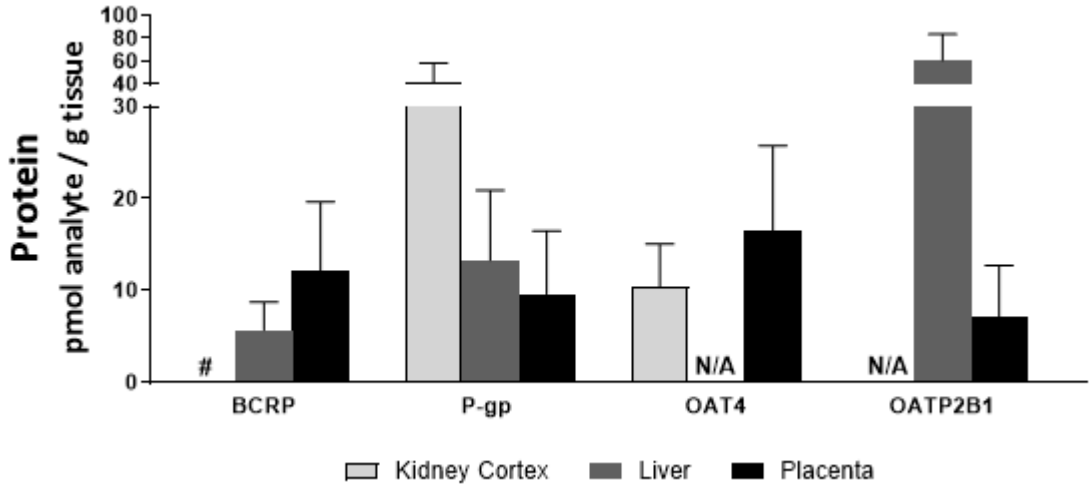

Figure 2.S4. Comparison of transporter protein abundance in human placenta, kidney and liver as measured by quantitative targeted proteomics. Placental protein abundance data are from the current study and represent pooled data across the three gestational age groups; liver data (Prasad et al., 2014; L. Wang et al., 2016); kidney data (Prasad, Johnson, et al., 2016). Data comparing abundance of SERT, NET and OCT3 are not shown as the corresponding data in the liver and kidney cortex are not available. N/A - data not available; # - below LLOQ.

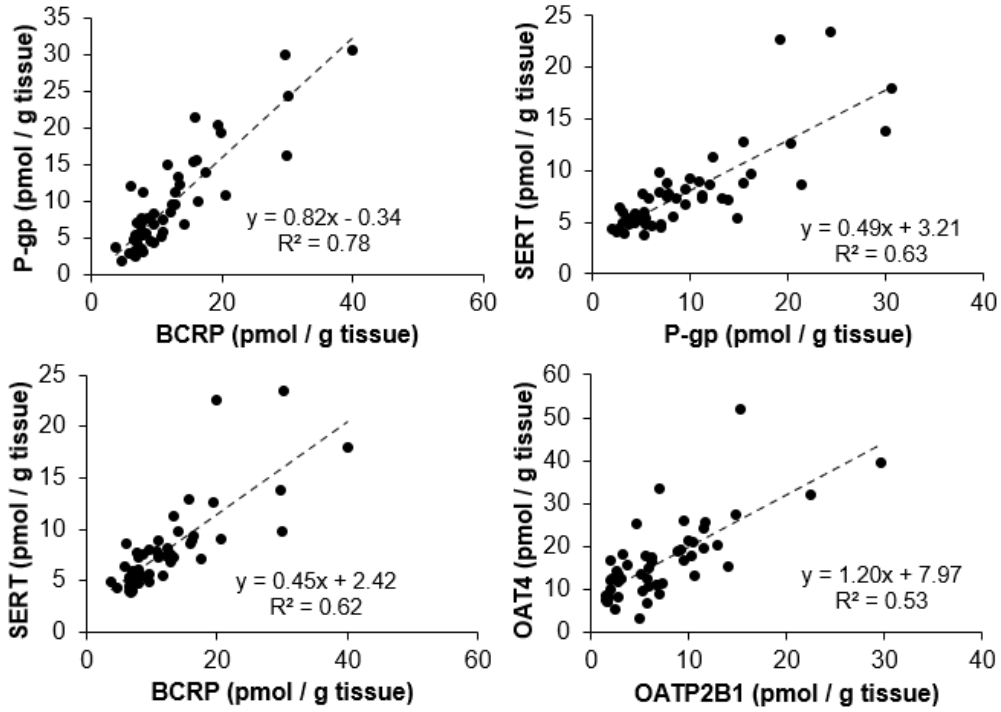

Figure 2.S5. Protein-protein correlation of placental transporter abundance (N=49). Correlations with Pearson correlation of R^2>0.5.

2.7 ABBREVIATIONS USED

%CV: percent coefficient of variation; ACOG: The American College of Obstetricians and Gynecologists; ALP: Alkaline Phosphatase; BCA: bicinchoninic acid; BCRP: breast cancer resistance protein; $CL_{invitro}$: *In Vitro* clearance; CL_{invivo}: *In Vivo* clearance; DDI: drug-drug interaction; DHEA-S: dehydroepiandrosterone; HIV; ELISA: Enzyme Linked Immunosorbent Assay; F_t: fraction transported; GA: gestational age; GW: gestational week; HEPES: N-2-hydroxyethylpiperazine-N'-2-ethanesulfonic acid; HIV: Human Immunodeficiency Virus; HPLC: high-performance liquid chromatography; IVIVE: in vitro to in vivo extrapolation; K_m: Michaelis-Menten constant; LC-MS/MS: liquid chromatography tandem mass spectrometry; LLOQ: lower limit of quantification; MP: maternal plasma; mRNA: messenger ribonucleic acid; Na^+/K^+-ATPase : sodium/potassium-ATPase; NET: norepinephrine transporter; OAT4: Organic anion transporter 4; OATP2B1: organic anion-transporting polypeptide; OCT3: organic cation transporter 3; m-f PBPK model: maternal-fetal physiologically-based pharmacokinetic model; P-gp: P-glycoprotein; PK: pharmacokinetics; SD: standard deviation; SERT: serotonin transporter; T1: 1^{st} trimester, T2: 2^{nd} trimester; UPLC: ultra-performance liquid chromatography; UV: umbilical vein; UWBDRL: University of Washington Birth Defect Research Laboratory; V_{max}: maximum velocity of reaction.

Chapter 3. SUCCESSFUL PREDICTION OF HUMAN FETAL EXPOSURE TO P-GP DRUGS USING THE PROTEOMICS-INFORMED RELATIVE EXPRESSION FACTOR APPROACH AND PBPK MODELING AND SIMULATION

3.1 ABSTRACT

Many women take drugs during their pregnancy to treat a variety of clinical conditions. To optimize drug efficacy and reduce fetal toxicity, it is important to determine or predict fetal drug exposure throughout pregnancy. Previously, we developed and verified a maternal-fetal physiologically based pharmacokinetic (m-f PBPK) model to predict fetal $K_{p,uu}$ (unbound fetal plasma AUC/unbound maternal plasma AUC) of drugs that passively cross the placenta. Here, we used *in vitro* transport studies in Transwell® systems, in combination with our m-f PBPK model, to predict fetal $K_{p,uu}$ of drugs that are effluxed by placental P-glycoprotein (P-gp). The probe substrates were dexamethasone, betamethasone, darunavir and lopinavir. Using Transwell® systems, we determined the efflux ratio (ER) of these drugs in hMDR1-MDCK$^{cP\text{-}gpKO}$ cells where human P-gp was overexpressed and the endogenous P-gp was knocked-out. Then, using the proteomics-informed efflux ratio-relative expressive factor (ER-REF) approach, we predicted the fetal $K_{p,uu}$ of these drugs at term. Finally, to verify our predictions, we compared predicted fetal $K_{p,uu}$ with the observed *in vivo* fetal $K_{p,uu}$ at term. The latter was estimated using our m-f PBPK model and published UV/MP, which is the fetal umbilical vein normalized for maternal plasma drug concentrations obtained at term). Fetal $K_{p,uu}$ predictions for dexamethasone (0.63), betamethasone (0.59), darunavir (0.17) and lopinavir (0.08) were successful as they fell within the 90% confidence interval ($CI_{90\%}$) of the corresponding *in vivo*

fetal $K_{p,uu}$ (0.30 – 0.66, 0.29 – 0.71, 0.11 – 0.22, 0.04 – 0.19, respectively). This is the first demonstration of successful prediction of fetal $K_{p,uu}$ of P-gp drug substrates from *in vitro* studies.

3.2 INTRODUCTION

More than half of all pregnant women take drugs (medication) throughout pregnancy and about 25% of pregnant women take drugs in the first trimester (Scaffidi et al., 2017). Drugs are administered either to treat the mother for various clinical conditions (e.g., depression, epilepsy, gestational diabetes) or to treat her fetus (e.g., to prevent poor lung development in case of preterm delivery or to prevent vertical transmission of HIV) (Sheffield et al., 2014). Despite the high frequency of drug use in pregnancy, little is known about the drug benefits and risks for the fetus, which are related to fetal drug exposure after maternal drug administration. Fetal drug exposure (defined as the fetal area under drug plasma concentration-time profile, AUC) is determined by maternal drug exposure, placental transport and metabolism, and fetal drug elimination (Zhang et al., 2017). The extent of fetal drug exposure can be evaluated by $K_{p,uu}$, the ratio of fetal-to-maternal unbound plasma AUCs after single or multiple dose drug administration or the corresponding average steady-state plasma concentrations (C_{ss}) after multiple dose administration (**Eq. 3.1**, where $f_{u,f}$ and $f_{u,m}$ are the fractions of unbound drug in fetal or maternal plasma, respectively).

$$K_{p,uu} = \frac{f_{u,f} \cdot AUC_f}{f_{u,m} \cdot AUC_m} = \frac{f_{u,f} \cdot C_{ss,f}}{f_{u,m} \cdot C_{ss,m}} \quad (3.1)$$

In the absence of placental transport, fetal $K_{p,uu}$ is unity (i.e., drugs passively diffuse across the placenta from the mother to the fetus, yielding equal maternal and fetal unbound plasma AUCs). When placental drug efflux by transporters abundant in the human placenta (e.g., by P-glycoprotein (P-gp) (Anoshchenko et al., 2020; Joshi et al., 2016; Mathias et al., 2005)) is present, $K_{p,uu}$ will be less than unity. Such placental drug efflux can modulate fetal exposure to

drugs and, therefore, compromise efficacy if the fetus is the therapeutic target or reduce potential fetal toxicity.

In order to determine fetal $K_{p,uu}$ of a drug at any gestational age, measurement of fetal and maternal drug plasma concentrations is necessary. However, except at term, for ethical and logistical reasons, it is impossible to measure fetal drug concentrations via the umbilical vein. Various *in vitro* systems have attempted to mimic the syncytiotrophoblast (SYT) placental barrier that could aid in $K_{p,uu}$ estimation (Arumugasaamy et al., 2020), but most of them have deficiencies. For example, cell systems (e.g., BeWo, JAR, Jeg-3 cell monolayers) fail to recapitulate the *in vivo* complexity of SYT layer, perfused human placenta experiments are laborious, and microphysiological systems are at very early stages of development. Due to the limitations of the aforementioned systems and the lack of clinical data at earlier gestational ages, an alternative is to **predict**, as opposed to **measure**, fetal $K_{p,uu}$. Such predictions can be made and verified at term using physiologically-based pharmacokinetic (PBPK) modeling and simulation.

We have previously developed and verified a maternal-fetal PBPK (m-f PBPK) model capable of predicting maternal-fetal exposure to drugs that are metabolized by various CYP enzymes (Ke, Nallani, Zhao, Rostami-Hodjegan, & Unadkat, 2012, 2014) and cross the placenta by passive diffusion (Zhang et al., 2017; Zhang & Unadkat, 2017). However, many drugs administered to pregnant women are substrates of efflux transporters that are highly expressed in the placenta such as P-glycoprotein (P-gp) and Breast Cancer Resistance Protein (BCRP) (Anoshchenko et al., 2020; Mathias et al., 2005). Both serve to reduce fetal exposure to drugs such as corticosteroids (Petersen, Nation, Ashley, & McBride, 1980; Tsuei et al., 1980), HIV protease inhibitors (Colbers, Greupink, Litjens, Burger, & Russel, 2016; Fauchet et al., 2015) or

anti-cancer drugs (e.g., imatinib) (Russell, Carpenter, Akhtar, Lagattuta, & Egorin, 2007). Therefore, to make our m-f PBPK model more comprehensive, we combined it with the efflux ratio-relative expression factor approach (ER-REF) to predict fetal $K_{p,uu}$ of drugs that are actively transported by the placenta. The ER-REF approach to predict $K_{p,uu}$ has been described previously to predict brain distribution of transporter substrates in humans and preclinical species (Storelli, Anoshchenko, et al., 2021; Trapa et al., 2019; Uchida et al., 2011; Uchida, Wakayama, et al., 2014). It relies on measurement of: 1) transport clearance of the drugs (i.e., via the efflux ratio, ER) in transporter-overexpressing cell lines (e.g., Transwell®) and 2) transporter abundance in both *in vivo* tissue (the placenta) and transporter-overexpressing cell lines using quantitative targeted proteomics to obtain a REF (see, **Figure 3.1** for workflow).

Using this efflux ratio-relative expression factor approach (ER-REF), combined with our m-f PBPK model, we predicted the fetal $K_{p,uu}$, of four model P-gp substrate drugs, namely two antenatal corticosteroids (ACS), dexamethasone (DEX) and betamethasone (BET), and two HIV protease inhibitors (PIs), darunavir (DRV) and lopinavir (LPV). Then, to verify our $K_{p,uu}$ predictions, we compared these predictions with the corresponding estimated *in vivo* fetal $K_{p,uu}$ of these drugs. The latter was estimated from m-f PBPK modeling of the observed maternal and fetal (umbilical vein) plasma concentrations of these drugs obtained at term or close to term from published maternal-fetal dyad data (**Figure 3.1**).

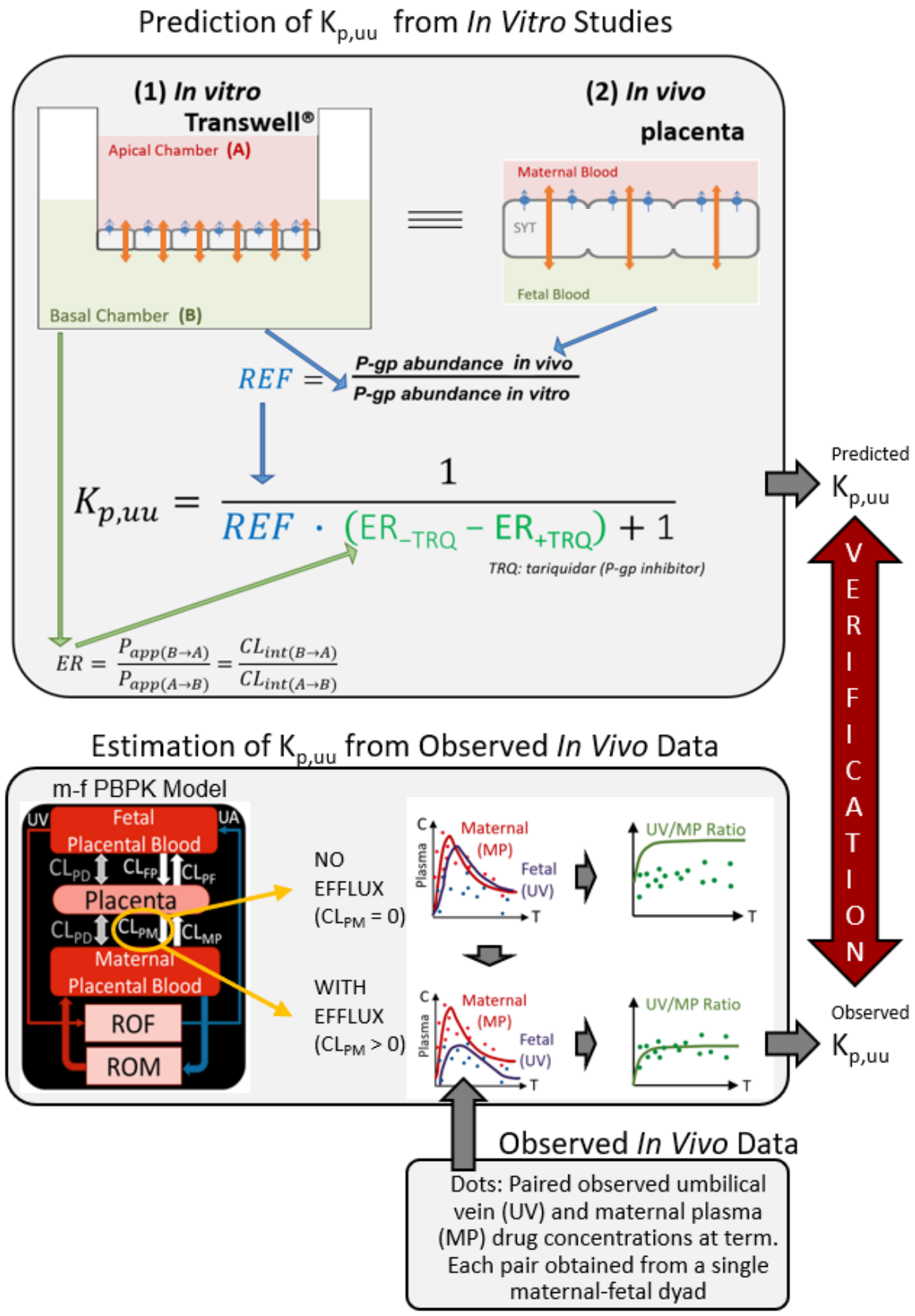
Prediction of $K_{p,uu}$ from *In Vitro* Studies
(1) *In vitro*
Transwell®
Apical Chamber (A)
Basal Chamber (B)
(2) *In vivo*
placenta
Maternal Blood
SYT
Fetal Blood
$REF = \frac{\text{P-gp abundance in vivo}}{\text{P-gp abundance in vitro}}$
$K_{p,uu} = \frac{1}{REF \cdot (ER_{-TRQ} - ER_{+TRQ}) + 1}$
TRQ: tariquidar (P-gp inhibitor)
$ER = \frac{P_{app(B\to A)}}{P_{app(A\to B)}} = \frac{CL_{int(B\to A)}}{CL_{int(A\to B)}}$
Predicted
$K_{p,uu}$
VERIFICATION
Estimation of $K_{p,uu}$ from Observed *In Vivo* Data
m-f PBPK Model
UV
Fetal
Placental Blood
UA
CL_{PD}
CL_{FP}
CL_{PF}
Placenta
CL_{PD}
CL_{PM}
CL_{MP}
Maternal
Placental Blood
ROF
ROM
NO
EFFLUX
(CL_{PM} = 0)
WITH
EFFLUX
(CL_{PM} > 0)
C
Plasma
Maternal
(MP)
Fetal
(UV)
T
UV/MP Ratio
T
Observed
$K_{p,uu}$
Observed *In Vivo* Data
Dots: Paired observed umbilical vein (UV) and maternal plasma (MP) drug concentrations at term. Each pair obtained from a single maternal-fetal dyad

Figure 3.1. Workflow for the prediction *in vivo* fetal $K_{p,uu}$ using the ER-REF approach and subsequent verification of the predicted $K_{p,uu}$ by comparison with the observed *in vivo* $K_{p,uu}$ estimated by m-f PBPK modeling and simulation. Top panel: Efflux transporter-overexpressing cell monolayer (e.g., hMDR1-MDCK$^{cP\text{-}gp\ KO}$) in the *in vitro* Transwell® system (indicated by 1 in the top panel) mimics the placental syncytiotrophoblast (SYT) layer *in vivo* (indicated by 2 in the top panel). That is, the apical and basal chambers in the *in vitro* system, respectively, mimic the *in vivo* maternal and fetal blood compartments allowing the use of the ER-REF approach to predict the *in vivo* fetal $K_{p,uu}$. For verification, this predicted $K_{p,uu}$ was compared with the observed *in vivo* $K_{p,uu}$ estimated by m-f PBPK modeling and simulation as depicted in the bottom panel. Orange arrows indicate bidirectional intrinsic passive diffusion clearance. Blue circles and blue arrows respectively represent apically localized efflux transporters and the direction of drug efflux/ intrinsic placental-maternal clearance (CL_{PM}, specified as $CL_{int,P\text{-}gp,placenta}$ in the text). ER-REF is efflux ratio-relative expression factor approach. $P_{app(B\rightarrow A)}$ and $P_{app(A\rightarrow B)}$ are apparent permeabilities and $CL_{int(B\rightarrow A)}$ and $CL_{int(A\rightarrow B)}$ are apparent intrinsic clearances of a drug in the indicated directions. **Bottom panel**: Estimation of $K_{p,uu}$ from the observed *in vivo* data with and without intrinsic active placental-maternal efflux clearance (CL_{PM}) incorporated into the model. For drugs that are effluxed by placental P-gp (i.e., $CL_{PM}>0$), CL_{PM} was adjusted until the m-f PBPK model-predicted UV/MP values best described the observed UV/MP values (dots). Then, based on **Eq 3.1**, the *in vivo* $K_{p,uu}$ was estimated. CL_{PD}: intrinsic passive diffusion clearance; CL_{FP}, CL_{PF}, CL_{MP}: intrinsic active clearance for fetal-placental, placental-fetal and maternal-placental compartments, respectively (assume 0 for drugs transported only by placental-maternal efflux transporters (CL_{PM})); ROM: rest of the maternal compartments, ROF: rest of the fetal compartments, UV: umbilical vein; UA: umbilical artery.

3.3 MATERIALS AND METHODS

3.3.1 *Chemicals and Reagents*

Dexamethasone (DEX), betamethasone (BET), and Lucifer Yellow CH dithiothreitol (LY) were purchased from Toronto Research Chemicals (Toronto, Canada). Quinidine (QND), prazosin hydrochloride (PZS), 12-well Transwell® plates with polyester membrane inserts (12 mm 0.4 µm), 96-well white flat bottom polystyrene microplates, HEPES [4-(2-hydroxyethyl)-1-piperazineethanesulfonic acid], ProteoExtract® Subcellular Proteome Extraction Buffer II (EBII buffer), tariquidar (TRQ), Ko143, ammonium bicarbonate, sodium dodecyl sulfate (SDS), and N-desmethyl loperamide were obtained from Sigma-Aldrich (St. Louis, MO, USA). Dulbecco's Modified Eagle's medium (DMEM) with 4.5 g/L glucose (high glucose) or 1 g/L glucose (low glucose), L-glutamine and sodium pyruvate, heat-inactivated fetal bovine serum (FBS), penicillin (10,000 U/mL)–streptomycin (10,000 g/mL), 0.25% trypsin –EDTA (ethylenediaminetetraacetic acid), DPBS, Glutamax™, geneticin, Hank's balanced salt solution (HBSS) with $CaCl_2$ and $MgCl_2$, Trypan Blue, Hygromycin B (50 mg/mL), human serum albumin, iodoacetamide, acetonitrile, formic acid, methanol, and chloroform were purchased from Thermo Fisher Scientific (Waltham, MA).

3.3.2 *Cell Culture for Transwell Transport Assays*

Human P-gp overexpressing MDCKII cells, where the endogenous canine P-gp was knocked-out (hMDR1-MDCK$^{cP\text{-}gpKO}$), were generously provided by Dr. Per Artursson, Uppsala University. hMDR1-MDCK$^{cP\text{-}gpKO}$ cells were cultured in high-glucose DMEM containing 10% FBS, 1% penicillin (10,000 U/mL)/streptomycin (10,000 g/mL), 2 mM Glutamax™ and 375 µg/mL Hygromycin B. The human BCRP-overexpressing MDCKII (hABCG2-MDCKII) cells,

generously provided by Dr. Qingcheng Mao, University of Washington, were cultured in low-glucose DMEM that contained 10% FBS, 1% penicillin (10,000 U/mL)/streptomycin (10,000 g/mL) and 500 µg/mL geneticin. Cells were grown at 37°C, 5% CO_2, and 95% humidity, harvested using trypsin and subcultured twice-a-week.

3.3.3 *Transwell Transport Assay*

The efflux ratios (ER) of DEX (2 µM), BET (2 µM), DRV (2 µM), LPV (0.4 µM [^{3}H]LPV + 0.6 µM LPV) were determined in four independent experiments conducted in triplicate in hMDR1-MDCK$^{cP\text{-}gpKO}$ cells. ER of DEX (2 µM) and BET (2 µM) were also determined in four independent experiments conducted in triplicate in hABCG2-MDCKII cells. Quinidine (QND, 3 µM), prazosin (PZS, 3 µM) and lucifer yellow (LY) were included in the above determinations as positive controls for P-gp activity, BCRP activity and integrity of tight junction, respectively. ER was estimated by conducting each experiment in two directions: A→B where the donor was the apical (A) compartment (volume = 0.5 mL) and the receiver (B) was the basal compartment (volume = 1 mL) or vice versa, B→A.

Briefly, on day 0, 6 x 10^5 cells/well were plated on apical side of the 12-well Transwell® polyester insert. Cells were grown in plates for 4 days prior to experiment with the change of medium on days 2 and 3. On day 4, cells were washed 3 times with 37°C transport buffer (10 mM HEPES in HBSS at pH 7.4) and incubated in an orbital shaker at 120 rpm. The donor solutions ± tariquidar (P-gp inhibitor at 5 µM) or ± Ko143 (BCRP inhibitor at 5 µM) were prepared in transport buffer containing the drug and 50 µM paracellular transport marker lucifer yellow (LY). The receiver solution contained transport buffer ± tariquidar (5 µM) or ± Ko143 (5 µM). Transport assay was initiated by adding the donor solution to the donor compartment and performed at 37°C with 120 rpm shaking. Donor compartments were sampled (10 µL) at time 0

and at the end of the transport experiment. Receiver compartments were sampled (100 µL) at 15, 30, 45 and 60 min (DEX, BET); 7, 15, 30, 45 min (DRV); 60, 120, 180 and 240 min (LPV) and replenished with the incubation medium. At the end of each experiment, cells were washed 3 times with ice-cold transport buffer and lysed for drug or marker assay, total protein content (BCA) and proteomic analysis.

3.3.4 *Quantification of Drugs and Markers*

[^{3}H]LPV was quantified using scintillation counting (PerkinElmer, Waltham, MA). DEX, BET, DRV, QND and PZS were quantified using liquid chromatography-tandem mass spectrometry (LC-MS/MS) on AB Sciex Triple Quad 6500 (SCIEX, Farmingham, MA) instrument coupled with Waters Acquity UPLC system (Waters, Hertfordshire, UK). Briefly, 100 µL of acetonitrile containing 0.5 nM N-desmethyl loperamide as internal standard (IS) was added to 50 µL of donor/receiver samples in 96-well plates. Samples were centrifuged at 3220 x g at 4°C for 15 min and the supernatant was injected into the LC-MS/MS (see **Tables 3.S1 and 3.S2** for details on LC-MS/MS method and chromatographic conditions). All drug concentrations (diluted where necessary) fell within the linear range of peak area ratios with a signal-to-noise ratio of >5. The permeability of the paracellular marker lucifer yellow (LY) was analyzed on Synergy HTX fluorescence reader (Biotek, Winooski, VT, USA) with excitation and emission wavelengths of 480 nm and 530 nm, respectively. The linearity of LC-MS/MS signal (in peak area units) and fluorescence reader signal (in relative fluorescent units) within the quantified work range, were confirmed by preliminary experiments (data not shown).

3.3.5 *Determination of in vitro Efflux Ratios (ER)*

ER in the absence and presence of P-gp or BCRP inhibitors were determined in the *in vitro* Transwell® assay (**Eq 3.2**),

$$ER = \frac{P_{app(B\rightarrow A)}}{P_{app(A\rightarrow B)}} = \frac{CL_{int(B\rightarrow A)}}{CL_{int(A\rightarrow B)}} = \frac{cA_{A(R)} \cdot AUC_{A(D)}}{AUC_{B(D)} \cdot cA_{B(R)}} \qquad (3.2)$$

where $P_{app(B\rightarrow A)}$ and $P_{app(A\rightarrow B)}$ are apparent permeabilities and since the surface area is identical in both direction, these are equivalent to $CL_{int(B\rightarrow A)}$ and $CL_{int(A\rightarrow B)}$, the apparent intrinsic clearances of a drug in indicated directions; $cA_{A(R)}$ and $cA_{B(R)}$ are cumulative amounts of drug in corresponding receiver compartment; $AUC_{A(D)}$ and $AUC_{B(D)}$ are AUC of the drug in corresponding donor compartment. $cA_{A(R)}$ and $cA_{B(R)}$ were corrected for the sampled volume at each time point. We used $AUC_{A(D)}$ and $AUC_{B(D)}$ instead of single donor drug concentration at time 0, because this approach corrects for the depletion of the drug in the donor compartment during the experiment. Only experiments with integral tight junctions (LY apparent permeability - $P_{app} < 2 \cdot 10^{-6}$ cm/s) were used for analyses. Likewise, only experiments with ER >7 for QND or PRZ were included in our analyses. Grouped statistical analysis of ER and P_{app} values was performed by Kruskal-Wallis with Dunn's multiple comparisons test and p values less than 0.05 were considered significant.

3.3.6 *Prediction of fetal $K_{p,uu}$ from in vitro studies using the ER-REF approach*

The *in vivo* $K_{p,uu}$ is related to the clearances mediating the entry and exit of the unbound drug into and from the fetal compartment, respectively, provided fetal elimination of the drug is negligible (see below for justification of this assumption) (**Eq. 3.3**).

$$K_{p,uu} = \frac{CL_{\text{int,PD,placenta}}}{CL_{\text{int,PD,placenta}} + CL_{\text{int,P-gp,placenta}}} \qquad (3.3)$$

Dividing by $CL_{int,PD,\ placenta}$ yields:

$$K_{p,uu} = \frac{1}{1 + \frac{CL_{int,P-gp,placenta}}{CL_{int,PD,placenta}}} \quad (3.4)$$

Therefore, the *in vivo* $K_{p,uu}$ (**Eq. 3.4**) can be related to the *in vitro* P-gp mediated ER as follows:

$$K_{p,uu} = \frac{1}{1+ \left(ER_{TRQ(+)} - ER_{TRQ(-)}\right) \cdot REF} \quad (3.5)$$

where the ER in the presence (+) and absence (-) of TRQ is the P-gp mediated ER. To scale this P-gp mediated ER to an *in vivo* value, the difference in the abundance of P-gp between *in vitro* (i.e., hMDR1-MDCK$^{cP\text{-}gpKO}$ cells) and *in vivo* should be accounted for. The relative expression factor (REF) corrects for this difference in abundance. P-gp abundance in cells and *in vivo* in human placentae was quantified as described below and in previous work (Anoshchenko et al., 2020), respectively.

$$REF = \frac{P-gp\ abundance\ in\ human\ placenta\ (pmol/mg\ HP)}{P-gp\ abundance\ in\ hMDR1-MDCKII^{cP-gp\ KO}\ cell\ line\ (pmol/mg\ HP)} \quad (3.6)$$

where HP is the total protein in the homogenate of the human placenta or hMDR1-MDCK$^{cP\text{-}gpKO}$ cells.

Based on the above equations, when a drug is not a substrate of P-gp and/or BCRP, $K_{p,uu}$ and ER will both equal 1. When a drug is actively effluxed, $K_{p,uu}$ will be <1 and ER>1. The fraction of a drug transported by P-gp ($f_{t,P\text{-}gp}$) was calculated from predicted $K_{p,uu}$ value of each drug ($f_{t,P\text{-}gp} = 1 - K_{p,uu}$).

3.3.7 *Quantification of P-gp Abundance in hMDR1-MDCK$^{cP\text{-}gpKO}$ Cells and Determination of the Relative Expression Factor (REF)*

After each experiment, cells were lysed on the semi-permeable membranes in 1:1 ratio of 2% SDS:EBII buffer for 60 min at room temperature. Total protein concentration was measured by BCA assay and approximately 110-160 µg of total protein was reduced, alkylated and trypsin digested in duplicate as described previously (Anoshchenko et al., 2020; Billington et al., 2019; Storelli, Billington, Kumar, & Unadkat, 2020). Ice-cold heavy-labeled IS peptide (NTTGALTTR) was prepared in a solution of 80% acetonitrile and 0.2% formic acid and spiked into the trypsin digest (in 1:4 IS:sample ratio) to terminate trypsin digestion. After centrifugation (5000 x g, 4°C), 5 µL of supernatant was injected onto the LC-MS/MS system and analyzed using settings and procedure described previously (Anoshchenko et al., 2020). Pooled human placental total membrane sample was used as a biological control and digested with experimental samples. The calibration curve (0.62 – 40 nM) and quality control samples (0.62, 10, 40 nM) were prepared in 50 mM ammonium bicarbonate buffer, 10 uL of unlabeled peptide standard and 20 µL of chilled labeled peptide internal standard (both in 80% acetonitrile and 0.2% formic acid). The published P-gp abundance in the homogenate of the term placenta (0.16 ± 0.07 pmol/mg of homogenate protein) was used to estimate the REF value in **Eq. 3.6** (Anoshchenko et al., 2020).

3.3.8 *Estimation of Fetal $K_{p,uu}$ Using the Observed in vivo Data*

Fetal *in vivo* $K_{p,uu}$ of DRV and LPV was estimated as described for DEX and BET (manuscript submitted for publication). DRV and LPV are usually administered in combination with ritonavir (RTV). The observed DRV and LPV data in non-pregnant and pregnant women (including UV plasma concentrations) are available only for the combination drug dosing

regimens, DRV/RTV or LPV/RTV. As an overview (see below for details), we first optimized SimCYP® PBPK model of DRV/RTV and LPV/RTV in non-pregnant individuals after oral drug administration of each combination drug regimen. To do so, the model was populated with physicochemical and pharmacokinetic parameters for DRV, LPV and RTV (Wagner et al., 2017) and verified using the observed drug plasma concentration-time profiles (C-T profiles) in the non-pregnant population (Boffito, Miralles, & Hill, 2008; Eron et al., 2004; V. Sekar et al., 2010; V. J. Sekar, Lefebvre, De Pauw, Vangeneugden, & Hoetelmans, 2008). Then, the parameters from non-pregnant population were incorporated into m-f PBPK model and adjusted for pregnancy-induced physiological changes (e.g., placental and hepatic blood flow, hepatic CYP3A induction, etc.) at the gestational week (average demographic) specified in the observed data sets. Finally, fetal-placental clearance parameters of DRV and LPV were optimized to estimate the *in vivo* fetal $K_{p,uu}$.

I. Optimization of PBPK Models of DRV and LPV in the Non-pregnant Population

We first predicted plasma concentration-time (C-T) profiles of DRV administered alone (PO 400 mg BID, data not shown), DRV/RTV (PO 600/100 mg BID and PO 800/100 mg QD) and LPV/RTV (PO 400/100 mg BID) in the non-pregnant population using SimCYP Simulator® version 19 (SimCYP Ltd., Certara, Sheffield, UK). The previously published DRV, LPV, RTV drug-specific parameters were used (Wagner et al., 2017) except that some of them (t_{lag}, k_a) were optimized (DRV: t_{lag} = 1.3 h, k_a = 0.4 h^{-1} and LPV: t_{lag} = 1.5 h) so the predicted steady-state DRV or LPV plasma concentration data better described the observed data. The observed DRV or LPV steady-state C-T data (Boffito et al., 2008; Eron et al., 2004; V. Sekar et al., 2010; V. J. Sekar et al., 2008) were digitized with WebPlotDigitizer

(https://automeris.io/WebPlotDigitizer/). RTV drug-specific parameters included the time-dependent inactivation and induction of CYP3A enzymes in the intestine and the liver.

II. Verification of the m-f PBPK Models of DRV (at Gestational Week - GW34 and GW38) and LPV (GW 38) in the Pregnant Population.

CYP3A inhibition by RTV in pregnancy was first generated in the SimCYP® pregnancy model. Then, the change in bioavailability of DRV or LPV in pregnancy, due to co-administration of RTV, was incorporated into our m-f PBPK model (13-fold for DRV and 112-fold for LPV). The DRV and LPV steady-state PK parameters obtained in non-pregnant population were incorporated into our m-f PBPK model built in MATLAB R2020a using our previously published approach. As per our previous publications, compared to non-pregnant individuals, we assumed maternal hepatic CYP3A activity was induced at term by 2-fold (Hebert et al., 2008; Zhang et al., 2015). For DRV, two sets of maternal C-T profile predictions were generated from intensively-sampled observed data at GW34 and sparsely sampled data at GW38 (latter, with matching sparsely-sampled fetal UV data).

III. Optimization of Fetal-Placental PK Parameters of DRV and LPV at Gestational Week 38 (GW38) to Estimate in vivo Fetal $K_{p,uu}$

As described previously (Zhang & Unadkat, 2017), we estimated the *in vivo* transplacental passive diffusion clearance ($CL_{int,PD,placenta}$) of DRV and LPV by scaling the *in vivo* midazolam $CL_{int,PD,placenta}$ by the ratio of the apparent permeabilities (P_{app}) of the two drugs in hMDR1-MDCK$^{cP\text{-}gpKO}$ cells (1.19×10^{-5} and 1.25×10^{-5} cm/s, respectively) and that of midazolam (MDZ $CL_{int,PD,placenta}$ = 500 L/h, $P_{app} = 4.9 \times 10^{-5}$ cm/s; determined in MDCKII or Caco-2 cells). The resulting DRV and LPV $CL_{int,PD,placenta}$ were 121 and 127 L/h, respectively. These values were much greater than the placental blood flow at term (~45 L/h). Therefore, DRV

and LPV $CL_{int,PD,placenta}$ were considered to be perfusion-limited (45 L/h). Fetal hepatic intrinsic clearance (fCL_{int}) was assumed to be negligible due to low CYP3A7 turnover of CYP3A metabolized drugs and low fetal liver weight (Zhang & Unadkat, 2017)(manuscript submitted for publication). As we have described elsewhere, the *in vivo* fetal $K_{p,uu}$ value was optimized by adjusting $CL_{int,P\text{-}gp,placenta}$ until the predicted unbound UV/MP best described the observed unbound UV/MP by minimizing the absolute average fold error, AAFE. The observed maternal and UV steady-state C-T profiles of DRV were obtained from published literature (Colbers et al., 2015; Murtagh et al., 2019; Stek et al., 2015). These C-T profiles were digitized with WebPlotDigitizer. Because the observed C-T profiles of LPV (Cressey et al., 2015; Fauchet et al., 2015) were highly variable, we used the UV and MP C-T profiles predicted by a population pharmacokinetic (PopPK) model developed by others to fit the UV and MP LPV C-T profiles (Cressey et al., 2015; Fauchet et al., 2015). To generate interindividual variability in the plasma C-T profiles, a virtual population of 100 individuals was simulated within m-f PBPK model to generate the mean, 5^{th} and the 95^{th} percentile profiles (90% confidence interval – $CI_{90\%}$).

3.3.9 *Prediction of DRV and LPV Pharmacokinetics in the Pregnant Population at an Earlier Gestational Age (Week 20; GW20)*

To illustrate the utility of our model to predict fetal exposure to drugs at an earlier gestational age, we predicted the DRV and LPV maternal-fetal profiles at gestational week 20 (GW20). GW20 was chosen since this is the earliest gestational age at which all the fetal physiological parameters (e.g., organ volumes, partition coefficients, blood flows) are available. First, the m-f PBPK model was populated with both maternal and fetal physiological and hepatic CYP3A activity applicable to GW20 using the gestational age-dependent changes in the parameters that we have published previously (Zhang et al., 2015; Zhang et al., 2017). Then,

$CL_{int,PD,placenta}$ and $CL_{int,P\text{-}gp,placenta}$ at GW20 for both drugs were adjusted for the GW20 placental surface area (Zhang et al., 2017) and total placental P-gp abundance (Anoshchenko et al., 2020). Finally, GW20 maternal and fetal C-T profiles at steady-state (dose 16) were generated after PO DRV/RTV 600/100 BID and PO LPV/RTV 400/100 BID.

3.3.10 *Statistical Analyses and Verification of Predictions*

Our acceptance criteria for non-pregnant PBPK and m-f PBPK model verifications were to predict pharmacokinetic parameters (C_{max}, AUC and CL) within 0.8 – 1.25-fold of the observed values and absolute average fold error (AAFE, where available) of <2. Interindividual variability and $CI_{90\%}$ (5^{th} and 95^{th} percentiles) for C-T profiles and $K_{p,uu}$ were generated in a virtual population of 100 individuals and included variability only in the maternal system-related parameters. The 90% confidence intervals ($CI_{90\%}$) of the predicted fetal $K_{p,uu}$ were generated using pooled variance approach (O'Neill., 2014), where the variability in ER and REF (P-gp abundances in the *in vitro* cell line and *in vivo* from placental tissue) were included. Verification of the predicted fetal $K_{p,uu}$ using the ER-REF approach was deemed successful if the mean predicted fetal $K_{p,uu}$ fell within $CI_{90\%}$ of the observed fetal $K_{p,uu}$.

3.4 RESULTS

3.4.1 *ER of DEX, BET, DRV and LPV in Transwell Assays using hMDR1-MDCK$^{cP\text{-}gp\ KO}$ or hABCG2-MDCKII cells*

DEX, BET, DRV and LPV were transported by P-gp as evidenced by their P-gp mediated efflux ratios ($ER_{P\text{-}gp}$) in hMDR1-MDCK$^{cP\text{-}gp\ KO}$ cells (**Figure 3.2, Table 3.1**). In the same experiments, the ER of the positive control quinidine (QND) was 11.1 ± 2.5 (mean ± SD, n=4 experiments, each conducted in triplicate, data not shown). In contrast, DEX and BET were not transported by BCRP. The ER of DEX and BET in hABCG2-MDCKII cells was 1.2 ± 0.3 and 1.1 ± 0.1, respectively (**Figure 3.2C**). In the same experiments, the ER of the BCRP positive-control substrate prazosin (PZS) was 7.1 ± 2.5 (mean ± SD, n=4 experiments, each conducted in triplicate, data not shown). The HIV PIs were not tested in hABCG2-MDCKII cells as published data indicate that they do not appear to be BCRP substrates (Agarwal, Pal, & Mitra, 2007; Konig et al., 2010).

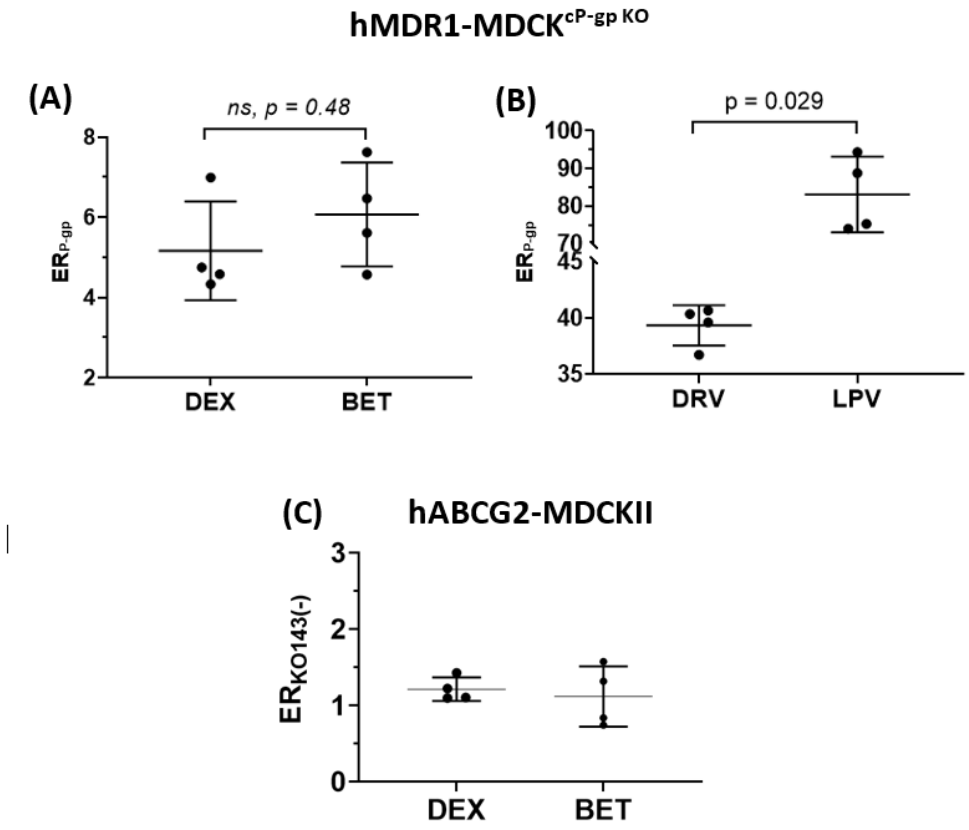

Figure 3.2. Efflux ratios (ER) of test compounds in Transwell assays using monolayer of (A, B) hMDR1-MDCK$^{cP\text{-}gp\ KO}$ or (C) hABCG2-MDCKII. All four drugs were substrates of P-gp in hMDR1-MDCK$^{cP\text{-}gp\ KO}$ cells as evidenced by their P-gp mediated efflux ratio, $ER_{P\text{-}gp}$ (i.e., $ER_{P\text{-}gp} = ER_{TRQ(-)} - ER_{TRQ(+)}$ where TRQ is tariquidar). **(A)** $ER_{P\text{-}gp}$ of DEX (5.2±1.2) and BET (6.1±1.3) were not significantly different, (Kruskal-Wallis test). **(B)** while the $ER_{P\text{-}gp}$ of LPV (83.1±10.1) and DRV (39.3±1.8) were significantly different from each other and greater than those of DEX and BET **(C)** neither DEX nor BET were substrates of BCRP in hABCG2-MDCKII cells (in the absence of KO143) as evidenced by their efflux ratios of 1.2±0.3 and 1.1±0.1, respectively. Drug concentrations in the donor compartments were 2 µM for DEX, BET and DRV, and 1 µM for LPV. Dots represent individual experiments, each conducted in triplicate; lines represent means and standard deviations. Detailed summary of the efflux ratios of test compounds is provided in **Table 3.1.**

Table 3.4. ER, REF and the predicted fetal $K_{p,uu}$ for P-gp Substrates using the ER-REF approach and P-gp overexpressing cells (hMDR1-MDCK$^{cP\text{-}gp\ KO}$).

Drug	Exp #	$ER_{TRQ(-)}$	$ER_{TRQ(+)}$	$ER_{P\text{-}gp}$	*In vitro* P-gp abundance (pmol/mg HP)	REF	Predicted $K_{p,uu}$		Observed $K_{p,uu}$	Predicted / Observed
				$ER_{TRQ(-)}$ - $ER_{TRQ(+)}$			Value	Mean ($CI_{90\%}$)	Mean ($CI_{90\%}$)	
DEX	1	5.42	0.85	4.58	1.16	0.14	0.61	0.63 (0.48 - 0.78)	0.48 (0.30 - 0.66)	1.31
	2	5.37	1.04	4.33	1.34	0.12	0.66			
	3	8.33	1.35	6.99	1.92	0.08	0.63			
	4	5.65	0.90	4.75	1.20	0.13	0.61			
	Mean ± SD	6.2 ± 1.43	1.03 ± 0.22	5.16 ± 1.23	1.41 ± 0.35	0.12 ± 0.02				
BET	1	6.56	0.95	5.61	1.16	0.14	0.56	0.59 (0.42 - 0.69)	0.5 (0.29 - 0.71)	1.18
	2	5.64	1.07	4.57	1.34	0.12	0.65			
	3	8.64	1.03	7.62	1.92	0.08	0.62			
	4	7.66	0.92	6.74	1.20	0.13	0.53			
	Mean ± SD	7.13 ± 1.31	0.99 ± 0.07	6.13 ± 1.33	1.41 ± 0.35	0.12 ± 0.03				
DRV	1	40.43	0.82	39.61	1.16	0.14	0.15	0.17 (0.10 - 0.23)	0.16 (0.11 - 0.22)	1.06
	2	41.83	1.48	40.35	1.34	0.12	0.17			
	3	37.86	1.12	36.74	1.92	0.08	0.25			
	4	41.73	1.06	40.67	1.20	0.13	0.16			

	Mean ± SD	40.46 ± 1.85	1.12 ± 0.27	39.34 ± 1.79	1.41 ± 0.35	0.12 ± 0.02				
LPV	1	95.37	1.02	94.35	1.30	0.12	0.08	0.08 (0.07 - 0.10)	0.11 (0.04 - 0.19)	0.73
	2	90.07	1.29	88.78	1.20	0.13	0.08			
	3	75.63	1.64	73.99	1.20	0.13	0.09			
	4	76.57	1.30	75.27	0.99	0.16	0.08			
	Mean ± SD	84.41 ± 9.84	1.31 ± 0.25	83.1 ± 10.05	1.17 ± 0.13	0.14 ± 0.02				

ER: efflux ratio; TRQ: tariquidar; $ER_{P\text{-}gp}$: transporter-mediated component of ER; LP: total protein in MDCK cell lysate; REF: relative expression factor measured by targeted proteomics; Predicted $K_{p,uu}$: value predicted using the ER-REF (efflux ratio-relative expression factor) approach; Observed $K_{p,uu}$: value estimated from *in vivo* UV/MP ratio at term; $CI_{90\%}$: 90% confidence interval. Note: *in vivo* P-gp abundance used in REF calculations was 0.16 ± 0.07 pmol/mg HP (Anoshchenko et al., 2020)

3.4.2 *Estimates of in vivo Fetal $K_{p,uu}$ Obtained Using our m-f PBPK Model*

To estimate the *in vivo* fetal $K_{p,uu}$ to verify our ER-REF predictions, we first successfully predicted C-T profiles and pharmacokinetic parameters of LPV and DRV in the non-pregnant population after DRV/RTV PO 600/100 BID (**Figure 3.3 A1, A2)**, DRV/RTV PO 800/100 QD (**Figure 3.S3 A1, A2)** or LPV/RTV PO 400/100 BID (**Figure 3.4 A1, A2**). Then, using our m-f PBPK model that incorporates pregnancy-induced changes in pharmacokinetic and physiological parameters by gestational week specified in observed data sets, we predicted the C-T profiles of LPV (GW38: **Figure 3.4 B1**) and DRV (GW34: **Figure 3.3 B1**; GW38 **Figure 3.3 C1**) in pregnant women who were administered the dosing regimens specified above. The predicted C-T profiles in pregnant women were successfully verified as evidenced by comparing the predicted and observed data (**Figure 3.3 B1** and **3.4 B1**: predicted $CI_{90\%}$ captured observed/PopPK predicted data; **Figure 3.3 C1**: AAFE = 1.93 and **Figure 3.S3 C1**: AAFE = 1.72) and the predicted pharmacokinetic parameters falling within 0.8 and 1.25-fold of the observed data (our predefined acceptance criteria) (**Figure 3.3 B2**; **Figure 3.S3 B2** and **Figure 3.4 B2,** respectively).

Once the maternal C-T profiles were verified, we optimized the *in vivo* placental P-gp mediated efflux clearance ($CL_{int,P\text{-}gp,placenta}$) for DRV and LPV using our m-f PBPK model and published UV/MP data at term (**Figures 3.3 and 3.4**). For DRV, *in vivo* placental efflux clearance ($CL_{int,P\text{-}gp,placenta}$ = 612 L/h), yielding $K_{p,uu}$ = 0.16, resulted in the best prediction of UV/MP ratio (AAFE = 1.63) compared with when no $CL_{int,P\text{-}gp,placenta}$ was invoked (AAFE = 8.35, $K_{p,uu}$ = 1) (**Figure 3.3 E1, E2**). For LPV, *in vivo* placental efflux clearance ($CL_{int,P\text{-}gp,placenta}$ = 1029 L/h) yielding $K_{p,uu}$ = 0.11 resulted in the best prediction of UV/MP ratio (AAFE = 1.17)

compared to when no $CL_{int,P\text{-}gp,placenta}$ was invoked (AAFE = 6.42, $K_{p,uu}$ = 1) (**Figure 3.4 D1, D2**). DEX and BET *in vivo* $K_{p,uu}$ were estimated in a similar (0.48 and 0.5, respectively) and obtained from our submitted publication.

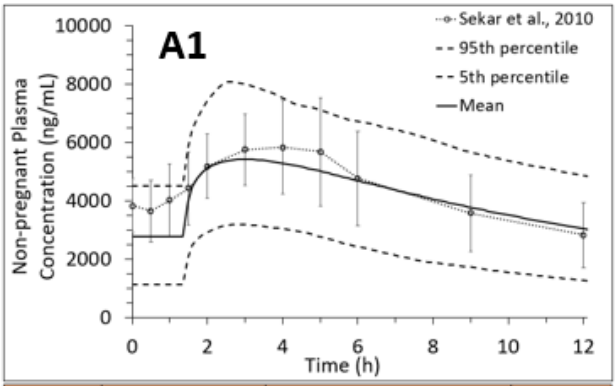

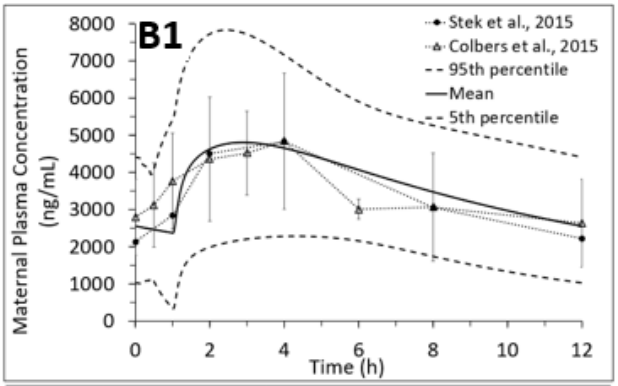

A2	Observed	Predicted (predicted / observed)	Unit
C_{max}	5821	5416 (0.93)	ng/mL
t_{max}	4	3.2 (0.8)	h
AUC_{0-12}	52601	50142 (0.95)	h*ng/mL
CL	11.4	12.0 (1.05)	L/h
AAFE	N/A	1.07	

B2	Observed	Predicted (predicted / observed)	Unit
C_{max}	4830*, 4839†	4805 (0.99)	ng/mL
t_{max}	4	3 (0.75)	h
AUC_{0-12}	41818*, 41694†	44126 (1.10)	h*ng/mL
CL	14.3*, 14.4†	13.6 (0.94)	L/h
AAFE	N/A	1.15	

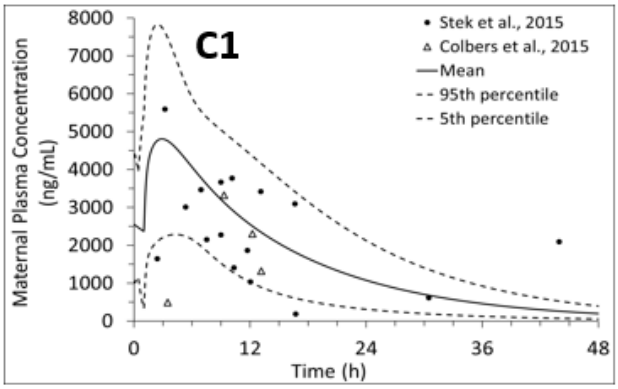

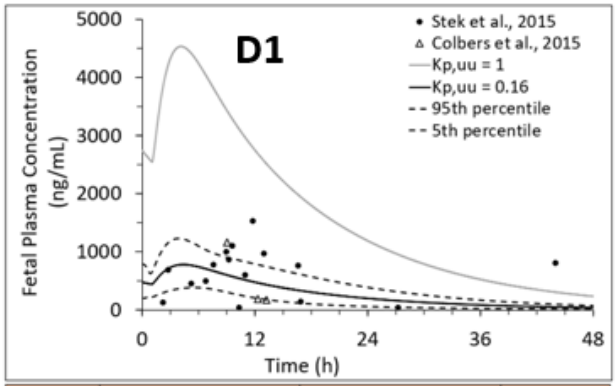

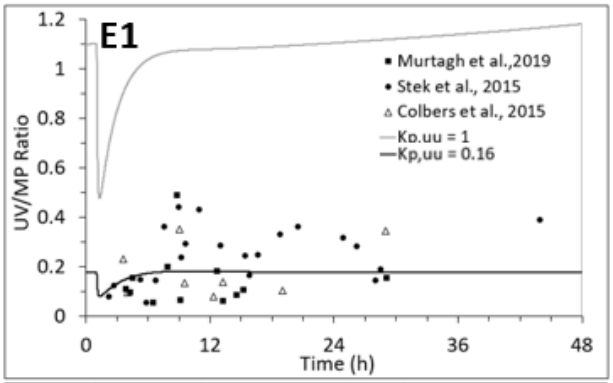

D2	Predicted $K_{p,uu}$=1	Predicted $K_{p,uu}$= 0.16	Unit
C_{max}	4536	780	ng/mL
t_{max}	4.1	4.4	h
AUC_{0-12}	43797	7577	h*ng/mL
AAFE	6.87	2.44	

E2	Observed	Predicted $K_{p,uu}$ = 1 (predicted / observed)	Predicted $K_{p,uu}$ = 0.16 (predicted / observed)
UV/MP	0.21	1.08 (5.14)	0.17 (0.81)
AAFE	N/A	8.35	1.63

Figure 3.3. PBPK predictions of DRV steady-state plasma concentrations in (A1) non-pregnant individuals, (B1) pregnant women at GW 34 (intensively sampled), (C1) pregnant women at GW 38 (sparsely sampled) and corresponding (D1) fetuses at GW38 (sparsely sampled) and (E1) umbilical vein (UV)/maternal plasma (MP) ratio at GW38 with and without incorporation of placental P-gp efflux. Subjects were administered DRV/RTV 600/100 mg PO BID. (A1) SimCYP® or **(B1, C1)** m-f PBPK predicted mean concentration-time profile (solid line) and $CI_{90\%}$ (dashed lines) are overlaid on the observed mean ± SD data (**A1**: circles, , n=8; **B1**: circles, n=32; triangles, n=6; or **C1**:n=20). **D1, D2:** The observed fetal UV concentration-time data were better predicted by our m-f PBPK model in the presence of P-gp efflux clearance ($K_{p,uu}$ = 0.16 - black solid line; dashed lines - 5th and 95th percentile profiles) vs. in the absence of P-gp efflux clearance (i.e., passive diffusion only resulting in $K_{p,uu}$ = 1 - grey solid line). **E1:** The m-f PBPK model better predicted UV/MP ratios in the presence of P-gp efflux clearance ($K_{p,uu}$= 0.16) vs. in the absence of P-gp efflux clearance ($K_{p,uu}$= 1). The observed UV/MP ratios are combined from two dosing regimens of DRV/RTV: 600/100 BID and 800/100 QD. **(A2, B2, D2, E2)** The predicted pharmacokinetic parameters in **A2, B2** met our *a priori* defined acceptance criteria and were within 0.8- to 1.25-fold of the observed data. The observed PK parameters were estimated from Stek *et al*., 2015 (*) or Colbers *et al*., 2015 (†).

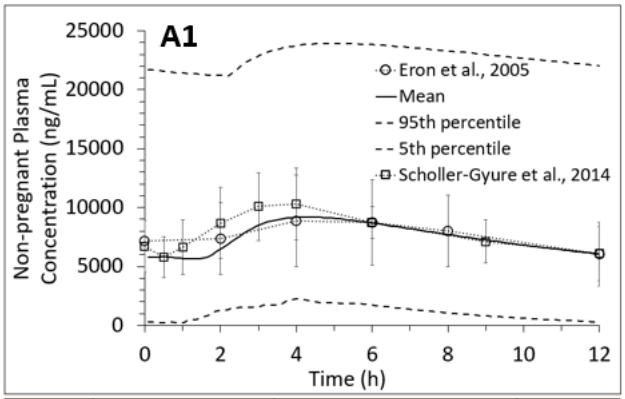

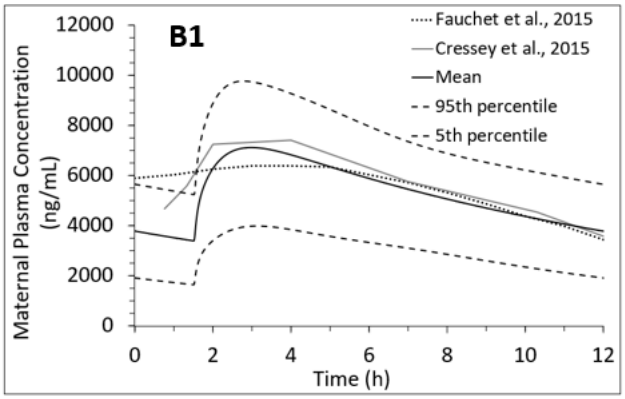

A2	Observed	Predicted (predicted / observed)	Unit
C_{max}	8885*, 10323†	8872 (0.99*,0.86†)	ng/mL
t_{max}	4	4.3 (1.07)	h
AUC_{0-12}	93333*, 96105†	90367 (0.97*, 0.94†)	h*ng/mL
CL	4.3*, 4.2†	4.4 (1.0)	L/h
AAFE	N/A	1.06*, 1.09†	

B2	PopPK Model	Predicted (predicted / observed)	Unit
C_{max}	6388*, 7409†	7064 (1.1*, 0.95†)	ng/mL
t_{max}	4	3 (0.75)	h
AUC_{0-12}	66361*, 67553†	62663 (0.94*, 0.93†)	h*ng/mL
CL	6.0*, 5.9†	6.4 (1.1)	L/h
AAFE	N/A	1.12*, 1.19†	

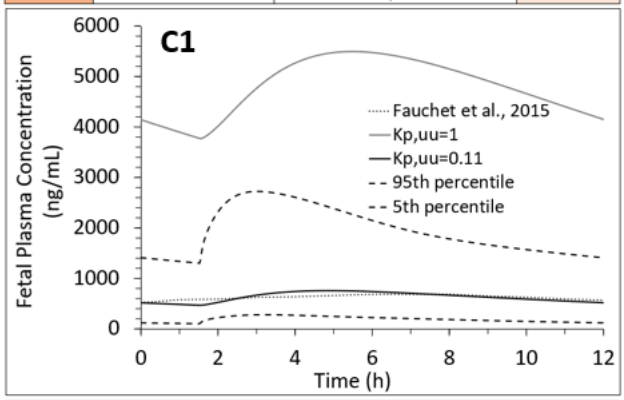

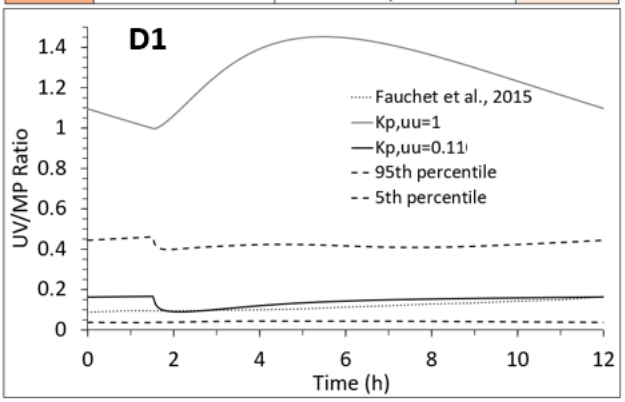

C2	PopPK Model	Predicted $K_{p,uu}$=1 (predicted / observed)	Predicted $K_{p,uu}$ = 0.11 (predicted / observed)	Unit
C_{max}	686	5494 (8.00)	756 (1.10)	ng/mL
t_{max}	7	5.48 (0.78)	4.9 (0.70)	h
AUC_{0-12}	7559	57491 (7.61)	7562 (1.00)	h*ng/mL
AAFE	N/A	7.58	1.08	

D2	PopPK Model	Predicted $K_{p,uu}$ = 1 (predicted / observed)	Predicted $K_{p,uu}$ = 0.11 (predicted / observed)
UV/MP	0.12	1.27 (10.73)	0.14 (1.20)
AAFE	N/A	6.42	1.17

Figure 3.4. PBPK predictions of LPV steady-state plasma concentrations in (A1) non-pregnant individuals, (B1) pregnant women and (C1) their fetuses at GW38 and (D1) umbilical vein (UV)/maternal plasma (MP) ratio with and without incorporation of placental P-gp efflux. Subjects were administered LPV/RTV 400/100 mg PO BID. (A1, B1) SimCYP® or m-f PBPK predicted mean concentration-time profile (solid line) and $CI_{90\%}$ (dashed lines) are overlaid on the observed data (**A1** - circles: mean ± SD, n=19; squares: mean ± SD, n=16) or **B1**, two published population pharmacokinetic (PopPK) profiles respectively (grey solid line). **(C1, C2)** The "observed" (i.e., PopPK predicted) fetal UV concentration-time profile (dotted line) was better predicted by our m-f PBPK model in the presence of P-gp efflux clearance ($K_{p,uu}$ = 0.11 - black solid line; dashed lines - 5th and 95th percentile profiles) vs. in the

absence of P-gp efflux clearance (i.e., passive diffusion only resulting in $K_{p,uu}$ = 1 - grey solid line). **(D1)** The m-f PBPK model better predicted the "observed" (i.e., PopPK predicted) UV/MP ratios in the presence of P-gp efflux clearance ($K_{p,uu}$ = 0.11) vs. in the absence of P-gp efflux clearance ($K_{p,uu}$ = 1). **(A2, B2, C2, D2)** The predicted pharmacokinetic parameters met our *a priori* defined acceptance criteria and were within 0.8- to 1.25-fold of the observed or PopPK predicted values. The published PopPK parameters were estimated from **(A2)** Eron *et al*., 2004 (*) and Scholler-Gyure et al., 2013 (†), or **(B2)** Fauchet et al., 2015 (*) or Cressey et al., 2015 (†).

3.4.3 *Prediction and Verification of Fetal $K_{p,uu}$ using the ER-REF Approach*

After the *in vitro* ER of DEX, BET, DRV and LPV, were scaled using the ER-REF approach (**Eq. 3.5, 3.6**), the mean predicted *in vivo* fetal $K_{p,uu}$ ($CI_{90\%}$) obtained were 0.63 (0.48 – 0.78), 0.59 (0.42 – 0.69), 0.17 (0.1 – 0.23), 0.08 (0.07 – 0.1) respectively (**Figure 3.5, Table 3.1**). The mean ER-REF predicted values fell within $CI_{90\%}$ of estimated from *in vivo* values for DEX (0.3 – 0.66), BET (0.29 – 0.71), DRV (0.11 – 0.22) and LPV (0.04 – 0.19), demonstrating success of the ER-REF approach (**Figure 3.5, Table 3.1**). These mean ER-REF predicted $K_{p,uu}$ resulted in UV/MP ratio profiles that predicted the observed values well (DRV, LPV **Figure 3.S4 A, B**), or modestly overpredicted the observed values (BET, DEX **Figure 3.S4 C, D**). These ER-REF predicted $K_{p,uu}$ values yielded mean *in vivo* fraction of drug transported by placental P-gp ($f_{t,P\text{-}gp} = 1 - K_{p,uu}$) of 0.37, 0.41, 0.84 and 0.92 for DEX, BET, DRV and LPV, respectively

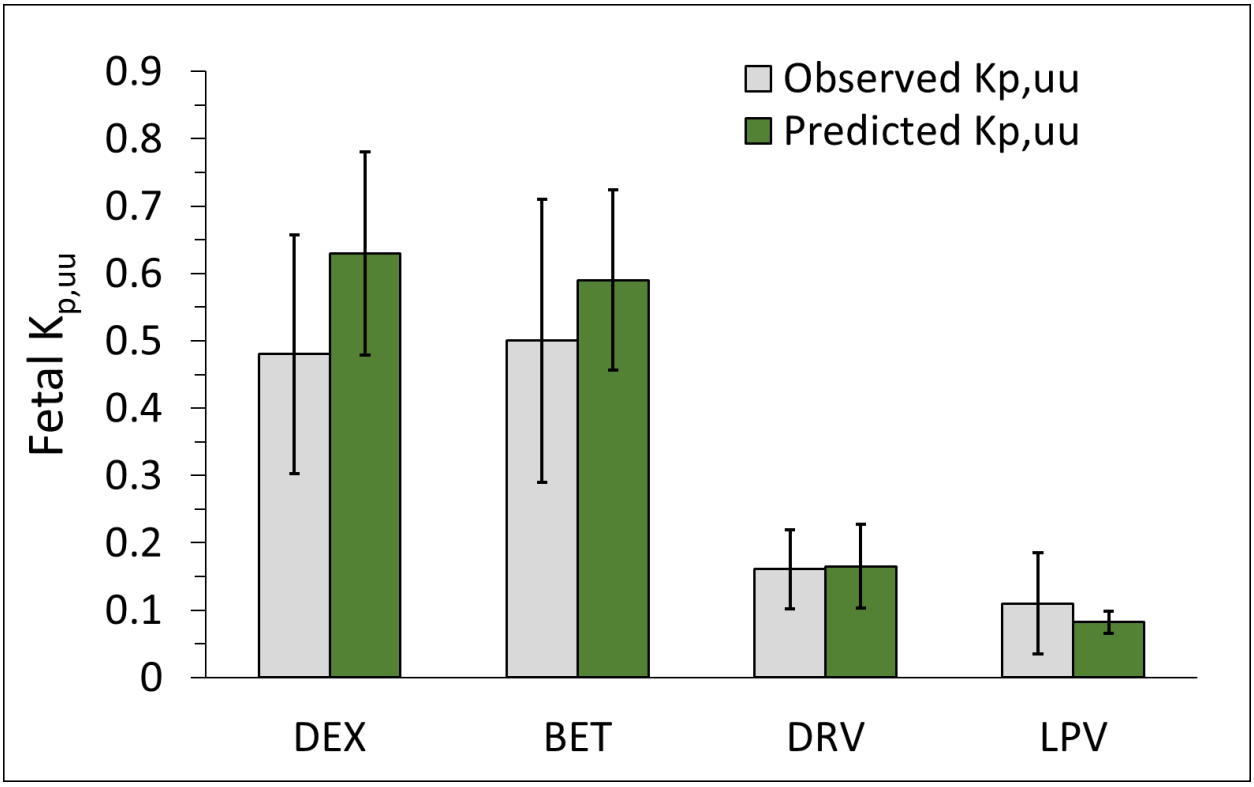

Figure 3.5. Successful prediction of fetal $K_{p,uu}$ by the REF-ER approach when compared with the *in vivo* $K_{p,uu}$ estimated by m-f PBPK modeling and simulation of the observed data. The mean ER-REF predicted $K_{p,uu}$ values of DEX, BET, DRV and LPV (green bars, error bars are $CI_{90\%}$) fell within $CI_{90\%}$ (error bars) of the mean observed values (grey bar), demonstrating the success of the ER-REF approach.

3.4.4 *Prediction of DRV/RTV and LPV/RTV $K_{p,uu}$ at an Earlier Gestational Age (GW20)*

At GW20, $CL_{int,PD,placenta}$ for DRV and LPV were 47.0 and 49.5 L/h, respectively, which was calculated from term $CL_{int,PD,placenta}$ values by adjusting for the change in placental surface area between two gestational ages. These values exceeded placental blood flow at this gestational age (27.5 L/h), yielding perfusion-limited $CL_{int,PD,placenta}$. $CL_{int,P\text{-}gp,placenta}$ at GW20, adjusted for decrease in total placental P-gp abundance at this gestational age (Anoshchenko et al., 2020), resulted in values 40% lower than the corresponding values at GW38 (367 and 617 L/h for DRV

and LPV, respectively). After gestational-age adjustment of other maternal-fetal physiological and pharmacokinetic parameters, the m-f PBPK model predicted fetal DRV and LPV UV plasma AUCs were 43% and 38%, respectively, of that at GW38. In contrast, the corresponding maternal plasma AUC of DRV was unchanged, while that of LPV was 1.15-fold higher at GW20 than at GW38 (**Figure 3.6**). These changes predicted DRV and LPV fetal $K_{p,uu}$ at GW20 of 0.11 and 0.07, respectively (69% and 64%, respectively, of the $K_{p,uu}$ at GW38).

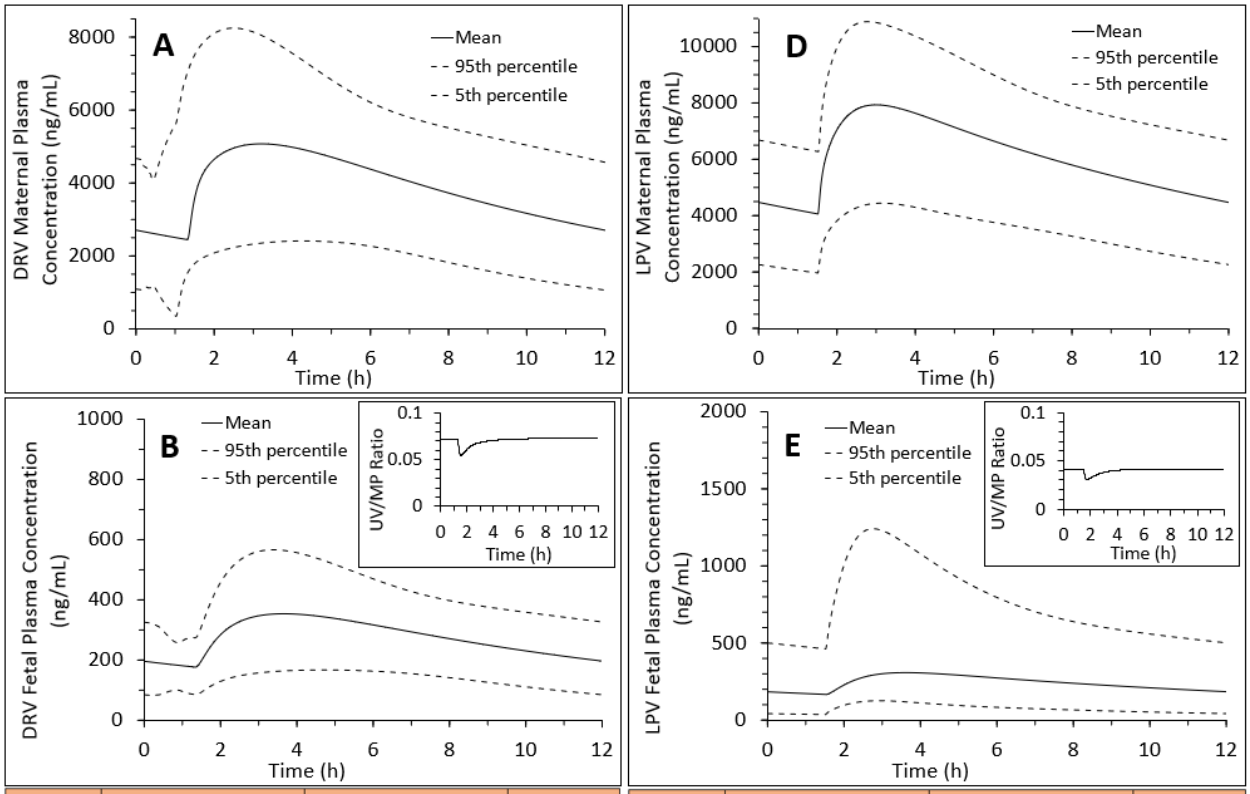

C	DRV Maternal Plasma	DRV Fetal Plasma	Unit
C_{max}	5074	353	ng/mL
t_{max}	3.2	3.6	h
AUC_{0-12}	46275	3266	h*ng/mL
UV/MP	0.07		

F	LPV Maternal Plasma	LPV Fetal Plasma	Unit
C_{max}	7935	308	ng/mL
t_{max}	3	3.6	h
AUC_{0-12}	71988	2873	h*ng/mL
UV/MP	0.04		

Figure 3.6. M-f PBPK model predictions of DRV or LPV steady-state plasma drug concentrations at gestational week 20 (GW20) after administration of (A-C) 600/100 mg PO DRV/RTV BID or (D-F) 400/100 mg PO LPV/RTV BID. (B, C) Fetal plasma DRV C_{max} and AUC_{0-12} at GW20 were 45% and 43% of that at GW38 (**Figure 3.3 D1, D2**), while maternal

plasma DRV C_{max} and AUC_{0-12} at GW20 **(A, C)** were approximately the same as that at GW38 (**Figure 3.3 B1, B2**), indicating that both P-gp efflux and passive diffusion clearance affect fetal rather than maternal DRV exposure. These values yielded DRV $K_{p,uu}$ of 0.11 at GW20 vs. $K_{p,uu}$ of 0.16 at GW38. **(B-inset, C)** DRV UV/MP ratio at GW20 was 41% of that at GW38 (**Figure 3.3 E1, E2**). **(E, F)** Fetal plasma LPV C_{max} and AUC_{0-12} at GW20 were 41% and 38% of that at GW38 (**Figure 3.4 C1, C2**), while maternal plasma LPV C_{max} and AUC_{0-12} at GW20 **(D, F)** were only modestly (1.12- and 1.15-fold, respectively) higher than at GW38 (**Figure 3.4 B1, B2**). These valued yielded LPV $K_{p,uu}$ = 0.07 at GW20 vs. $K_{p,uu}$ of 0.11 at GW38. **(E-inset, F)** The LPV UV/MP ratio at GW20 was 29% of that at GW38 (**Figure 3.4 D1, D2**).

3.5 DISCUSSION

Using our m-f PBPK model, we successfully predicted and verified fetal exposure to drugs that passively cross the placenta (Zhang & Unadkat, 2017). However, pregnant women often take drugs that are effluxed by placental transporters. We previously showed that the REF approach can successfully predict transporter-based clearance and tissue concentrations of drugs (Ishida, Ullah, Toth, Juhasz, & Unadkat, 2018; A. R. Kumar et al., 2021; V. Kumar et al., 2018; Sachar, Kumar, Gormsen, Munk, & Unadkat, 2020; Storelli, Anoshchenko, et al., 2021). Similarly, we determined if our ER-REF approach, combined with our m-f PBPK model, could predict fetal exposure to drugs that are transported by placental transporters. We tested this hypothesis using the placental P-gp transporter as our model transporter because, of all the transporters expressed in the placenta, it is arguably the most important in modulating fetal drug distribution. This is because it is highly abundant in the human placentae (Anoshchenko et al., 2020; Joshi et al., 2016; Mathias et al., 2005) and is capable of transporting wide variety of marketed drugs (Schinkel & Jonker, 2003). Indeed, many drugs (e.g., antibiotics, cardiac drugs, antiemetics, and HIV drugs) taken by pregnant women are effluxed by placental P-gp. Using the ER-REF approach, combined with our m-f PBPK model, we present the first successful prediction of fetal $K_{p,uu}$ at term for drugs that are transported by the human placentae. Moreover, our predicted fetal $K_{p,uu}$ were verified by observed maternal-fetal data at term. Although we would have preferred to conduct verification of our prediction at several gestational ages, such verification is not possible due to inability to collect UV and MP data at gestational ages other than at term.

Our ER-REF approach deliberately incorporated several elements to enhance our success in $K_{p,uu}$ predictions. First, we used a transfected MDCK cell line that had the endogenous canine

P-gp knocked out. Therefore, our measured ER and predicted fetal $K_{p,uu}$ were not confounded by endogenous canine P-gp activity. Second, we measured P-gp abundance in hMDR1-MDCK$^{cP\text{-}gpKO}$ cells in each independent transport experiment and, hence, our REF was not confounded by differences in *in vitro* transporter abundance between cell passage numbers (**Table 3.1**). Third, the quantification of P-gp abundance *in vitro* was performed using the same method as for *in vivo* placental tissue (Anoshchenko et al., 2020), within the same lab and minimizes interlaboratory variability in proteomics quantification bias in determining REF. Fourth, we chose to study drugs that were selective for P-glycoprotein. Thus, the presence of other transporters in the placenta (e.g., BCRP) did not confound the observed or predicted *in vivo* fetal $K_{p,uu}$. Indeed, we showed that the ACS were not substrates of BCRP (ER<2 in hABCG2-MDCKII cells, **Figure 3.2C**). And, literature data suggest that the PIs, DRV and LPV, are also unlikely substrates of BCRP (Agarwal et al., 2007; Konig et al., 2010). Fifth, none of the drugs are likely to be metabolized to a significant degree in the placenta, which would also confound interpretation of the *in vivo* $K_{p,uu}$. All four drugs are primarily metabolized by CYP3A, an enzyme with relatively low placental abundance and activity (Myllynen et al., 2009; Myllynen, Pasanen, & Vahakangas, 2007; Pasanen, 1999). Besides CYP3A, DEX and BET can also be metabolized by 11β-hydroxysteroid dehydrogenase-2 that is present in placenta, although the rate and extent of such metabolism relative to $CL_{int,PD,placenta}$ and $CL_{int,P\text{-}gp,placenta}$ is low (e.g., ~10-15% of DEX/BET metabolized over 6 h *in vitro* in placental microsomes) (Blanford & Murphy, 1977; Murphy et al., 2007). Sixth, we confirmed that the ER of the ACS drugs in our Transwell® assays was independent of concentration over the range of 2 - 250 µM. Due to low solubility of DRV and LPV (16 and 3 µM, respectively, DrugBank database), verification of ER over a wide range of PI concentrations was not feasible. Therefore, for our Transwell® assays, we selected

the lowest concentration of all four drugs that was quantifiable by our analytical method (2 µM for DEX/BET/DRV and 1 µM for LPV). Although RTV has been reported to be a P-gp inhibitor, based on the reported *in vivo* plasma concentration of the drug at the doses administered together with DRV or LPV, RTV is highly unlikely to inhibit placental P-gp *in vivo*. The highest reported maternal plasma RTV unbound C_{max} is 13 nM (Stek et al., 2015) (at 100 mg, BID), much lower than the lowest reported RTV IC_{50} for P-gp (240 nM, (Vermeer, Isringhausen, Ogilvie, & Buckley, 2016). Additionally, *in vivo* data (Gimenez, Fernandez, & Mabondzo, 2004) also support the fact that low-dose RTV is unlikely to inhibit brain P-gp in human (Tayrouz et al., 2001) or mice (Gimenez et al., 2004; Huisman et al., 2001). Therefore, in determining DRV or LPV ER in hMDR1-MDCK$^{cP\text{-}gp\ KO}$ cells, RTV was not added to the donor compartment. Seventh, although the *in vivo* $K_{p,uu}$ of the PIs was estimated from data obtained when the drugs were co-administered with RTV (a potent intestinal CYP3A inhibitor), incorporating 2-fold induction of hepatic CYP3A4 in pregnancy (Hebert et al., 2008) into the m-f PBPK model did not result in a proportional 2-fold increase in the PI maternal clearance. Instead, the increase was rather modest: 1.1-fold for DRV and 1.5-fold for LPV. The reason for this observation is likely due to inhibition of hepatic (and intestinal) CYP3A enzymes by RTV (Kirby et al., 2011). Incorporation of such inhibition in our m-f PBPK recapitulated the observed increase in maternal clearance of 1.2-fold and 1.4-fold, respectively (**Figure 3.2 B-D, Figure 3.3 B-D).** Finally, our prediction of $K_{p,uu}$ was based on UV/MP values that are obtained from multiple maternal-fetal dyads, rather than based on UV values alone. Inter-individual variability in maternal plasma concentration can result in significant inter-individual variability in UV C-T profile. However, the variability is mitigated considerably when UV/MP values are used.

Our *in vitro* findings confirmed previous data (Crowe & Tan, 2012; Prasad & Unadkat, 2015; Ueda et al., 1992) that all four drugs are moderate to excellent P-gp substrates (defined by FDA as efflux ratios of >2 in P-gp overexpressing cell lines (Administration, 2017)) (**Figure 3.2, Table 3.1**). As expected, because DEX and BET are epimers, their efflux ratios in the P-gp overexpressing cell line and the corresponding predicted fetal $K_{p,uu}$ were not different (**Figure 3.2A, Table 3.1**), consistent with their similar *in vivo* $K_{p,uu}$ (manuscript submitted for publication). Based on these data, the estimated *in vivo* $f_{t,P\text{-}gp}$ for DEX and BET were 0.52 and 0.50, respectively. LPV showed higher ER and $f_{t,P\text{-}gp}$, and lower ER-REF predicted $K_{p,uu}$ than DRV (**Figure 3.2B, Table 3.1**). Hence, our *in vitro* predictions indicate lower fetal LPV exposure at term compared to DRV in agreement with DRV and LPV *in vivo* $K_{p,uu}$ observations (**Figure 3.3 E-F, 4 E-F,** respectively). Also, placental P-gp drug efflux resulted in decreased fetal drug exposure to all four drugs ($K_{p,uu} < 1$, **Figure 3.5**) when compared with their corresponding fetal exposure ($K_{p,uu} = 1$) if only passive placental diffusion of the drug was assumed.

The mean ER-REF predicted $K_{p,uu}$ values were in good to excellent agreement with the estimated *in vivo* $K_{p,uu}$ values demonstrating success of the ER-REF approach (**Figure 3.5, Table 3.1**). For DEX and BET, the observed *in vivo* $K_{p,uu}$ was modestly overpredicted by the ER-REF approach. The successful predictions enhance our confidence in using the ER-REF approach to predict fetal exposure to drugs at earlier gestational ages. This is important because many drugs (e.g., DRV, LPV) are administered to pregnant women both earlier in gestation and throughout pregnancy. Indeed, our m-f PBPK model predicted lower fetal exposure to DRV or LPV at GW20 vs. at term (**Figure 3.6**). This finding is a result of an interplay between two clearance processes defining transplacental passage of the drugs (**Eq. 3.4**). Alternatively stated, it is the

ratio of $CL_{int,P\text{-}gp,placenta}$ and $CL_{int,PD,placenta}$ that determines $K_{p,uu}$ of drugs. Although P-gp abundance per gram of placenta is higher at GW20 than at term, because the placenta size is smaller at GW20, the abundance of P-gp in the whole placenta is also lower at GW20. Both the size and total placental P-gp abundance at GW20 term resulted in a greater decrease in $CL_{int,PD,placenta}$ of the drugs (80% decrease due to lower placental surface area) than in the decrease in $CL_{int,P\text{-}gp,placenta}$ (40% decrease due to lower total P-gp abundance) resulting in a lower predicted *in vivo* $K_{p,uu}$ of the drugs at GW20 compared to at term. Unfortunately, the predicted fetal drug exposure at GW20 cannot be verified due to the lack of observed UV data. Nevertheless, these predictions demonstrate the ability of our m-f PBPK model to predict fetal exposure to drugs at earlier gestational ages.

There are several limitations to our study. First, verification of LPV $K_{p,uu}$ was challenging because of the large variability in the maternal-fetal dyad data. Hence, we resorted to the use of previously published PopPK model predictions. When data for additional drugs appropriate for PBPK modeling are available (criteria for such data sets were described before in the manuscript submitted for publication), we will be able to verify our model with greater confidence and for additional P-gp substrates. Second, we modestly overpredicted DEX UV/MP ratio profile based on the ER-REF predicted $K_{p,uu}$ value (**Figure 3.S4D**). This over-prediction may be due to lack of observed UV/MP values over a duration necessary to accurately estimate its $K_{p,uu,}$ involvement of efflux transporters other than P-gp or BCRP or metabolism in the placenta. Third, we could not predict fetal exposure to drugs earlier than GW20 as fetal physiological parameters are not reliably available at that stage of gestation (Abduljalil, Jamei, & Johnson, 2018; Zhang et al., 2017). Additionally, the lack of established maternal-placental blood circulation before GW13

(Chang, Wakeland, & Parast, 2018) that would restrict overall drug access to the fetus, precludes the use of this model application from the first trimester of pregnancy.

Despite the high prevalence of drug use in pregnancy (~80% of pregnant women using at least one drug (Scaffidi et al., 2017)), 90% of drugs on the market still lack guidance on their administration in this population, leaving both mother and her fetus as "drug orphans". Although we have some understanding of maternal drug exposure and changes therein during pregnancy (Abduljalil et al., 2012; Abduljalil, Pansari, & Jamei, 2020; Anderson, 2005), this is not the case for fetal drug exposure and related fetal drug efficacy and toxicity. This study is the first to address this significant gap in health care knowledge by developing a method to successfully predict fetal exposure to drugs irrespective of transport. Since, UV/MP data at term are not readily available for all drugs prescribed to pregnant women and these studies are logistically and ethically challenging to conduct, our approach provides a means to predict fetal exposure to drugs incorporating diffusion and transport when necessary. Moreover, together with placental transporter abundance that was previously quantified (Anoshchenko et al., 2020), this ER-REF approach can be used to predict fetal exposure to placental transported drugs at gestational ages other than term (e.g., for GW20). Our ER-REF scaling approach can easily be adapted to substrates of multiple placental transporters (e.g., P-gp and BCRP) as for transport-mediated hepatic uptake and distribution of drugs (Trapa et al., 2016; Trapa et al., 2019). In conclusion, our study provides a tool to prospectively predict the fetal exposure to drugs at various gestational ages to help assess potential fetal benefits and risks associated with maternal drug administration.

3.6 SUPPLEMENTARY INFORMATION

Table 3.S1. LC-MS/MS parameters for quantification

Compound	Parent Ion	Fragment Ions	Declustering Potential	Collision energy
Dexamethasone	393.3	373.3, 355.3	32,45	10,17
Betamethasone	393.3	373.3, 355.3	32,45	10,17
Darunavir	548.2	392.3	25	20
Quinidine	325.2	307.1, 172.0	31, 45	32, 47
Prazosin	384.2	247.2	45	40
N-desmethyl loperamide (internal standard)	463.2	252.3	71	20

Table 3.S2. LC conditions for the compounds quantified

Column	UPLC column (ACQUITY UPLC® BEH C18 column, 1.7 µm, 2.1 mm x 50 mm, Waters)
Guard Column	C18 VanGuard Precolumn (C18, 2.1 mm x 5 mm)
Run Time	4 min
Injection Volume	5 µL
Column Oven Temperature	25°C
Autosampler Temperature	4°C

Gradient Table

Time (min)	Flow Rate (ml/min)	%A	%B
Initial	0.3	95	5
2	0.3	95	5
2	0.3	5	95
3	0.3	5	95
3.05	0.3	95	5
4	0.3	95	5

A = 0.1% formic acid in water; B = 0.1% formic acid in acetonitrile

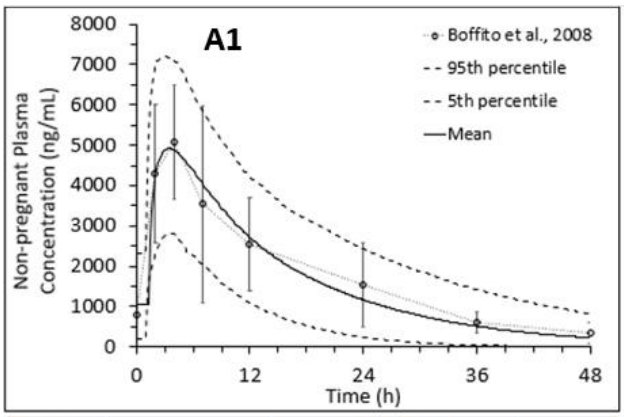

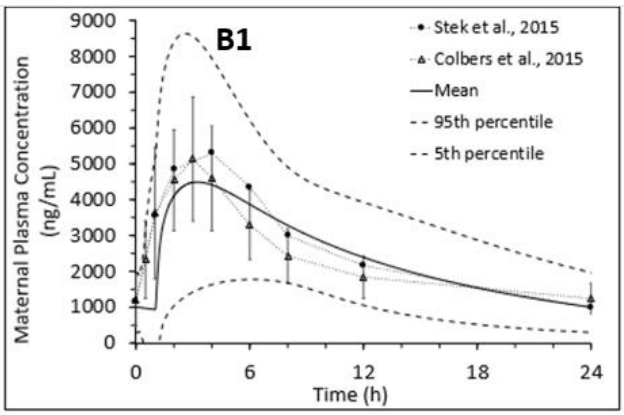

A2	Observed	Predicted (predicted / observed)	Unit
C_{max}	5079	4921 (0.97)	ng/mL
t_{max}	4	3.6 (0.9)	h
AUC_{0-24}	67007	65151 (0.97)	h*ng/mL
CL	11.9	12.3 (1.0)	L/h
AAFE	N/A	1.3	

B2	Observed	Predicted (predicted / observed)	Unit
C_{max}	5297*, 5135†	4490 (0.85*, 0.87†)	ng/mL
t_{max}	4*, 3†	3.36 (0.84*, 1.12†)	h
AUC_{0-24}	62890*, 56797†	58686 (0.93*, 1.00†)	h*ng/mL
CL	12.7*, 14.1†	13.6 (1.10*, 0.96†)	L/h
AAFE	N/A	1.38	

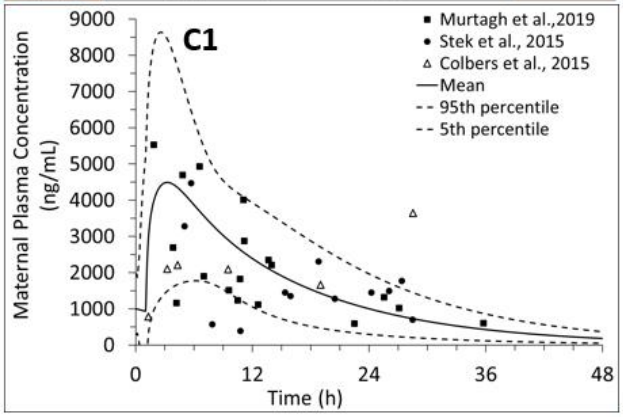

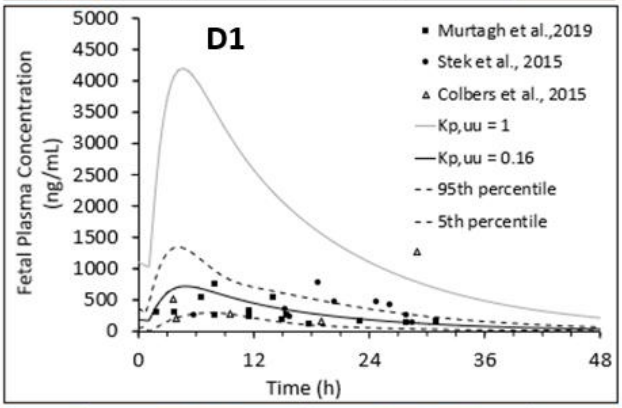

D2	Predicted $K_{p,uu}$=1	Predicted $K_{p,uu}$ = 0.16	Unit
C_{max}	4192	718	ng/mL
t_{max}	4.6	4.9	h
AUC_{0-24}	58646	10062	h*ng/mL
AAFE	6.56	1.83	

Figure 3.S3. PBPK predictions of DRV steady-state plasma concentrations in (A1) non-pregnant individuals, (B1) pregnant women at GW34 (intensively sampled), (C1) pregnant women at GW38 (sparsely sampled) and their (D1) fetuses at GW38 (sparsely sampled) with and without incorporation of placental P-gp efflux. Subjects were administered DRV/RTV 800/100 mg PO QD. (A1) SimCYP® or **(B1, C1)** m-f PBPK predicted mean concentration-time profile (solid line) and $CI_{90\%}$ (dashed lines) are overlaid on the observed data (**A1**, circles: mean ± SD, n=7; **B1**, circles: mean ± SD, n=32, triangles: mean ± SD, n=17; **(C1)** sparsely-sampled observed data). **(D1, D2)** The observed fetal UV concentration-time data were better predicted by our m-f PBPK model in the presence of P-gp efflux clearance ($K_{p,uu}$ = 0.16 - black solid line; dashed lines - 5th and 95th percentile profiles) vs. in the absence of P-gp efflux clearance (i.e., passive diffusion only resulting in $K_{p,uu}$ = 1 - grey solid line). **(A2, B2, D2)**

Predicted pharmacokinetic parameters in **A2, B2** met our *a priori* defined acceptance criteria of within 0.8- to 1.25-fold of the observed data). The observed PK parameters were estimated from Stek *et al*., 2015 (*) or Colbers *et al*., 2015 (†).

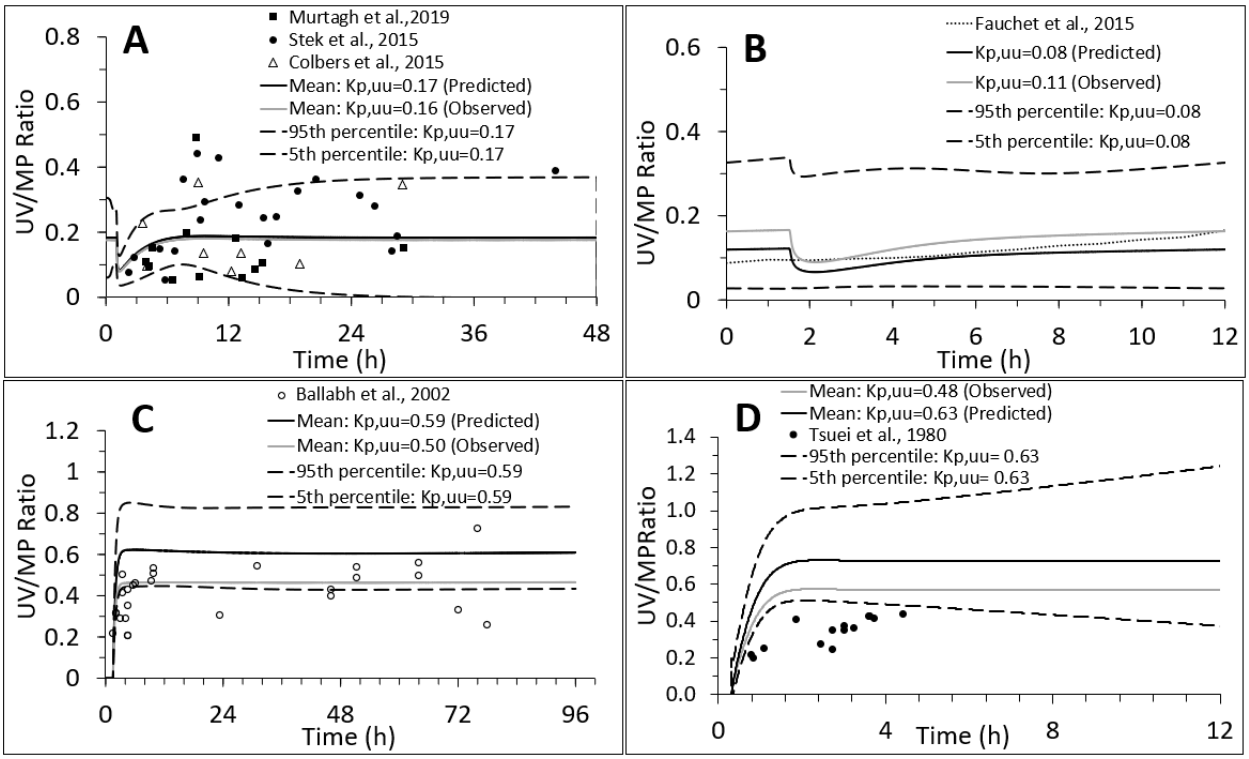

Figure 3.S4. M-f PBPK model predictions of UV/MP ratios for (A) darunavir, (B) lopinavir, (C) betamethasone and (D) dexamethasone overlaid on the observed data (A, C, D: symbols or B: PopPK predicted – dotted line) data. Mean UV/MP ratio profile of DRV and LPV based on ER-REF predicted $K_{p,uu}$ (black lines) were in excellent agreement with the profile based on their $K_{p,uu}$ estimated from *in vivo* studies (grey lines). In contrast, as expected from Fig. 3.6, the UV/MP profiles of BET and DEX based on ER-REF $K_{p,uu}$ modestly over-estimated the profiles generated based on their $K_{p,uu}$ estimated from *in vivo* studies. Dashed lines - 5th and 95th percentiles around ER-REF predicted $K_{p,uu}$ values that include variability in the virtual maternal population (See **Method**).

3.7 ABBREVIATIONS USED

5^{th} percentile: 5^{th} percentile confidence value; 95^{th} percentile: 95^{th} percentile confidence value; AAFE: absolute average fold error; AUC_f: area under the curve of total fetal plasma concentration-time profile; AUC_m: area under the curve of total maternal plasma concentration-time profile; BCRP: breast cancer resistance protein; BID: *Bis in die*, twice daily; $CI_{90\%}$: 90% confidence interval spanning between 5th and 95th percentiles; $CL_{int,PD,placenta}$: intrinsic placental passive diffusion clearance; $CL_{int,Pgp,placenta}$: *in vivo* P-gp mediated efflux clearance from the placenta; C_{max}: maximum plasma drug concentration; C-T profile: drug plasma concentration-time profile; CYP: cytochrome P450; DEX: dexamethasone; DRV: darunavir; ER: efflux ratio; ER-REF: efflux ratio-relative expression factor; fCL_{int}: fetal intrinsic hepatic clearance; $f_{t,P\text{-}gp}$: fraction of a drug transported by P-glycoprotein; $f_{u,f}$: unbound fraction in fetal plasma; $f_{u,m}$: unbound fraction in maternal plasma; GW: gestational week; hABCG2-MDCKII: Madin-Darby canine kidney cells II with overexpressed human ABCG2 [BCRP]; hMDR1-MDCK$^{cP\text{-}gp\ KO}$: Madin-Darby canine kidney II cells with overexpressed human multidrug resistance protein 1 [P-gp] and knocked out canine P-gp; IC_{50}: 50% of maximal inhibitory concentration; IV: intravenous; k_a: absorption rate constant; K_p: partition coefficient; $K_{p,uu}$: unbound partition coefficient; LC-MS/MS: liquid chromatography tandem mass spectrometry; LPV: lopinavir; LY: lucifer yellow; MDCK: Madin-Darby canine kidney; m-f PBPK model: maternal-fetal physiologically based pharmacokinetic model; MP: maternal plasma; P_{app}: apparent permeability; PIs: HIV protease inhibitors; PK: pharmacokinetic; PO: peroral; PopPK: population pharmacokinetic; PZS: prazosin; QD: *Quaque die*, once daily; QND: quinidine; REF: relative expression factor; RTV: ritonavir; SYT: syncytiotrophoblast; T_{lag}: lag time; TRQ: tariquidar; UV: Umbilical vein.

Chapter 4. PREDICTING MATERNAL-FETAL ANTENATAL CORTICOSTEROID EXPOSURE TO INFORM RE-DESIGNING ACS DRUG DOSING TO PREVENT NEONATAL RESPIRATORY DISTRESS SYNDROME

4.1 ABSTRACT

Antenatal dosing of corticosteroids (ACS - dexamethasone, DEX, and betamethasone, BET) promotes fetal lung maturation and reduces the risk of neonatal respiratory distress syndrome (RDS) in preterm babies. Due to historical, ethical, and logistical reasons, ACS dosing regimens and their maternal-fetal exposure to prevent RDS have never been optimized. Our existing maternal-fetal physiologically based pharmacokinetic (m-f PBPK) model was modified to predict m-f pharmacokinetic exposure following various ACS regimens currently used in the clinic, including the dexamethasone phosphate (DEX-P: 6 mg IM every 12 h over 48 h) and betamethasone phosphate:acetate (BET-P:A: 12 mg IM every 24 h over 48 h) (reference dosing regimens). To do so, we incorporated P-glycoprotein-mediated ACS placental efflux into our m-f PBPK model. To illustrate the utility of our m-f PBPK model to improve the efficacy and toxicity of the currently used reference regimens, we simulated potential alternative dosing regimens of DEX and BET that were convenient to administer, maintained maternal-fetal exposure (AUC) and/or C_{max}, or minimized maternal exposure while maintaining fetal drug plasma concentrations above a minimum therapeutic threshold. Besides these dosing regimens, our m-f PBPK model could be used in the future to devise other ACS dosing regimens. The efficacy and toxicity of any alternative ACS dosing regimens need to be tested in the clinic prior to their routine use.

4.2 INTRODUCTION

Preterm births account for over 11% of all live births worldwide and up to 60% of live births in low-to-middle income countries such as Sub-Saharan African countries and India (Blencowe et al., 2013; A. C. Lee et al., 2013). Infants born prematurely are at high risk of neonatal respiratory distress syndrome (RDS), a major cause of neonatal mortality and disability (Blencowe et al., 2013). Respiratory failure due to RDS is one of the most common causes of death in premature infants in the United States neonatal intensive care units. Even among infants who survive, RDS is associated with a 2-fold increased risk of cerebral palsy and a 1.4-fold increased risk of epilepsy (Dyer, 2019; Thygesen et al., 2018).

Dexamethasone (DEX) and betamethasone (BET) are the most common antenatal corticosteroids (ACS) used to prevent RDS (Roberts et al., 2017). These two epimers were developed in the early 1960s to treat rheumatoid arthritis. Dosing regimens for pregnant women that maximize their efficacy in preventing RDS and minimize their toxicity (i.e., maternal infection (Roberts et al., 2017; Vogel et al., 2017), fetal neurodevelopmental disorders (Crowther et al., 2007; Raikkonen et al., 2020) and hypoglycemia (Vogel et al., 2017)) have never been optimized. To prevent RDS, the conventional ACS dosing regimens administered to pregnant women of 24 to 36 gestational weeks (GW) are intramuscular (IM) administration of 6 mg dexamethasone phosphate (DEX-P) every 12 h for 48 h, or 12 mg of 1:1 betamethasone phosphate:acetate mixture (BET-P:A) every 24 h for 48 h (American College of & Gynecologists' Committee on Practice, 2016; Boland, 1962) (henceforth referred to as the reference dosing regimens). In several clinical trials, when these reference regimens were used, their efficacy was modest to none (the relative risk ratio [RR] of developing RDS with ACS treatment relative to placebo was 0.6 - 1.16. For example, investigators found that the risk of

both neonatal death and RDS in preterm babies was reduced by only one-sixth when the DEX reference regimen was administered to pregnant women at imminent risk of preterm birth (within 48 hours) in a recent large clinical trial in low to middle income countries (Roberts et al., 2017). Alternatively stated, despite ACS therapy, the relative risk of RDS or infant mortality within 28 days of birth remained high (RR of 0.81 and 0.84 respectively). Collectively, these data suggest a need to further optimize ACS dosing regimens.

Optimizing ACS dosing regimens to prevent RDS is a challenge for several reasons. First, defining the maternal or fetal exposure vs. efficacy/toxicity relationship of the ACS is difficult. Measurement of fetal exposure to ACS can be obtained only by measuring fetal ACS drug plasma concentrations over time. However, such a measurement can be obtained only at delivery by simultaneously sampling the umbilical vein (UV) and maternal peripheral vein. Single-point sampling does not provide a measure of fetal exposure to ACS as DEX-P and BET-P:A dosing regimens used in clinic are not designed for the fetal plasma drug concentrations to reach steady-state that are proportional to drug exposure (AUC) (Zhang et al., 2017). Second, maternal drug exposure is not a good surrogate of fetal exposure as these drugs do not passively cross the placenta. Both drugs are substrates of P-glycoprotein (P-gp) (Crowe & Tan, 2012; Yates et al., 2003), an efflux transporter that is abundant in the human placenta (Anoshchenko et al., 2020; Ceckova-Novotna, Pavek, & Staud, 2006; Han et al., 2018; Mathias et al., 2005) and acts to diminish fetal ACS exposure relative to that in the mother (Ballabh et al., 2002; Foissac et al., 2020; Tsuei et al., 1980). The extent of this diminution and the variability therein has not been well defined, but is likely to increase as pregnancy progresses due to the increase of P-gp protein abundance per whole placenta (Anoshchenko et al., 2020). Finally, even though DEX and BET are epimers, they differ in their pharmacokinetic characteristics. For example, BET has

lower hepatic clearance and longer half-life than DEX (Petersen, Nation, McBride, Ashley, & Moore, 1983; Tsuei, Moore, Ashley, & McBride, 1979). In addition, the formulation of the two ACS used for intramuscular administration differ, resulting in different absorption pharmacokinetics. BET is administered as the 1:1 mixture of BET phosphate (BET-P; fast release) and BET acetate (BET-A; slow release) resulting in a sustained release of BET from the IM depot site compared to the rapid release of DEX following dexamethasone phosphate (DEX-P) IM administration (Schmidt et al., 2018).

To overcome challenges in defining optimal dosing regimens of ACS to prevent RDS, methods to accurately predict (rather than measure) fetal exposure to ACS are needed. One such method is physiologically-based pharmacokinetic (PBPK) modeling. We previously published a maternal-fetal PBPK (m-f PBPK) model that can estimate fetal drug exposure for several drugs (Zhang et al., 2017). Our model accounts for physiological changes in pregnancy, including changes in hepatic activity of cytochrome P450 (CYP) enzymes and incorporates placental transport (e.g., by P-glycoprotein [P-gp]). Our model successfully predicted maternal and fetal drug exposure to drugs that passively diffuse across the placenta and are not metabolized in that tissue, such as midazolam, theophylline, and zidovudine (Zhang & Unadkat, 2017). To extend the model, we optimized the magnitude of placental P-gp efflux clearance ($CL_{int,Pgp,placenta}$) of each ACS to explain the observed fetal plasma concentrations of the drugs in maternal-fetal dyad pairs. As a result, our PBPK model can now predict fetal plasma concentration of ACS for a given ACS dosing regimen. An additional goal of this chapter was to use the m-f PBPK model with placental P-gp efflux to design alternative ACS dosing regimens that either make the dosing regimen more convenient by reducing the frequency of administration (DEX) or minimize maternal-fetal drug exposure and hence toxicity (BET). For DEX, we assumed that its efficacy

and toxicity were related to the maternal and fetal plasma exposure (AUC). For BET-P:A, we designed alternative dosing regimens that maintained BET fetal plasma concentrations above 1 ng/mL, a threshold defining fetal efficacy in sheep (Foissac et al., 2020; Jobe, Milad, Peppard, & Jusko, 2020; Schmidt et al., 2018).

4.3 MATERIALS AND METHODS

4.3.1 *Optimization of SimCYP PBPK Model of ACS in the Non-pregnant Caucasian Population*

Our m-f PBPK model requires, as input, drug physiological and pharmacokinetic (PK) parameters in the non-pregnant population. The majority of these parameters were as described previously by Ke et al., 2019 (Ke & Milad, 2019) and some (described in the following subsections) were optimized for the two ACS for the non-pregnant population in SimCYP Simulator® version 19 (SimCYP Ltd., Certara, Sheffield, UK). Our acceptance criterion was set to predict PK parameter values within 0.8- to 1.25-fold of the observed values (**Figure 4.1**). The concentration-time values for observed data were obtained from the literature using the WebPlotDigitizer (https://automeris.io/WebPlotDigitizer/) and PK parameters were estimated using non-compartmental analysis in Phoenix version 8.1 by the linear trapezoid method, if needed. Due to the limited ACS PK data available in the literature, we used observed data in the Caucasian and Indian population to train our PBPK model after IV (Petersen, Nation, et al., 1983; Tsuei et al., 1979) and IM administration of ACS (Jobe et al., 2020), respectively. The Indian population training data set was used to estimate the differential release characteristics of BET from BET-P and BET-A in the IM BET-P:A formulation. Such data are not available in the Caucasian population.

The SimCYP Simulator® was populated with the ACS PK parameters as follows. The molar dose of the ACS drug in the administered formulation (DEX-P, BET-P or BET-P:A) was used. The observed clearances (CL) for DEX (14.2 L/h) (Petersen, Nation, et al., 1983; Tsuei et al., 1979) and BET (10.3 L/h) (Petersen, Nation, et al., 1983; Tsuei et al., 1979) were converted to hepatic intrinsic clearance ($CL_{hep,int}$) using the well-stirred model within SimCYP Simulator®.

Dexamethasone $CL_{hep,int}$ was assigned to CYP3A4 (f_m = 0.95) and an additional minor unidentified pathway (f_m = 0.022) based on itraconazole inhibition studies (Ke & Milad, 2019). Betamethasone $CL_{hep,int}$ was assigned to CYP3A4 (f_m = 0.938) based on a previously published report (Ke & Milad, 2019). The renal clearance for both drugs, a minor clearance pathway, comprised 0.41 L/h (f_e = 0.028) for DEX (Tsuei et al., 1979) and 0.49 L/h (f_e = 0.062) for BET (Petersen, Collier, Ashley, McBride, & Nation, 1983). The volume of distribution at steady-state (V_{ss}) was extracted from the literature as 0.71 L/kg for DEX (Tsuei et al., 1979) and 1.4 L/kg for BET (Petersen, Nation, et al., 1983) for non-pregnant individuals. Binding of the ACS to non-albumin proteins was assumed to be negligible as previously reported (Peets, Staub, & Symchowicz, 1969). For IM administration of DEX-P or BET-P, the absorption-rate constant (k_a = 2 h^{-1}) and lag time (T_{lag} = 1 h) of the drugs were optimized to describe the observed profiles (Jobe et al., 2020). After IM administration of BET-P:A, each prodrug was assigned a different absorption rate constant from the site of administration (k_a = 1.5 and 0.02 h^{-1}) to take into account the different release characteristics of the phosphate and acetate prodrug, respectively (Jobe et al., 2020). The remaining baseline physicochemical parameters were as described by Ke and Milad (Ke & Milad, 2019).

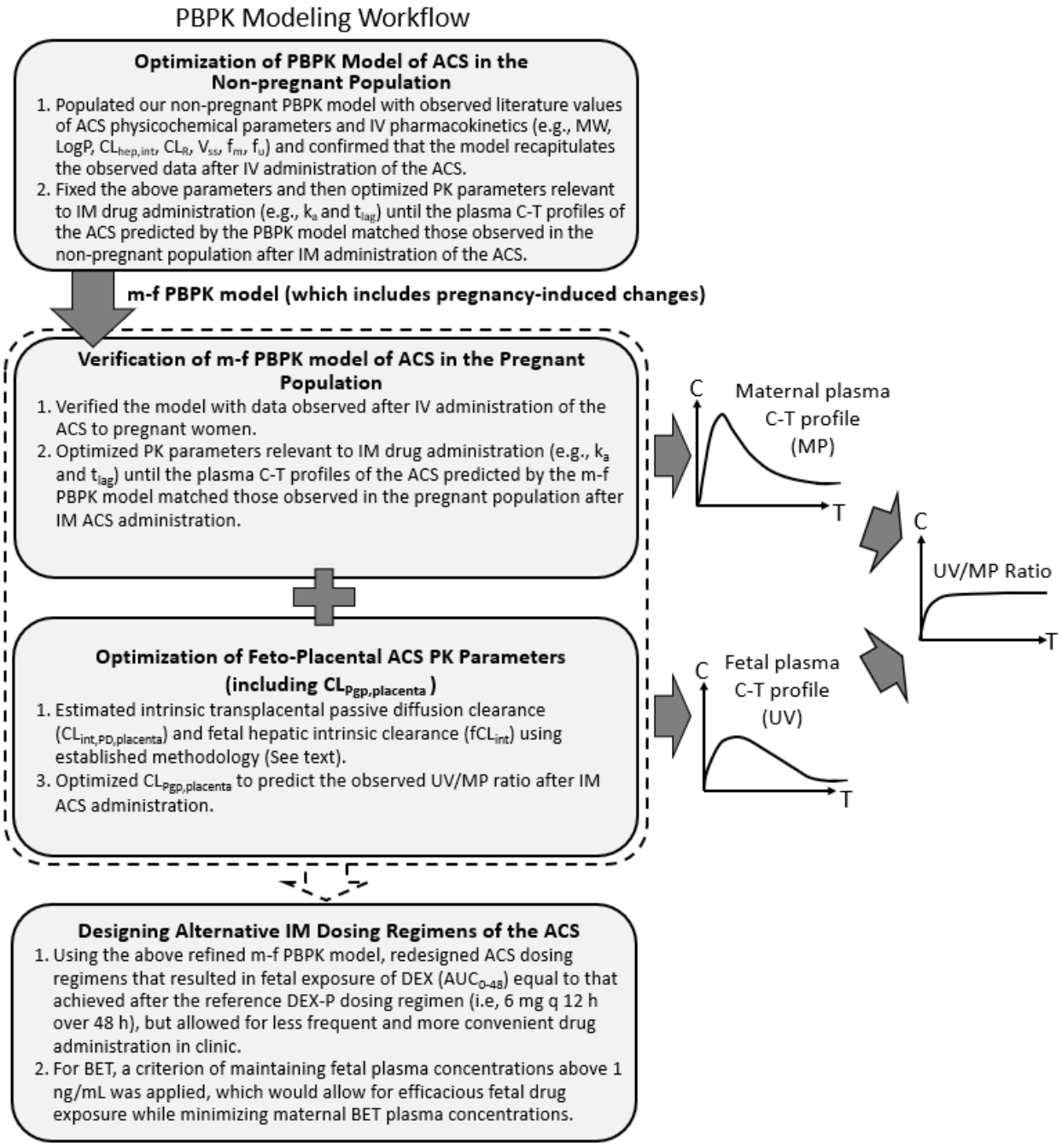

Figure 4.1. General Workflow of PBPK Modeling and Simulation. Of note, the m-f PBPK model used was exactly the same as previously described by us. Our m-f PBPK model incorporated P-gp placental efflux clearance. Since the ACS are P-gp substrates, we utilized this functionality in predicting fetal ACS concentrations.

4.3.2 *Verification of m-f PBPK Model of ACS in the Pregnant Population*

The ACS baseline pharmacokinetic parameters from non-pregnant population were incorporated without changes, except as noted below, into our previously published m-f PBPK model built in MATLAB R2020a and adjusted for pregnancy using the approach described previously (Zhang et al., 2017) (**Figure 4.1**). First, using our m-f PBPK model, DEX and BET plasma concentration-time profiles were predicted in pregnant women at term (GW 37-38) after IV administration of DEX-P and BET-P. Maternal hepatic CYP3A4 activity was assumed to be induced 2-fold (100%) at term (Hebert et al., 2008; Zhang et al., 2015). We chose to use 100% induction of CYP3A in pregnancy because this value was obtained using the selective CYP3A substrate midazolam. In contrast, though other studies have reported varying degrees of CYP3A induction during pregnancy (3-60%), these values were obtained using drugs that are not selective probes of CYP3A enzymes (Dallmann, Ince, Coboeken, Eissing, & Hempel, 2018; De Sousa Mendes et al., 2017; Xia, Heimbach, Gollen, Nanavati, & He, 2013). Then, using these IV pharmacokinetic parameters, the plasma concentration-time profiles of ACS, after IM administration of DEX-P and BET-P:A, were predicted using our m-f PBPK model. The values of k_a and T_{lag} were optimized to describe the observed IM DEX plasma concentration-time profiles. As was the case in non-pregnant individuals, to predict the plasma concentration-time profiles after IM BET-P:A administration, distinct rates of absorption of the phosphate and the acetate from the IM site were incorporated into our model. To generate interindividual variability in the plasma concentration-time profiles, a virtual population of 100 individuals was simulated and the mean, lower 5^{th} and the upper 95^{th} percentile profiles (90% confidence interval - CI) were generated. All of the maternal system-dependent parameters used in the model were varied as per the variability assigned within SimCYP® (~30% for each parameter). Due to the lack of

data about the variability in the fetal system-dependent parameters, only variability in the maternal system-dependent parameters was included. The trial designs for model verification of IM DEX-P in pregnancy were obtained from Tsuei *et al.* (Tsuei et al., 1980) and for IM BET-P:A from Ballabh et al. and Foissac et al. (Ballabh et al., 2002; Foissac et al., 2020). Pharmacokinetic data in pregnancy from other sources were excluded due to the lack of information on the time of sampling post-last dose of BET-P:A (Ballard, Granberg, & Ballard, 1975; Gyamfi et al., 2010). Our predictions were evaluated by computing the absolute average fold error (AAFE) in the predicted vs. observed maternal and fetal plasma concentration-time data (**Eq. 4.1**).

$$AAFE = 10^{\frac{1}{n}\sum |log\frac{predicted}{observed}|} \quad (4.1)$$

4.3.3 *Optimization of Feto-Placental ACS Pharmacokinetic Parameters (Including $CL_{int,Pgp,placenta}$)*

Several factors determine fetal exposure to drugs including its transplacental clearance (i.e. intrinsic passive diffusion [$CL_{int,PD,placenta}$], intrinsic P-gp-mediated efflux clearance [$CL_{int,Pgp,placenta}$], intrinsic clearance via other placental transporters), placental metabolic clearance, placental blood flow, and fetal hepatic intrinsic clearance. These factors collectively determine $K_{p,uu}$ of the drug, that is the fetal:maternal unbound drug plasma concentration ratio at steady-state or the corresponding AUC ratio after a single dose or during the dosing interval at steady-state. Our m-f PBPK model was populated with gestational age-dependent dynamic changes in maternal-fetal plasma protein concentrations (e.g., albumin and alpha-1-acid glycoprotein) and placental blood flow. Since we do not have an estimate of the $CL_{int,Pgp,placenta}$ of the ACS, we optimized its value to best explain the observed fetal-maternal ACS plasma

concentration-time profiles. To do so, we first estimated $CL_{int,PD,placenta}$ and fetal hepatic intrinsic clearance and then estimated the $K_{p,uu}$ of the drugs as presented in detail below (**Figure 4.1**).

I. *Intrinsic Transplacental Passive Diffusion Clearance ($CL_{int,PD,placenta}$) of the ACS*: The $CL_{int,PD,placenta}$ for DEX and BET was determined as previously described (Zhang & Unadkat, 2017). Briefly, we obtained the ratio of the apparent permeability of DEX and BET through Caco-2 cell monolayer relative to that of midazolam ($P_{app,\ DEX/BET} = 11.65 \times 10^{-6}$ cm/s). The *in vivo* $CL_{int,PD,placenta}$ of midazolam (500 L/h) was scaled using this ratio to arrive at the $CL_{int,PD,placenta}$ of DEX and BET. The estimated value for DEX and BET $CL_{int,PD,placenta}$ of 118.9 L/h was higher than the placental blood flow at term (~45 L/h). Hence, the m-f PBPK model apparent $CL_{int,PD,placenta}$ value for the ACS was set to 45 L/h (i.e. perfusion-limited transplacental clearance).

II. *Fetal Hepatic Intrinsic Clearance of the ACS:* Fetal hepatic intrinsic clearance was conservatively estimated from total intrinsic clearance in human liver microsomes phenotyping study (unpublished data). This value was scaled with total protein content per gram of liver tissue (26 mg) and the weight of fetal liver (~130 g) (Abduljalil et al., 2012; Zhang & Unadkat, 2017). Fetal hepatic intrinsic clearance of DEX and BET was scaled to 1.18 L/h. This value is much smaller than the estimated placental intrinsic passive diffusion clearance of these drugs (45 L/h) and is therefore not expected to affect fetal exposure to the ACS as was also noted for other drugs (Zhang et al., 2017). Though fetal livers typically express CYP3A7, while adult livers express CYP3A4/5, our estimate is a conservative one as CYP3A7 turnover of CYP3A substrates tends to be lower than that by CYP3A4/5 (Stevens et al., 2003; Williams et al., 2002).

III. Optimization *of* $K_{p,uu}$ through sensitivity analysis*:* For BET, maternal and fetal plasma concentration-time profiles were simulated with various values of $CL_{int,Pgp,placenta}$ until the predicted UV/MP ratio best described the observed data as determined by minimizing AAFE. $CL_{int,Pgp,placenta}$ was expressed as a fraction of $CL_{int,PD,placenta}$.

$$K_{p,uu} = \frac{CL_{\text{int,PD,placenta}}}{CL_{\text{int,PD,placenta}} + CL_{\text{int,Pgp,placenta}}} \qquad (4.2)$$

For this optimization, we used UV/MP ratio rather than the actual fetal plasma concentration-time profiles because the UV/MP ratios is less confounded by the observed large inter-individual variability in maternal and fetal plasma concentrations. The UV/MP values, each obtained at a single time point, were derived from many maternal-fetal pairs. The observed BET data up to 96 h (Ballabh et al., 2002) allowed us to determine the value of UV/MP ratio plateau, which reflects pseudo-equillibrium between maternal and fetal plasma concentrations. For DEX, a plateau value was not observed within the short sampling duration of 6.5 h(Tsuei et al., 1980). Hence for DEX, we estimated the "theoretical" value of this plateau by fitting a simple Emax model to the observed data using non-linear regression. Then, $CL_{int,Pgp,placenta}$ was adjusted within the m-f PBPK model as described above until the simulated UV/MP ratio plateau achieved the Emax model-derived plateau.

4.3.4 *Designing Alternative IM ACS Dosing Regimens by Predicting Maternal-fetal Exposure of ACS using the m-f PBPK Model*

Once the m-f PBPK model parameters for IM DEX-P and BET-P:A were optimized, they were adjusted for gestational age to GW30 (as the median gestational age when DEX and BET are administered). The m-f PBPK model used to design alternative IM dosing regimens for these ACS that fulfilled the following criteria:

1) Maintain fetal DEX AUC or 5th percentile BET C_{min} as follows:

a) For DEX, fetal drug exposure (AUC_{0-48}) should be no less than that obtained after the reference DEX dosing regimen (6 mg every 12 h for 48 h) (Oladapo et al., 2020).

b) For BET, the fetal 5th percentile C_{min} must be maintained above 1 ng/mL for 48 h. Briefly, the downward adjustment of the dose was carried out until the predicted fetal 5th percentile BET C_{min} reached 1 ng/mL. The cutoff value of 1 ng/mL was based on sheep data, where maintaining BET fetal plasma concentrations >1 ng/mL over 36-48 h after drug administration was necessary for fetal lung maturation (Kemp et al., 2018; Schmidt et al., 2018).

2) Not exceed maternal AUC or 95th percentile C_{max} (or both) of the reference dosing regimen. Alternatively stated, if the maternal AUC of the reference regimen is maintained, maternal 95th percentile C_{max} may be exceeded.

3) The ACS dosing regimen must be convenient to administer (i.e., administer the ACS no more frequently than every 12 h).

4.4 RESULTS

4.4.1 *Verification of SimCYP PBPK Model of ACS using the Observed Data from Non-pregnant Indian Population*

When the SimCYP Simulator® was populated with observed clearance, V_{ss}, renal clearance (CL_R), and other pharmacokinetic parameters obtained in the non-pregnant Caucasian population after IV administration of DEX and BET, the model recapitulated the observed ACS plasma concentration-time profiles within the *a priori* defined acceptance criteria (data not shown). When the model, populated with these parameters, was used to predict $AUC_{0-\infty}$ and clearance in the Indian population after BET-P:A IM administration, the predicted values fell within 0.8- to 1.25-fold of the observed values (except $T_{1/2,\beta}$) (**Figure 4.2 C, D**). In contrast, based on our acceptance criteria, after DEX-P (**Figure 4.2 A, B**) and BET-P IM administration (**Figure 4.2 E, F**), the model underpredicted the $AUC_{0-\infty}$ and overpredicted the clearance observed in the Indian population. The data in Indian non-pregnant population were used for verification after IM administration of BET-P:A because similar data sets in the Caucasian population were not available.

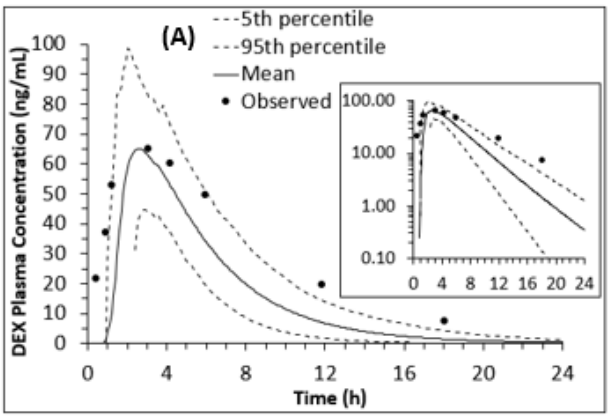

(B)	Observed	Predicted (observed / predicted)	Unit
C_{max}	65	65.2 (1.00)	ng/mL
t_{max}	3	2.6 (1.15)	h
$AUC_{0-\infty}$	643	368.5 (1.74)	h*ng/mL
CL	9.5	14.5 (0.66)	L/h
$T_{1/2,\beta}$	5.2	3 (1.73)	h

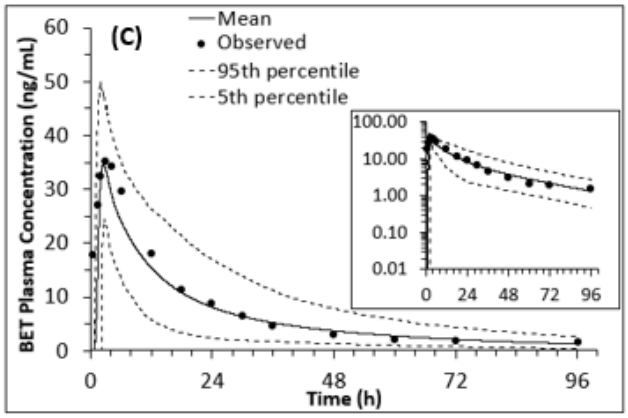

(D)	Observed	Predicted (observed / predicted)	Unit
C_{max}	35.2	34.7 (1.01)	ng/mL
t_{max}	2.9	2.7 (1.07)	h
$AUC_{0-\infty}$	800	690 (1.16)	h*ng/mL
CL	6.2	7.2 (0.86)	L/h
$T_{1/2,\beta}$	51.6	32.7 (1.58)	h

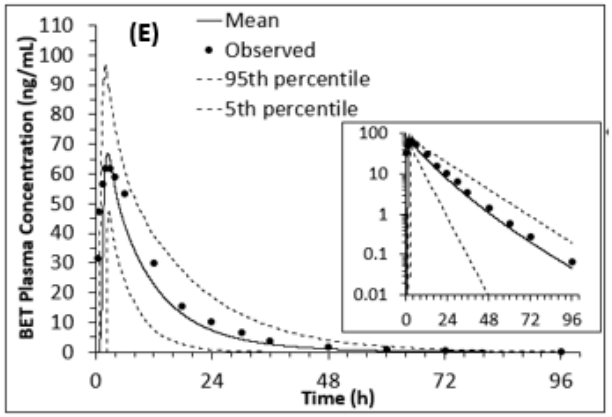

(F)	Observed	Predicted (observed / predicted)	Unit
C_{max}	61.6	66.9 (0.92)	ng/mL
t_{max}	2.2	2.6 (0.85)	h
$AUC_{0-\infty}$	905	700 (1.29)	h*ng/mL
CL	5.4	7.0 (0.77)	L/h
$T_{1/2,\beta}$	7.0	7.0 (1.00)	h

Figure 4.2. Verification of model predicted plasma concentration-time profile after IM betamethasone or dexamethasone administration to Indian non-pregnant women (A) 6 mg DEX-P **(C)** 6 mg BET-P:A **(E)** 6 mg BET-P. Model predicted mean values and their 5th and 95th percentiles are solid and dashed lines respectively **(B, D, F).** Comparison of the observed and predicted pharmacokinetic parameters of profiles shown in A, B, and C respectively showed that model predicted plasma concentration-time profiles were verified for BET-P:A **(D)** but not for DEX-P **(B)** or BET-P **(F)**. BET profiles in **C** were generated using dual absorption input function, where half of the dose (phosphate) was absorbed from the IM site with k_{a1} = 1.5 h^{-1} and

the other half (acetate) was absorbed with k_{a2} = 0.02 h^{-1}. Observed PK parameters were reported previously (Jobe et al., 2020) or estimated from the digitized mean concentration-time profiles using non-compartmental analysis in Phoenix 8.1. Insets show the ACS concentrations plotted on a log scale.

4.4.2 *Verification of m-f PBPK model of ACS in the Pregnant Population*

Consistent with our previous observations (Zhang et al., 2015), to predict the IV plasma concentration-time profiles of the ACS in the Caucasian population at term, we assumed that CYP3A-mediated hepatic intrinsic clearance of the ACS was induced 2-fold by pregnancy (i.e., DEX $CL_{hep,int}$ = 106 L/h and BET $CL_{hep,int}$ = 62 L/h). Using our acceptance criteria, these model-predicted plasma concentration-time profiles were successfully verified by comparing them with the observed profiles after IV administration of BET-P (**Figure 4.3 A, B**) or DEX-P (**Figure 4.3 C, D)**. Then, the m-f PBPK model-predicted plasma concentration-time profiles of the ACS were compared with the observed data after IM administration of DEX-P to pregnant women at term (one data point per subject (Tsuei., et al 1980); **Figure 4.4 A**). For DEX, the values for k_a (3 h^{-1}) and T_{lag} (0.3 h) were optimized to better describe the observed data (AAFE = 1.3). In contrast, simulating a 2-fold induction of BET $CL_{hep,int}$ failed to predict maternal concentrations after IM administration of BET-P:A mixture (AAFE = 2.03) (one data point per subject; **Figure 4.5A**). Surprisingly, the $CL_{hep,int}$ that accurately described maternal BET concentrations with an AAFE of 1.41 was 11.2 L/h, a value much lower than that in the non-pregnant population (**Figure 4.5 B**).

Optimization of DEX and BET $K_{p,uu}$ through sensitivity analysis: For BET, *in vivo* placental efflux clearance yielding $K_{p,uu}$= 0.5 resulted in the best match between the predicted and observed UV/MP ratio ($AAFE_{Kp,uu=0.5}$ = 1.47) vs. when no $CL_{Pgp,placenta}$ was invoked

($AAFE_{Kp,uu=1}$ =2.19) (**Figure 4.5 D**). For DEX, the theoretical UV/MP ratio plateau was estimated as 0.59 using the simple E_{max} model as a mathematical approximation (**Figure 4.4 C**). This value improved model predictions of UV/MP ratios compared to when $CL_{Pgp,placenta}$ of the drug was not incorporated in the model ($AAFE_{Kp,uu=0.48}$ = 1.8; $AAFE_{Kp,uu=1}$ = 3.46) (**Figure 4.4 D**). Furthermore, adjusting the value of $K_{p,uu}$ to 0.31 (0.20 – 0.42 90% CI) allowed the model predicted UV/MP ratios to best match the observed values ($AAFE_{Kp,uu=0.31}$ = 1.43). To develop alternative dosing regimens of the ACS (described below), BET $K_{p,uu}$=0.5 (0.29 – 0.71 90% CI) and DEX $K_{p,uu}$=0.48 (0.30 - 0.66 90% CI) were used. The use of the latter is justified in the discussion.

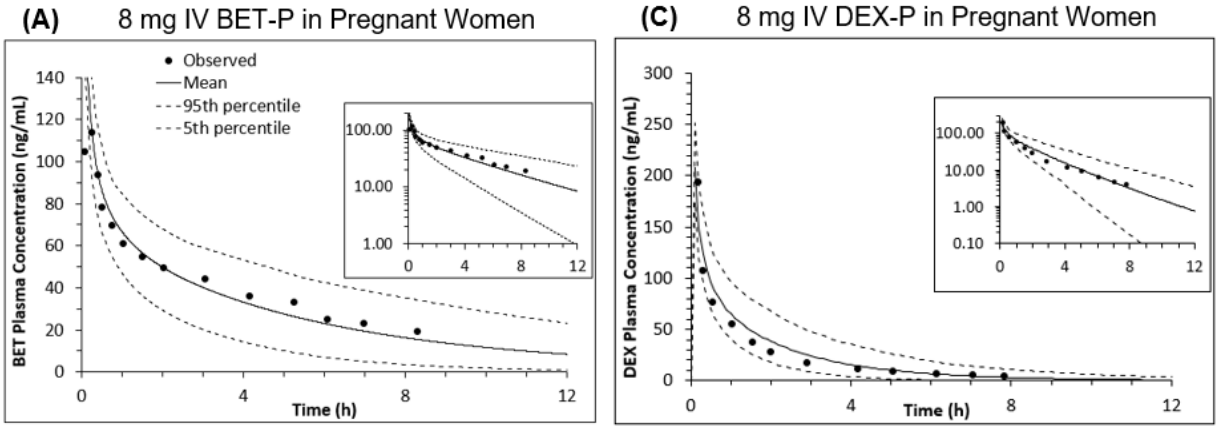

(B)	Observed	Simulated Parameter (observed/predicted)	Unit
$AUC_{0-\infty}$	467	438 (1.07)	h*ng/mL
CL	16.3	18.1 (0.90)	L/h
$T_{1/2,\beta}$	4.4	3.8 (1.16)	h

(D)	Observed parameter (Subject JM)	Simulated parameter (observed/ predicted)	Unit
$AUC_{0-\infty}$	242	243 (1.00)	h*ng/mL
CL	27.5	27.4 (1.00)	L/h
$T_{1/2,\beta}$	1.7	1.6 (1.06)	h

Figure 4.3. Verification of our m-f PBPK model in the pregnant Caucasian population after IV administration of ACS as evidenced by the model predictions falling within our *a priori* defined acceptance criteria. Predicted (mean - solid lines; 5th and 95th percentile – dashed lines) and observed (circles) data after IV administration of **(A)** 8 mg of BET-P at GW37 (one representative subject (Petersen, Collier, et al., 1983)) and **(C)** 8 mg of DEX-P at GW38 (mean of 8 subjects (Tsuei et al., 1980)). Insets in panel A and C show the ACS concentrations plotted on a log scale. **(B, D)** Comparison of observed and predicted pharmacokinetic parameters from data in A and B respectively show that the predicted values met our *a priori* defined acceptance criteria.

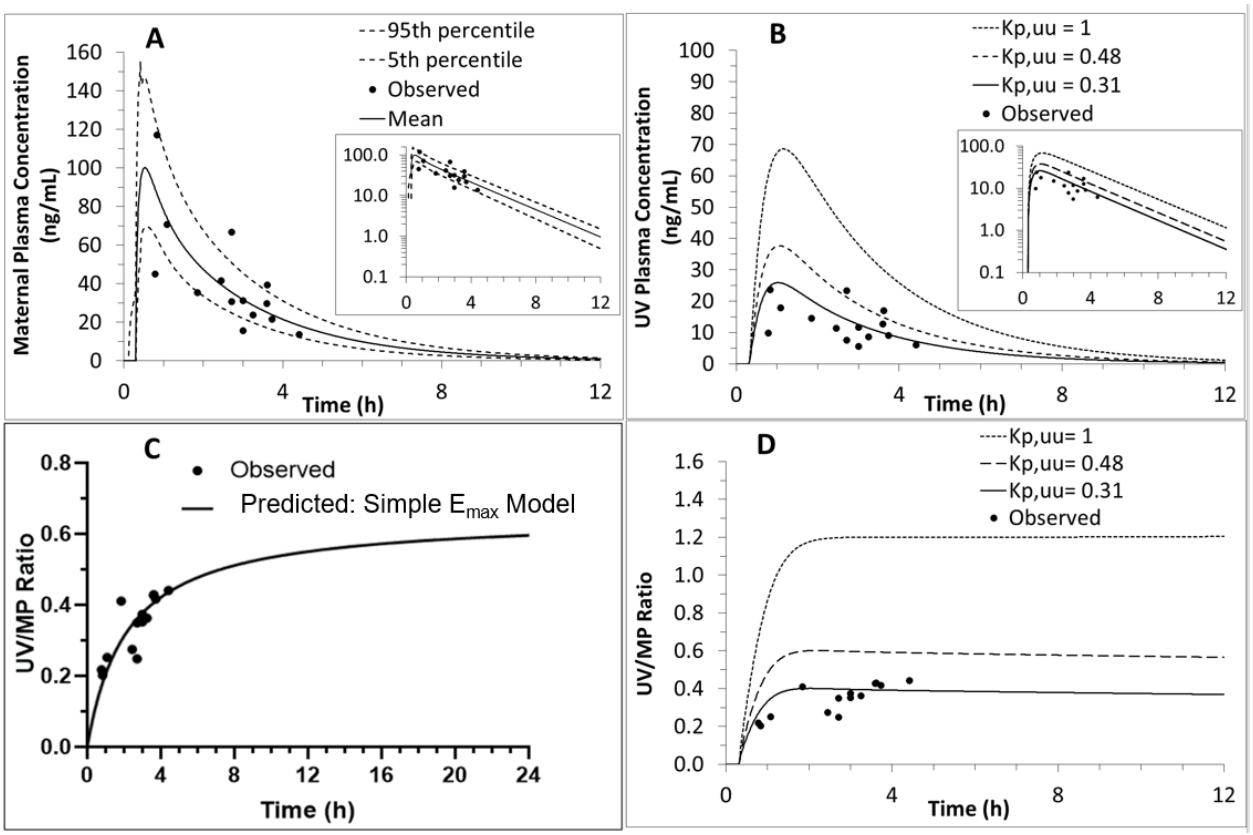

Figure 4.4. m-f PBPK model predictions after IM DEX-P administration for maternal and UV plasma DEX concentration-time profiles as well as UV/MP ratio with and without placental $CL_{int,Pgp,placenta}$ incorporated into our m-f PBPK model. (A) The m-f PBPK model predicted mean maternal plasma concentration-time profile (solid line) described the observed maternal concentrations at the time of delivery (circles; pooled from 14 mothers at GW38 (Tsuei et al., 1980)) after optimization of k_a (3 h^{-1}) and T_{lag} (0.3 h) (AAFE = 1.3). **(B)** The m-f PBPK model predicted umbilical vein (UV) plasma concentration-time profile with $CL_{int,Pgp,placenta}$ ($K_{p,uu}$ = 0.48, dashed line and $K_{p,uu}$ = 0.31, solid line) better described the observed UV plasma concentration-time profile (black circles) than when placental P-gp was not incorporated into the model ($K_{p,uu}$ = 1, dotted line) (UV: $AAFE_{Kp,uu=1}$ = 3.46; $AAFE_{Kp,uu=0.48}$ = 1.8, $AAFE_{Kp,uu=0.31}$ = 1.43). In panels A and B, insets show DEX plasma concentrations plotted on a log scale. **(C)** Predicted plateau value (0.59) of the observed UV/MP ratio determined by fitting the simple Emax model (black line) to the observed data (black circles). This plateau value translates to a $K_{p,uu}$ = 0.48. **(D)** The m-f PBPK model predicted UV/MP ratios without placental $CL_{int,Pgp,placenta}$ ($K_{p,uu}$ = 1, dotted line), with $CL_{int,Pgp,placenta}$ derived from panel C ($K_{p,uu}$ = 0.48, dashed line) or one that allows the model to best describe the observed UV/MP ratios ($K_{p,uu}$ = 0.31, solid line; UV/MP: $AAFE_{Kp,uu=1}$ = 3.30; $AAFE_{Kp,uu=0.48}$ = 1.64, $AAFE_{Kp,uu=0.31}$ = 1.17). Observed data (Tsuei et al., 1980) are shown as filled circles (8 mg DEX-P IM at GW38). Simulated mean profiles are shown as solid lines, 5th and 95th percentile profiles are shown as dotted lines. For the fetus, see **Figure S1** for the 5th and 95th percentile profiles**.**

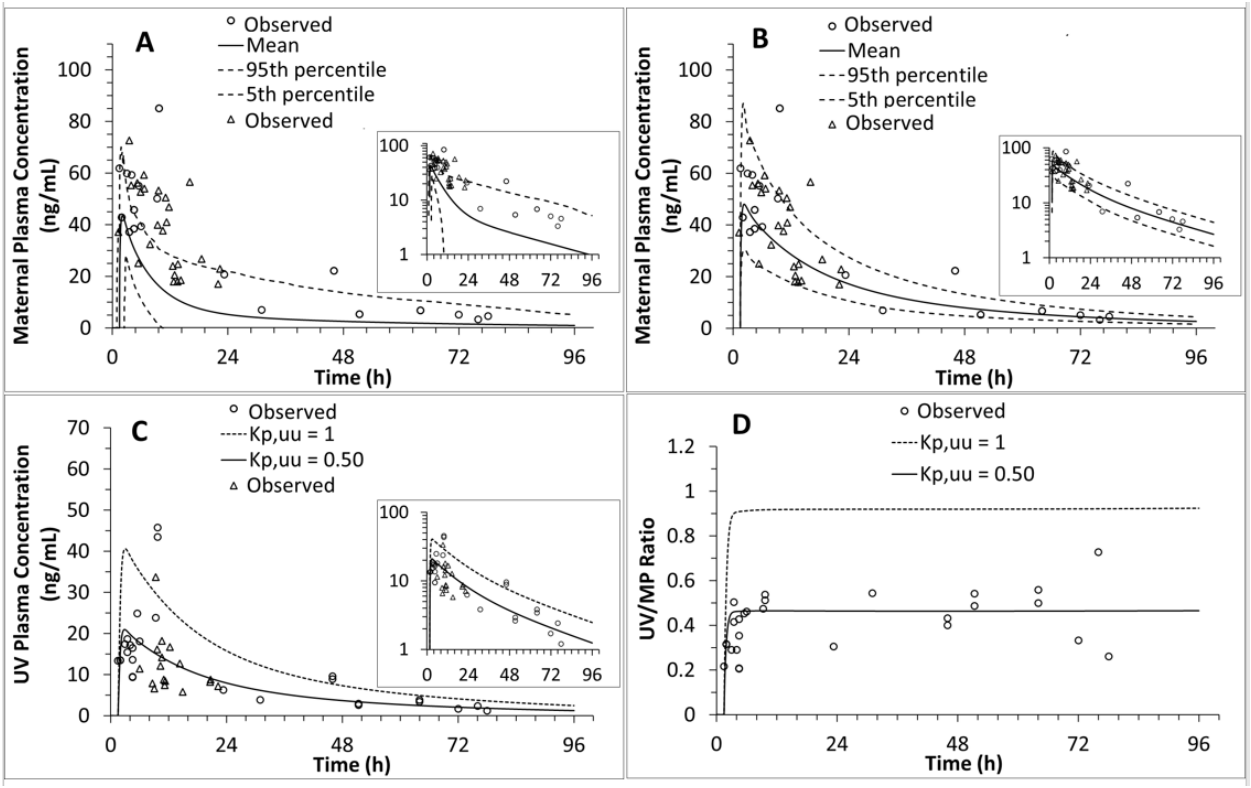

Figure 4.5. m-f PBPK model predictions after IM BET-P:A of maternal and UV plasma BET concentration-time profiles as well as UV/MP ratio with and without $CL_{int,Pgp,placenta}$ incorporated into our m-f PBPK model. (A) Predicted mean maternal plasma concentration-time profile (solid line) with $CL_{hep,int}$ (62 L/h); (a 2-fold increase of clearance compared to non-pregnant individuals). Simulated maternal plasma concentration-time profile poorly predicted the observed data (AAFE = 2.03). The observed data were pooled from 56 mothers at the time of delivery (12 mg BET-P:A IM at GW32; (Ballabh et al., 2002; Foissac et al., 2020)). The open triangles and circles were from 25 and 31 women, respectively. The 5th and 95th percentile profiles are shown as dotted lines. **(B)** When $CL_{hep,int}$ was reduced to 22 L/h, the predicted mean maternal plasma concentration-time profile described the observed data better (AAFE = 1.41). The predicted maternal plasma concentration-time profiles incorporated two rates of absorption k_a (k_{a1} = 1.5 and k_{a2} = 0.02 h^{-1}) and a T_{lag} (1.5 h). **(C)** Predicted mean umbilical vein C-T profile with $CL_{int,Pgp,placenta}$ incorporated into the model ($K_{p,uu}$ = 0.50, solid line) better described the observed concentrations than predictions without $CL_{int,Pgp,placenta}$ ($K_{p,uu}$ = 1, dotted line) ($AAFE_{kp,uu=1}$ = 2.19; $AAFE_{kp,uu=0.5}$ = 1.47). For fetal 5th and 95th percentile profiles see **Figure 4.S1. (D)** Predicted UV/MP ratios with $CL_{int,Pgp,placenta}$ incorporated into the model ($K_{p,uu}$ = 0.50; $AAFE_{kp,uu=0.50}$ =1.26) and no transport ($K_{p,uu}$ = 1; $AAFE_{kp,uu=1}$ = 2.22) demonstrate that $CL_{int,Pgp,placenta}$ was necessary to explain the observed data.

4.4.3 *Designing Alternative IM Dosing Regimens for ACS using m-f PBPK model at GW30*

For the alternative ACS dosing regimens, maternal and fetal C_{max}, C_{min} and AUC_{0-48} over the entire 48 h dosing regimen were computed. The reference regimen of 6 mg IM every 12 h is shown in **Figure 4.6 A.** An alternative DEX-P regimen of 12 mg administered every 24 h (**Figure 4.6 B**) maintained fetal AUC_{0-48} of the reference regimen (342 ng*h/mL). Fetal 5th percentile C_{min} decreased from 0.06 to <0.01 ng/mL. This alternative regimen also resulted in a 2-fold increase in maternal 95th percentile C_{max} (259.0 ng/mL) compared to the 95th percentile C_{max} (129.6 ng/mL) for the reference regimen. As expected, the total maternal exposure (AUC_{0-48}) with the new dosing regimen remained at 771 ng*h/mL, comparable to that for the reference regimen.

Reducing the reference BET-P:A dose to 2.4 mg every 24 h for 48 h (regimen 1; administered as often as the reference regimen; 20% of the total reference dose) (**Figure 4.7 A**) resulted in an 80% decrease in fetal AUC_{0-48} (145 ng*h/mL) and maintained fetal drug plasma concentrations >1 ng/mL for 48 h. Fetal 5th percentile C_{min} of 1 ng/mL was observed at the 48 h time point and decreased by 80% compared to reference regimen (**Figure 4.7 B**). Maternal 95th percentile C_{max} (18.7 ng/mL) and maternal AUC_{0-48} (285 ng*h/mL) also decreased by 80% compared to the BET reference regimen values of 94 ng/mL and 1424 ng*h/mL, respectively (**Figure 4.7 B**).

BET-P:A alternative dosing regimen 2 of single 5.4 mg dose (**Figure 4.7 C**; 22.5% of the total reference dose) decreased fetal AUC_{0-48} by 74% from 724 to 191 ng*h/mL. Fetal 5th percentile C_{min} decreased by 80% from 5 to 1 ng/mL and remained >1 ng/mL for 48 h. Maternal 95th percentile C_{max} (33.7 ng/mL) decreased by 64% vs. the BET-P:A reference regimen (94 ng/mL). Total maternal mean AUC decreased by 74% (375 ng*h/mL) for regimen 2.

We also predicted BET plasma concentrations for a dosing regimen currently used in BETADOSE clinical trial (Schmitz et al., 2019). BET-P:A alternative dosing regimen 3 is a single 12 mg BET-P:A dose (**Figure 4.7 D**; 50% of the total reference dose). Compared to the reference regimen, the fetal $AUC_{0\text{-}48}$ decreased by 41% from 724 to 424 ng*h/mL and fetal 5th percentile C_{min} by 53% from 5 to 2.3 ng/mL, but remained >1 ng/mL for 48 h. Maternal 95th percentile C_{max} (75 ng/mL) decreased by 22% from the BET-P:A reference regimen (94 ng/mL). Total maternal $AUC_{0\text{-}48}$ decreased by 42% (833 ng*h/mL).

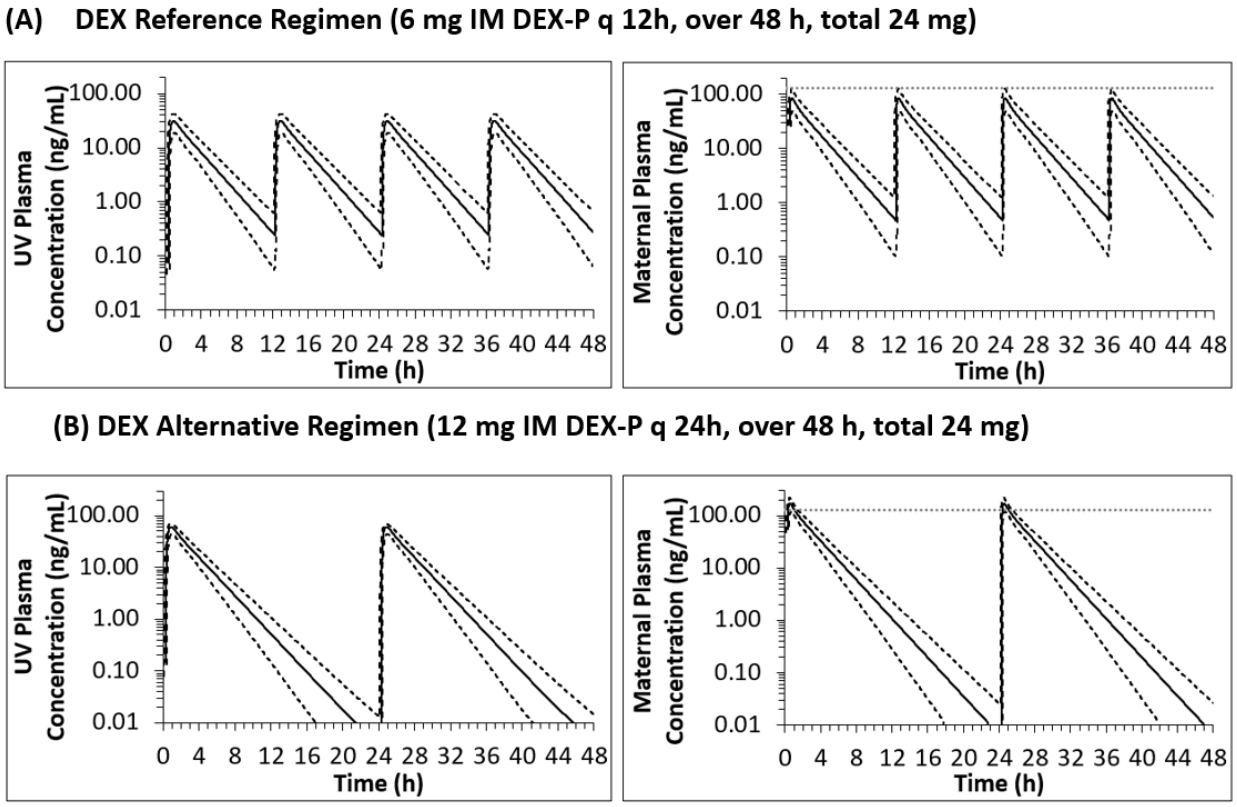

Figure 4.6. Predicted fetal (UV) and maternal plasma concentration-time profiles at GW30 for IM DEX-P reference (A) and an alternative (B) dosing regimen using our final m-f PBPK model. (A) The reference dosing regimen resulted in fetal $AUC_{0\text{-}48}$ of 342 ng*h/mL, UV 5th percentile C_{min} of 0.06 ng/mL (dashed line) and mean UV C_{min} of 0.24 ng/mL (solid line). The corresponding maternal values were 771 ng*h/mL for $AUC_{0\text{-}48}$ and 129.6 ng/mL 95th percentile C_{max} (dashed line). **(B)** The alternative dosing regimen maintained fetal $AUC_{0\text{-}48}$ of

342 ng/mL, decreased fetal UV 5th percentile C_{min} to <0.01 ng/mL. The maternal 95th percentile C_{max} (259.0 ng/mL) increased 2-fold while maintaining AUC_{0-48} at 771 ng*h/mL. Predicted mean plasma concentration-time profiles are solid lines, 5th and 95th percentiles are dashed lines. Horizontal dotted lines in maternal plasma concentration-time profiles denote maximum targeted cut-off value for maternal 95th percentile C_{max} (129.6 ng/ml defined by the reference dosing regimen). The C_{min} and C_{max} values were values determined over the entire 48 h period.

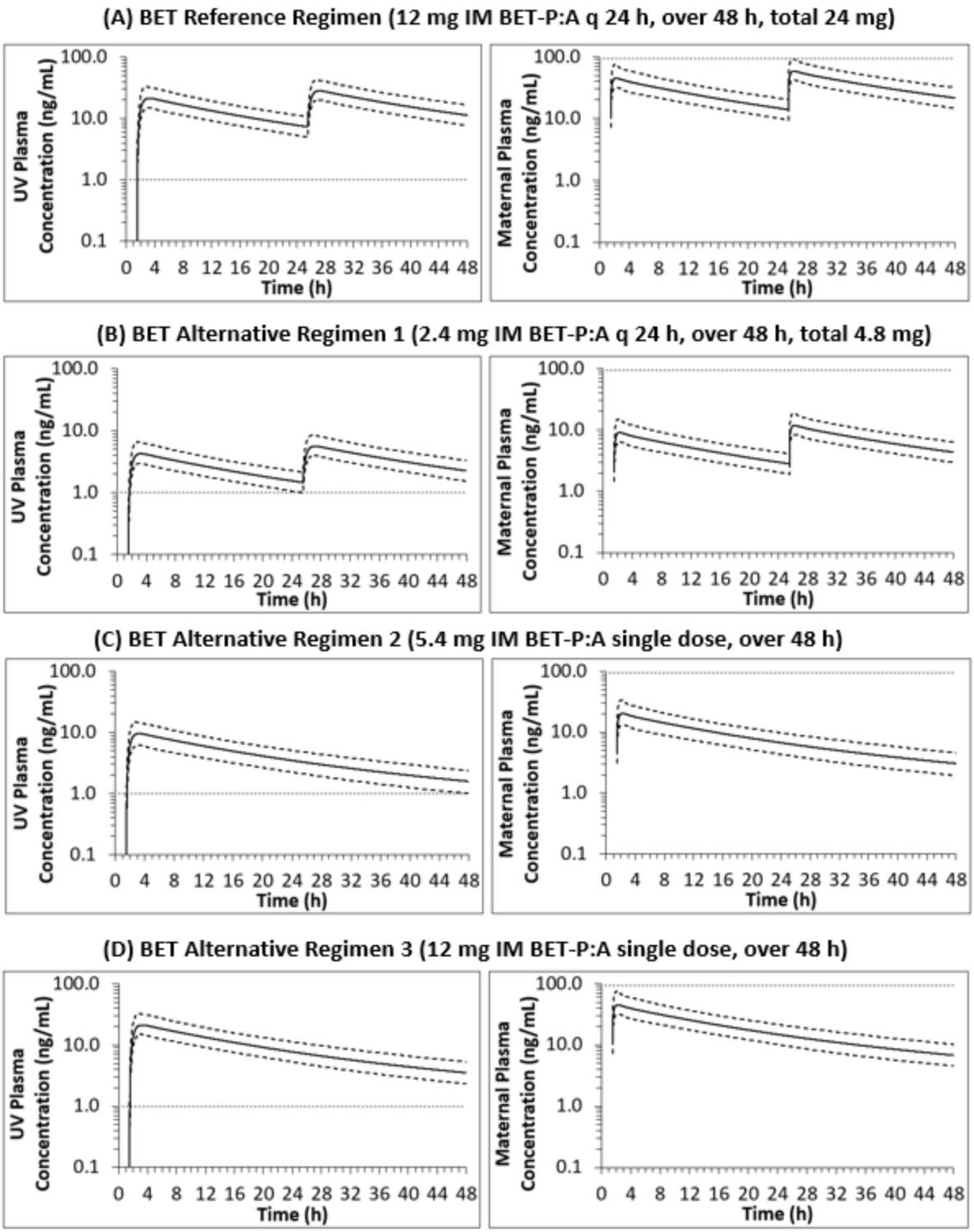

Figure 4.7. Predicted fetal and maternal UV plasma concentration-time profiles at GW30 for the IM BET-P:A reference (A) and alternative dosing regimens (B-D) using our final m-f PBPK model (A) The reference dosing regimen resulted in greater than 1 ng/mL fetal UV 5th percentile C_{min} (5 ng/mL) and mean UV C_{min} (7.3 ng/mL). Fetal AUC_{0-48} was 724 ng*h/mL. The

corresponding maternal values were 94 ng/mL and 1424 ng*h/mL respectively. **(B)** The alternative dosing regimen 1 decreased fetal UV 5th percentile C_{min} by from 5 to 1 ng/mL and maintained UV plasma concentration above 1 ng/mL for the duration of drug administration (48 hr). Fetal AUC_{0-48} decreased to 145 ng*h/mL, maternal 95th percentile C_{max} to 18.7 ng/mL and maternal AUC_{0-48} to 285 ng*h/mL. Fetal UV 5th percentile C_{min}, fetal AUC_{0-48} and maternal 95th percentile C_{max} as well as the total dose decreased by 80% compared to reference BET:P-A dosing regimen. **(C)** The alternative dosing regimen 2 decreased fetal UV 5th percentile C_{min} by 80% (from 5 to 1 ng/mL) and maintained UV plasma concentration above 1 ng/mL for the duration of drug administration (48 hr). Fetal AUC_{0-48} decreased by 74% to 191 ng*h/mL. The maternal 95th percentile C_{max} (33.7 ng/mL) decreased by 64% and the AUC_{0-48} (375 ng*h/mL) decreased by 74%. **(D)** The alternative dosing regimen 3 (currently used in BETADOSE clinical trial (Schmitz *et al.*, 2019)) decreased fetal UV 5th percentile C_{min} by 53% (from 5 to 2.3 ng/mL) and maintained UV plasma concentration above 1 ng/mL for the duration of drug administration (48 hr). Fetal AUC_{0-48} decreased by 41% to 424 ng*h/mL. The maternal 95th percentile C_{max} (75 ng/mL) decreased by 22% and the AUC_{0-48} (833 ng*h/mL) decreased by 42%. Predicted mean plasma concentration-time profiles are solid lines, 5th and 95th percentiles are dashed lines. Horizontal dotted line in maternal plasma concentration-time profiles denote maximum cut-off value for maternal 95th percentile C_{max} (94 ng/mL defined by the reference dosing regimen). Horizontal dotted line in fetal plasma concentration-time profiles denote minimum cut-off value for fetal 5th percentile C_{min} (1 ng/mL). These C_{min} and C_{max} values are values determined over the entire 48 h period.

4.5 DISCUSSION

Safe and efficacious ACS dosing is critical to reduce morbidity and mortality due to preterm delivery. In the present work, we used m-f-PBPK modeling to predict and verify maternal-fetal exposure to ACS. We used our m-f-PBPK model to propose alternative ACS dosing regimens that could maximize ACS efficacy while minimizing ACS toxicity or could be more convenient to implement in the clinic due to reduced frequency of administration.

To develop our ACS m-f-PBPK model, we first ensured that our PBPK model could describe ACS exposure after IM administration to non-pregnant Indian population (**Figure 4.2**). The m-f PBPK successfully verified the observed data (**Figure 4.2 C, D**). However, our model modestly over-predicted BET clearance in this population perhaps due to ethnic differences in BET clearance. The overprediction was not unduly concerning as this data set was used to estimate the two k_a for BET-P:A necessary to describe two distinct absorption (or release) phases of the phosphate and acetate prodrug (Ke & Milad, 2019). Once the PBPK model was verified for the non-pregnant population, the drug-dependent parameters were fixed and our m-f-PBPK model was populated with these parameters. Then, we verified our m-f PBPK model after IV administration of ACS in pregnancy (**Figure 4.3**). To do so, we incorporated the previously reported 2-fold induction of hepatic CYP3A4 activity at term (Zhang et al., 2015). BET and DEX are cleared from the body predominately by CYP3A metabolism (Gentile, Tomlinson, Maggs, Park, & Back, 1996; Varis, Kivisto, Backman, & Neuvonen, 2000). Indeed, this magnitude of induction was consistent with the observed 2-fold increase in midazolam clearance (a selective CYP3A probe) during the 3rd trimester (**Figure 4.3**). While others have reported different magnitudes of CYP3A induction in the 3rd trimester, these findings have been based on studies where a selective CYP3A probe was not utilized (Dallmann, Ince, et al., 2018; De Sousa

Mendes et al., 2017; Xia et al., 2013). However, for BET, the observed clearance after BET-P:A administration in pregnancy (5.7 L/h (Ballabh et al., 2002)) was surprisingly lower than after IV BET-P administration (16.3 L/h) (**Figure 4.5A**). The reasons for this decrease are not clear and should be explored further. Since the goal of this study was to *predict* fetal rather than maternal drug plasma concentrations, it was important to accurately *describe* maternal BET plasma concentration-time profiles. Hence, we decreased BET maternal $CL_{hep,int}$ to best describe BET maternal plasma concentration-time profile after intramuscular BET-P:A administration (**Figure 4.5 B**).

In order to accurately predict fetal DEX and BET plasma concentration-time profiles, it is important to account for the processes that govern transplacental transfer of these drugs into the fetus (i.e., passive diffusion and active placental efflux clearances). Since both drugs are substrates of P-gp (Crowe & Tan, 2012; Yates et al., 2003), which is highly abundant in placenta (Anoshchenko et al., 2020; Ceckova-Novotna et al., 2006; Han et al., 2018; Mathias et al., 2005), we aimed to optimize their magnitude of P-gp mediated efflux to obtain fetal drug exposure (*in vivo* $K_{p,uu}$) that agreed with the observed data. Our PBPK modeling showed that the *in vivo* $CL_{int,PD,placenta}$ for both drugs was indeed large and limited by placental blood flow (~45 L/h in 3rd trimester). Moreover, not accounting for placental efflux resulted in overestimation of fetal drug exposure and therefore underestimation of the maternal dose needed to maintain a fetal plasma concentration of >1 ng/mL.

The obtained $K_{p,uu}$ value for BET (0.5) was determined with greater confidence (**Figure 5**) than for DEX ($K_{p,uu}$ = 0.48 or 0.31) (**Figure 4.4**) due to excellent agreement of our model predicted BET UV/MP ratio with observed data (Ballabh et al., 2002; Ballard et al., 1975; Gyamfi et al., 2010). In preliminary Transwell® efflux studies in P-gp overexpressing MDCKII

cells, we found similar *in vitro* efflux ratios of DEX and BET (**Chapter 3**) suggesting that the *in vivo* $K_{p,uu}$ of these drugs should be similar. For this reason, to develop alternative dosing regimens for DEX, we used $K_{p,uu}$ = 0.48, a value close to that of BET. However, the *in vivo* DEX UV/MP data suggest that DEX $K_{p,uu}$ could just as well be 0.31. To resolve this discrepancy, additional *in vivo* DEX data sets are needed to better define its *in vivo* $K_{p,uu}$. DEX and BET do not appear to be transported by BCRP (**Chapter 3**).

In practice, the efficacy of the ACS reference regimens in reducing RDS is modest. When the reference ACS regimens are used, the relative risk of RDS (compared with placebo) ranges from 0.6 to 1.16 (Collaboration, 1981; Gyamfi-Bannerman & Thom, 2016; Liggins & Howie, 1972; Oladapo et al., 2020) suggesting a need to optimize the ACS dosing regimens. However, increasing the ACS dosing rate could potentially enhance ACS toxicity. For example, when the reference DEX-P regimen is used, maternal infections significantly increased from 6% in the placebo arm to 10% in the ACS arm (odds ratio of 1.64) (Althabe et al., 2015). Likewise, there are concerns of long-term neonatal neurodevelopmental toxicity (Crowther et al., 2007; Raikkonen et al., 2020; Wapner et al., 2006). Therefore, we used the m-f PBPK model to propose alternative ACS dosing regimens that could enhance ACS efficacy while minimizing their toxicity. It is not clear whether the efficacy and toxicity of these ACS is related to their maternal-fetal exposure (AUC) or C_{max} or both. In the absence of this information when designing alternative ACS dosing regimens, we took the conservative approach of not exceeding the reference regimen ACS maternal-fetal exposure (AUC) or C_{max} or both. In addition, for BET only, we designed dosing regimens based on maintaining fetal plasma concentration >1 ng/mL based on the efficacy data in sheep (Schmidt et al., 2018). When designing these alternative

dosing regimens, we also took into consideration the dosing frequency of the regimen so that it was convenient to implement in the clinic (not more frequent than twice a day).

To design a convenient alternative dosing regimen for IM DEX-P (**Figure 4.6 B**), fulfilling criterion 3 in **Methods**), we reduced the number of doses since the reference regimen is already administered every 12 h (**Figure 4.6 A**). Administering a two-fold higher dose, but less frequently (every 24 h) helped us maintain maternal and fetal AUCs (fulfilled criterion 1a and 2). As a consequence, maternal peak concentrations rose, which in clinic may increase efficacy but produce higher incidence of adverse events than observed after reference dosing regimen (maternal infection rate of 5-6% (Oladapo et al., 2020)). Due to the lack of animal or human data on fetal efficacy after lower IM DEX-P doses, we refrained from designing a regimen that would decrease fetal and maternal AUC. However, when such data are available, our model could be used to design regimens with lower doses.

To design a convenient alternative dosing regimen for IM BET-P:A (criterion 3) (**Figure 4.7 B**), we could increase (every12 h), maintain (every 24 h) (**Figure 4.7 B**) or decrease (single dose over 48 h) (**Figure 4.7 C, D**) the number of administered BET-P:A doses. Increasing the number of doses to every 12 h to maintain maternal and fetal AUC as for DEX-P above, produced similar maternal and fetal BET C_{max} and C_{min} as in reference regimen, and was therefore not considered further. Availability of sheep data (Kemp et al., 2018; Schmidt et al., 2018) gave us a new guideline for efficacious fetal drug plasma concentrations >1 ng/mL (criterion 2b). These data allowed us to decrease BET-P:A dose from 12 to 2.4 mg every 24 h (**Figure 4.7 B**) or to a 5.4 mg single dose (**Figure 4.7 C**) and fulfill criteria 1b and 2. These decreased doses resulted in decreases in fetal AUC and C_{max} and relied on the assumption that efficacious BET plasma concentrations can be translated from sheep to humans. This assumption

and proposed dosing regimens should be assessed in the clinic to ensure fetal therapeutic benefit. The ongoing BETADOSE clinical trial (Schmitz et al., 2019) is exploring the efficacy and safety of another BET-P:A dosing regimen that reduces the total administered IM BET-P:A dose (12 mg IM BET-P:A administered as a single dose). Simulations of maternal-fetal drug plasma concentrations for this dosing regimen are provided (**Figure 4.7 D**). Overall, lower BET drug plasma concentrations, smaller fluctuations and less frequent administration make it more attractive therapeutic option than DEX, but this conclusion should be tested in the clinic.

There are several limitations to this study, most of which are related to the limited clinical data for these ACS in pregnancy. First, maternal-fetal pharmacokinetic data on these ACS are limited, especially for DEX-P and therefore any inaccuracies in the published data will result in inaccuracies in the predicted dosing regimens. Second, limited clinical data and PK are available for different ethnic populations, especially those from countries where preterm delivery rates and ACS use are high. DEX and BET clearance for non-pregnant Caucasian population was 15 L/h and 7-17 L/h, respectively (Ke & Milad, 2019), which are higher than the values for the Indian non-pregnant women (DEX: 9-10 L/h; BET: 5-6 L/h) (**Figure 4.2 B, D, F;** (Jobe et al., 2020)). A similar observation was made for nifedipine, another CYP3A substrate (Ahsan et al., 1993). Therefore, we used PK parameters from Caucasian non-pregnant population and verified our m-f PBPK model with data from Caucasian pregnant women. Hence, PK/PD studies in pregnant Indian women are needed and are underway (Oladapo et al., 2020). A study conducted by World Health Organization is investigating the efficacy of IM BET-P at 2 mg every 12 h for 48h. Therefore, for comparison, we predicted the maternal-fetal exposure to BET for this dosing regimen (**Figure 4.S2**). If this regimen is found to be efficacious as the BET-P:A reference regimen, it has the potential to reduce maternal-fetal risks. Ideally, future studies will produce

high-quality data sets with maternal-fetal paired sampling, that include accurate recording of time post-last dose, and stabilization of hydrolysis of the ACS prodrugs after collection. The *in vivo* hydrolysis could be a source of error. The *in vivo* cleavage of BET-P to the BET is rapid and appears to be complete within 60 min (Samtani, Schwab, Nathanielsz, & Jusko, 2004). Corresponding data for DEX-P or BET-A are not available. Since *in vivo* hydrolysis of BET-A is slower than BET-P, if substantial amount of BET-A is present in the drawn blood sample and is subsequently hydrolyzed to BET prior to freezing, this could potentially explain the lower than anticipated clearance of BET in pregnant women when BET-P:A is administered but not when BET-P is administered. Parenthetically, the ACS UV/MP data used in these analyses were obtained at least 60 min after ACS prodrug administration.

To our knowledge, this is the first study to simulate maternal-fetal ACS exposure in pregnancy. Here we provide a tool, our m-f PBPK model, to predict maternal-fetal exposure to ACS that can be adapted for other ACS dosing regimens. Due to the longer half-life of BET and the slower release of BET-P:A from the IM site, our simulations suggest that BET could be administered at a lower dose than currently recommended and yet maintain its efficacy based on sheep data. Studies to verify these predictions are urgently needed to promote the optimal dose of ACS for fetal lung development in imminent preterm labor, especially in low-to-middle income countries, where rates of preterm birth are high.

4.6 SUPPLEMENTARY INFORMATION

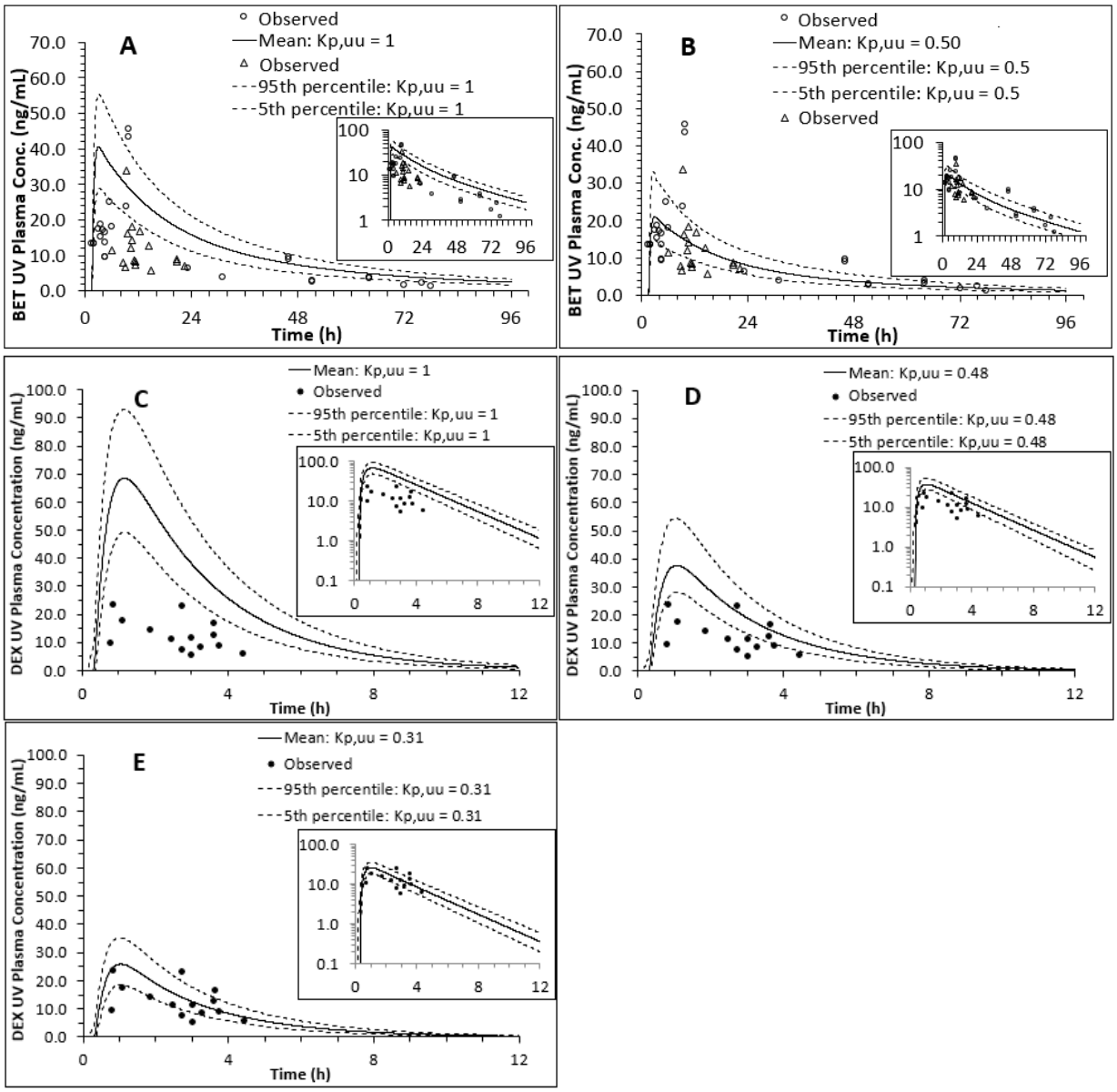

Figure 4.S1. Optimization of fetal plasma concentrations generated by our m-f PBPK model after intramuscular administration of BET-P:A (A-B) or DEX-P (C-E) to Caucasian pregnant women. (A-B) Predicted mean BET UV C-T profiles (solid lines) and 5th and 95th percentile (dashed lines) without (A: $K_{p,uu}$=1) and with (B: $K_{p,uu}$=0.50) P-gp efflux transport incorporated into the model. Observed data (empty triangles and circles) are from Ballabh *et al.*(Ballabh et al., 2002) and Foissac *et al.*(Foissac et al., 2020), respectively. **(C-E)** Predicted mean DEX UV C-T profiles (solid lines) and 5th and 99th percentiles (dotted lines) without (C: $K_{p,uu}$=1) and with (D: $K_{p,uu}$=0.48 or E: $K_{p,uu}$=0.31) Pgp efflux transport incorporated into the model. Observed data (filled circles) are from Tsuei *et al.*(Tsuei et al., 1980).

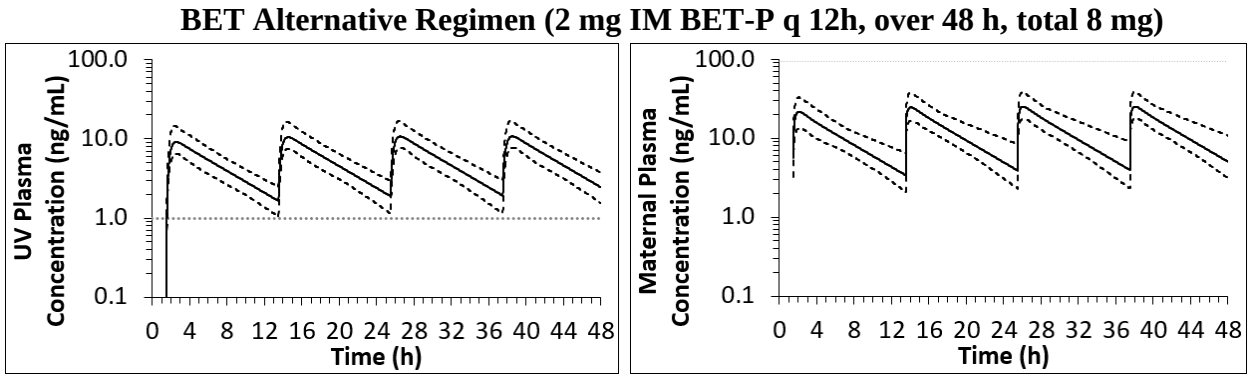

Figure 4.S2. Predicted fetal and maternal UV C-T profiles for an IM BET-P regimen. This dosing regimen of IM BET-P resulted in fetal $AUC_{0\text{-}48}$ of 248 ng*h/mL which is 66% lower than $AUC_{0\text{-}48}$ of BET P:A reference regimen (724 ng*h/mL). Fetal UV 5th percentile C_{min} remained above 1 ng/mL for the duration of drug administration (48 hr). Maternal $AUC_{0\text{-}48}$ (542 ng*h/mL) and 95th percentile C_{max} (38.2 ng/mL) were 38% and 41%, respectively, of the BET-P:A reference regimen. Predicted mean C-T profiles are solid lines, 5th and 95th percentiles are dashed lines. Horizontal dotted lines in maternal C-T profiles denote maximum targeted cut-off value for maternal 95th percentile C_{max} (94 ng/mL defined by the reference dosing regimen). Horizontal dotted lines in fetal C-T profiles denote minimum targeted cut-off value for fetal 5th percentile C_{min} (1 ng/mL).

4.7 ABBREVIATIONS USED

5^{th} percentile: 5^{th} percentile confidence values; 95^{th} percentile: 95^{th} percentile confidence values; ACS: antenatal corticosteroids; AAFE: absolute average fold error; AUC_f: area under the curve of total fetal plasma concentration-time profile; AUC_m: area under the curve of total maternal plasma concentration-time profile; BCRP: breast cancer resistant protein; BET: betamethasone; BET-P: betamethasone phosphate; BET-P:A: 1:1 betamethasone phosphate and acetate mixture; C-T: plasma concentration-time profile of a drug; CI: confidence interval; $CL_{int,PD,placenta}$: unbound intrinsic placental passive diffusion clearance; $CL_{hep,int}$: intrinsic hepatic clearance; $CL_{int,Pgp,placenta}$: *in vivo* P-gp mediated efflux clearance from placenta; CL_{PM}: total placental-maternal plasma clearance; C_{max}: maximum plasma drug concentration; C_{min}: minimum plasma drug concentration; CYP: cytochrome P450; DEX: dexamethasone; DEX-P: dexamethasone phosphate; E_{max}: maximum effect; fCL_{int}: intrinsic fetal hepatic clearance; F_t: fraction transported; IM: intramuscular; IV: intravenous; k_a: absorption rate constant; HLM: human liver microsomes; K_p: partition coefficient; $K_{p,uu}$: unbound partition coefficient; ; m-f PBPK model: maternal-fetal physiologically based pharmacokinetic model; MDCK: Madin-Darby canine kidney; MP: maternal plasma; P_{app}: apparent permeability; P-gp: P-glycoprotein; PK: pharmacokinetics; RDS: respiratory distress syndrome; T_{lag}: lag time; UV: umbilical vein; V_{ss}: volume of distribution at steady-state; WHO: World Health Organization.

Chapter 5. CONCLUSIONS

5.1 GENERAL CONCLUSIONS

Although 80% of pregnant women take medication (drugs), the issue of risks and benefits to the fetus (who is *de facto* exposed to drugs the mother takes), remain unaddressed (Scaffidi et al., 2017). These fetal risks and benefits are likely linked to fetal drug exposure and hence determining fetal drug exposure is key to safe and efficacious drug administration in pregnancy. Since measuring fetal drug exposure in the clinic is not routinely feasible, predicting it *in silico* presents an alternative. Hence, we extended our m-f PBPK model, previously successfully verified for drugs that only passively diffuse through placenta (Zhang et al., 2017; Zhang & Unadkat, 2017), to drugs that are transported by the placenta (e.g., by the efflux transporter, P-gp). Therefore, our **goal** was to **predict *in vivo* human fetal plasma drug exposure to placental transporter drug substrates using *in vitro* to *in vivo* extrapolation (IVIVE) and then to verify these predictions by comparing them with the corresponding *in vivo* data**. We focused our study on one transporter, P-gp, because it is highly abundant in the placenta (Anoshchenko et al., 2020; Mathias et al., 2005) and it is arguably the most important transporter for drugs routinely administered to pregnant women (e.g., HIV drugs, antenatal corticosteroids, anti-diabetics, antibiotics). We selected for our study four model P-gp substrates: dexamethasone (DEX), betamethasone (BET), darunavir (DRV) and lopinavir (LPV). For DEX and BET, the fetus is the therapeutic target, as these antenatal corticosteroids (ACS) are used to prevent respiratory distress syndrome (RDS). For DRV and LPV, both the mother and the fetus are the therapeutic target. For all the drugs, maternal-fetal safety and efficacy are critical to assess and maintain.

Fetal drug exposure can be quantified by fetal $K_{p,uu}$, the ratio of fetal to maternal unbound plasma AUCs. Since a recent IVIVE method was successful in predicting **brain** $K_{p,uu}$ of efflux transporter substrates in preclinical species (Trapa et al., 2019; Uchida et al., 2011; Uchida, Wakayama, et al., 2014) and in humans (Storelli, Anoshchenko, et al., 2021), we used this approach to predict **fetal** $K_{p,uu}$ for DEX, BET, DRV and LPV. We measured the efflux ratio (ER) of the four P-gp substrates in our *in vitro* system (hMDR1-MDCK$^{cP\text{-}gpKO}$) and scaled it with the relative expression factor (REF) to predict *in vivo* fetal $K_{p,uu}$ (ER-REF approach). The REF accounts for the difference in transporter abundance between the placental tissue and hMDR1-MDCK$^{cP\text{-}gpKO}$ cells. We found that P-gp abundance was approximately 10-fold higher in the hMDR1-MDCK$^{cP\text{-}gpKO}$ cells (**Chapter 3**) than in term human placentae (**Chapter 2**). To verify our ER-REF $K_{p,uu}$ predictions, we compared predicted $K_{p,uu}$ values to the observed $K_{p,uu}$ values estimated by our m-f PBPK model using the UV/MP ratio data for these drugs at term (**Chapter 3 and 4**). We concluded that our verification was successful, as our ER-REF predicted $K_{p,uu}$ values fell within the 90% confidence interval ($CI_{90\%}$) of the observed values (**Chapter 3**).

To illustrate the utility of our m-f PBPK model and our estimated $K_{p,uu}$ values, we designed alternative dosing regimens of DEX and BET at gestational week 30 (GW30) (**Chapter 4**). Dosing regimen optimization of these drugs is warranted due to concerns of limited efficacy and the observed adverse events associated with their currently used dosing regimens (reference regimen) (Althabe et al., 2015; Crowther & Harding, 2007; Oladapo et al., 2020; Raikkonen et al., 2020; Roberts et al., 2017; Vogel et al., 2017). For DEX-phosphate we developed an alternative regimen at a higher dose that could be administered less frequently than the reference regimen, while maintaining the total dose administered over 48 h. For BET-phosphate:acetate mixture we developed two dosing regimens that decreased the total administered dose by 78-

80% when compared to the reference regimen. These alternative dosing regimens should be rigorously evaluated for their efficacy and toxicity prior to their use in clinic.

In summary, this dissertation describes a method to successfully predict fetal exposure to drugs irrespective of whether they are transported. Since UV/MP ratios at term are not available for all drugs prescribed in pregnancy, and studies in pregnant women historically have been difficult to conduct, our method allows the prediction of fetal exposure to drugs, regardless of their mode of transplacental passage. With knowledge of placental transporter abundance (Anoshchenko et al., 2020), the ER-REF approach can predict fetal exposure to placental transported drugs at various gestational ages. Our ER-REF scaling approach can easily be adapted to substrates of multiple placental transporters (e.g., P-gp and/or BCRP; see below) as was shown previously for transport-mediated brain uptake and distribution (Trapa et al., 2016; Trapa et al., 2019). Overall, our m-f PBPK model provides means to prospectively predict fetal exposure to drugs at various gestational ages to help evaluate potential fetal benefits and risks associated with maternal drug administration.

5.2 Challenges and Future Directions

When ER-REF predicted $K_{p,uu}$ was incorporated into our m-f PBPK model, we observed excellent agreement of predicted DRV and LPV UV/MP ratio profiles with the observed data, but modest overprediction of the DEX and BET observed UV/MP ratios (**Chapter 3**). In other words, by accounting only for placental P-gp efflux of DEX and BET, we overpredicted the magnitude of net fetal drug transfer, and, hence, underpredicted the magnitude of all placental/fetal drug elimination processes. This finding highlights the complexity of drug transfer through the placenta and suggests that there are other processes, besides P-gp efflux, responsible for further elimination of fetal drug. One such process is placental drug efflux by other transporters. Our study demonstrated that neither DEX nor BET are substrates of BCRP in BCRP-overexpressed MDCKII cells. Although the possibility of BCRP contributing to the lower-than-expected fetal DEX/BET UV/MP ratios was excluded, other transporters such as multidrug resistance-associated protein 2 (MRP2) should be investigated. Another process that can contribute to UV/MP ratio overprediction is placental metabolism of DEX and BET. These drugs are known to be metabolized by 17β-hydroxysteroid dehydrogenase 2 (17β -HSD2), but the consensus as to rate and extent of such metabolism has not yet been established (Blanford & Murphy, 1977; Levitz, Jansen, & Dancis, 1978; Murphy et al., 2007; Smith, Thomford, Mattison, & Slikker, 1988). Additional *in vitro* (e.g., human placental microsome) or perfused placenta studies could address this issue.

We encountered an additional challenge in our m-f PBPK modeling of BET maternal plasma concentrations after IM BET-P:A administration (**Chapter 4**). We expected enhanced BET clearance after BET P and BET P:A administration in pregnant women based on the 2-fold induction of CYP3A enzymes, the predominant enzymes for BET metabolism, in pregnancy

compared to non-pregnant population (Hebert et al., 2008; Zhang et al., 2015). After IV administration of BET-P, BET clearance was increased 2-fold in pregnant women, though surprisingly, that was not the case after BET P:A administration (Ballabh et al., 2002). The reasons for these discrepant observations are not clear, but they emphasize the importance of further investigation of hepatic and extrahepatic metabolism of BET by other CYP and non-CYP enzymes, including 17β -HSD2. Esterase-mediated cleavage of acetate of BET-A in unstabilized samples following IM BET-P:A administration can result in artificially higher observed BET concentrations, a higher AUC and, hence lower clearance after the IM BET-P:A administration and can potentially contribute to the observed lack of induction in drug clearance in pregnancy. While BET-P stabilization by sodium arsenate and ethylenediaminetetraacetic acid has been studied (Samtani et al., 2004), stabilization of BET-A has not and needs to be further evaluated.

Lastly, we acknowledge the elasticity in estimates of the observed DEX fetal $K_{p,uu}$ (0.31 or 0.48). Informed by our Transwell assays, DEX and BET have similar efflux ratios in hMDR1-MDCK$^{cP\text{-}gpKO}$, and we chose the value of DEX fetal $K_{p,uu}$ (0.48) closest to the one for BET (0.5) to design the DEX alternative dosing regimen. The observed DEX $K_{p,uu}$ value cannot be determined accurately from the UV/MP ratio profile, since the UV/MP ratio plateau was not reached within the sampling time frame of 6.5 h (Tsuei et al., 1980). Thus, the $K_{p,uu}$ value for DEX can range from 0.31 to 0.48.. To accurately estimate observed fetal DEX $K_{p,uu}$, additional data beyond 6.5 h on observed DEX UV/MP ratios at term are needed.

Overall, the most prominent challenge with our m-f PBPK model verification was the paucity and quality of observed data. In order for a data set to be useful for such modeling efforts, it needs to include: 1) paired UV and MP data; 2) recorded time after dosing for both the UV and MP samples; 3) UV/MP ratio over a span that allows this ratio to reach pseudo-

equilibrium; 4) gestational age of the mothers and a sufficient number of subjects in the clinical study for a reliable pooled analysis; 5) accurate information on drug dose and formulation; 6) a rich maternal plasma concentration data set to accurately predict maternal plasma concentrations that influence the fetal drug plasma concentrations. The availability of such data sets will further increase confidence in our m-f PBPK predictions.

In future studies, we aim to verify our ER-REF approach and m-f PBPK model for additional placental efflux transporter substrates. These will include additional substrates of P-gp (e.g., nelfinavir), BCRP (e.g., efavirenz) or both P-gp and BCRP (e.g., imatinib). Both the ER-REF approach and our model can incorporate dual transporter substrates. With model verification for additional drugs, we will gain even greater confidence in our model and approach. Additionally, some drugs administered in pregnancy are substrates of placental influx transporters with reported UV/MP ratios of greater than 1. Such drugs include metformin, an anti-diabetic drug and a placental OCT3 substrate (Lee et al., 2018; Vanky, Zahlsen, Spigset, & Carlsen, 2005). The potential of these influx transporters to affect the UV/MP ratio of these drugs should be investigated, albeit in the context of their overlapping selectivity for transport by P-gp or/and BCRP. Overall, our m-f PBPK model is flexible and capable of integrating such complexities, is informed by high-quality *in vivo* and *in vitro* data, accurately predicts fetal drug exposure and advances the mechanistic understanding of drug therapy in pregnancy.

BIBLIOGRAPHY

Abduljalil, K., & Badhan, R. K. S. (2020). Drug dosing during pregnancy-opportunities for physiologically based pharmacokinetic models. *J Pharmacokinet Pharmacodyn*. doi:10.1007/s10928-020-09698-w

Abduljalil, K., Furness, P., Johnson, T. N., Rostami-Hodjegan, A., & Soltani, H. (2012). Anatomical, physiological and metabolic changes with gestational age during normal pregnancy: a database for parameters required in physiologically based pharmacokinetic modelling. *Clin Pharmacokinet, 51*(6), 365-396. doi:10.2165/11597440-000000000-00000

Abduljalil, K., Jamei, M., & Johnson, T. N. (2018). Fetal Physiologically Based Pharmacokinetic Models: Systems Information on the Growth and Composition of Fetal Organs. *Clin Pharmacokinet*. doi:10.1007/s40262-018-0685-y

Abduljalil, K., Jamei, M., & Johnson, T. N. (2019). Fetal Physiologically Based Pharmacokinetic Models: Systems Information on the Growth and Composition of Fetal Organs. *Clin Pharmacokinet, 58*(2), 235-262. doi:10.1007/s40262-018-0685-y

Abduljalil, K., Pansari, A., & Jamei, M. (2020). Prediction of maternal pharmacokinetics using physiologically based pharmacokinetic models: assessing the impact of the longitudinal changes in the activity of CYP1A2, CYP2D6 and CYP3A4 enzymes during pregnancy. *J Pharmacokinet Pharmacodyn, 47*(4), 361-383. doi:10.1007/s10928-020-09711-2

Administration, U. F. a. D. (2017). *In Vitro Metabolism and Transporter Mediated Drug-Drug Interaction Studies: Guidance for Industry (FDA)*. Silver Spring, MD.

Agarwal, S., Pal, D., & Mitra, A. K. (2007). Both P-gp and MRP2 mediate transport of Lopinavir, a protease inhibitor. *Int J Pharm, 339*(1-2), 139-147. doi:10.1016/j.ijpharm.2007.02.036

Ahsan, C. H., Renwick, A. G., Waller, D. G., Challenor, V. F., George, C. F., & Amanullah, M. (1993). The influence of dose and ethnic origins on the pharmacokinetics of nifedipine. *Clin Pharmacol Ther, 54*(3), 329-338. doi:10.1038/clpt.1993.155

Althabe, F., Belizan, J. M., McClure, E. M., Hemingway-Foday, J., Berrueta, M., Mazzoni, A., . . . Buekens, P. M. (2015). A population-based, multifaceted strategy to implement antenatal corticosteroid treatment versus standard care for the reduction of neonatal mortality due to preterm birth in low-income and middle-income countries: the ACT cluster-randomised trial. *Lancet, 385*(9968), 629-639. doi:10.1016/S0140-6736(14)61651-2

American College of, O., & Gynecologists' Committee on Practice, B.-O. (2016). Practice Bulletin No. 171: Management of Preterm Labor. *Obstet Gynecol, 128*(4), e155-164. doi:10.1097/AOG.0000000000001711

Andany, N., & Loutfy, M. R. (2013). HIV protease inhibitors in pregnancy : pharmacology and clinical use. *Drugs, 73*(3), 229-247. doi:10.1007/s40265-013-0017-3

Anderson, G. D. (2005). Pregnancy-induced changes in pharmacokinetics: a mechanistic-based approach. *Clin Pharmacokinet, 44*(10), 989-1008. doi:10.2165/00003088-200544100-00001

Anoshchenko, O., Prasad, B., Neradugomma, N. K., Wang, J., Mao, Q., & Unadkat, J. D. (2020). Gestational Age-Dependent Abundance of Human Placental Transporters as Determined by Quantitative Targeted Proteomics. *Drug Metab Dispos, 48*(9), 735-741. doi:10.1124/dmd.120.000067

Arumugasaamy, N., Rock, K. D., Kuo, C. Y., Bale, T. L., & Fisher, J. P. (2020). Microphysiological systems of the placental barrier. *Adv Drug Deliv Rev*. doi:10.1016/j.addr.2020.08.010

Atkinson, D. E., Sibley, C. P., Fairbairn, L. J., & Greenwood, S. L. (2006). MDR1 P-gp expression and activity in intact human placental tissue; upregulation by retroviral transduction. *Placenta, 27*(6-7), 707-714. doi:10.1016/j.placenta.2005.06.008

Balkovetz, D. F., Tiruppathi, C., Leibach, F. H., Mahesh, V. B., & Ganapathy, V. (1989). Evidence for an imipramine-sensitive serotonin transporter in human placental brush-border membranes. *J Biol Chem, 264*(4), 2195-2198.

Ballabh, P., Lo, E. S., Kumari, J., Cooper, T. B., Zervoudakis, I., Auld, P. A., & Krauss, A. N. (2002). Pharmacokinetics of betamethasone in twin and singleton pregnancy. *Clin Pharmacol Ther, 71*(1), 39-45. doi:10.1067/mcp.2002.120250

Ballard, P. L., Granberg, P., & Ballard, R. A. (1975). Glucocorticoid levels in maternal and cord serum after prenatal betamethasone therapy to prevent respiratory distress syndrome. *J Clin Invest, 56*(6), 1548-1554. doi:10.1172/JCI108236

Bawdon, R. E., Gravell, M., Hamilton, R., Sever, J., Miller, R., & Gibbs, C. J. (1994). Studies on the placental transfer of cell-free human immunodeficiency virus and p24 antigen in an ex vivo human placental model. *J Soc Gynecol Investig, 1*(1), 45-48. doi:10.1177/107155769400100109

Bawdon, R. E., Gravell, M., Roberts, S., Hamilton, R., Dax, J., & Sever, J. (1995). Ex vivo human placental transfer of human immunodeficiency virus-1 p24 antigen. *Am J Obstet Gynecol, 172*(2 Pt 1), 530-532. doi:10.1016/0002-9378(95)90568-5

Billington, S., Salphati, L., Hop, C., Chu, X., Evers, R., Burdette, D., . . . Unadkat, J. D. (2019). Interindividual and Regional Variability in Drug Transporter Abundance at the Human Blood-Brain Barrier Measured by Quantitative Targeted Proteomics. *Clin Pharmacol Ther, 106*(1), 228-237. doi:10.1002/cpt.1373

Blanco-Castaneda, R., Galaviz-Hernandez, C., Souto, P. C. S., Lima, V. V., Giachini, F. R., Escudero, C., . . . Sosa-Macias, M. (2020). The role of xenobiotic-metabolizing enzymes in the placenta: a growing research field. *Expert Rev Clin Pharmacol*, 1-17. doi:10.1080/17512433.2020.1733412

Blanford, A. T., & Murphy, B. E. (1977). In vitro metabolism of prednisolone, dexamethasone, betamethasone, and cortisol by the human placenta. *Am J Obstet Gynecol, 127*(3), 264-267.

Blencowe, H., Cousens, S., Chou, D., Oestergaard, M., Say, L., Moller, A. B., . . . Born Too Soon Preterm Birth Action, G. (2013). Born too soon: the global epidemiology of 15 million preterm births. *Reprod Health, 10 Suppl 1*, S2. doi:10.1186/1742-4755-10-S1-S2

Boffito, M., Miralles, D., & Hill, A. (2008). Pharmacokinetics, efficacy, and safety of darunavir/ritonavir 800/100 mg once-daily in treatment-naive and -experienced patients. *HIV Clin Trials, 9*(6), 418-427. doi:10.1310/hct0906-418

Boland, E. W. (1962). Clinical comparison of the newer anti-inflammatory corticosteroids. *Ann Rheum Dis, 21*, 176-187. doi:10.1136/ard.21.2.176

Bottalico, B., Larsson, I., Brodszki, J., Hernandez-Andrade, E., Casslen, B., Marsal, K., & Hansson, S. R. (2004). Norepinephrine transporter (NET), serotonin transporter (SERT), vesicular monoamine transporter (VMAT2) and organic cation transporters (OCT1, 2 and EMT) in human placenta from pre-eclamptic and normotensive pregnancies. *Placenta, 25*(6), 518-529. doi:10.1016/j.placenta.2003.10.017

Burton, G. J., & Fowden, A. L. (2015). The placenta: a multifaceted, transient organ. *Philos Trans R Soc Lond B Biol Sci, 370*(1663), 20140066. doi:10.1098/rstb.2014.0066

Carey, J. L., Nader, N., Chai, P. R., Carreiro, S., Griswold, M. K., & Boyle, K. L. (2017). Drugs and Medical Devices: Adverse Events and the Impact on Women's Health. *Clin Ther, 39*(1), 10-22. doi:10.1016/j.clinthera.2016.12.009

Ceckova-Novotna, M., Pavek, P., & Staud, F. (2006). P-glycoprotein in the placenta: expression, localization, regulation and function. *Reprod Toxicol, 22*(3), 400-410. doi:10.1016/j.reprotox.2006.01.007

Cha, S. H., Sekine, T., Kusuhara, H., Yu, E., Kim, J. Y., Kim, D. K., . . . Endou, H. (2000). Molecular cloning and characterization of multispecific organic anion transporter 4 expressed in the placenta. *J Biol Chem, 275*(6), 4507-4512.

Chang, C. W., Wakeland, A. K., & Parast, M. M. (2018). Trophoblast lineage specification, differentiation and their regulation by oxygen tension. *J Endocrinol, 236*(1), R43-R56. doi:10.1530/JOE-17-0402

Colbers, A., Greupink, R., Litjens, C., Burger, D., & Russel, F. G. (2016). Physiologically Based Modelling of Darunavir/Ritonavir Pharmacokinetics During Pregnancy. *Clin Pharmacokinet, 55*(3), 381-396. doi:10.1007/s40262-015-0325-8

Colbers, A., Molto, J., Ivanovic, J., Kabeya, K., Hawkins, D., Gingelmaier, A., . . . Network, P. (2015). Pharmacokinetics of total and unbound darunavir in HIV-1-infected pregnant women. *J Antimicrob Chemother, 70*(2), 534-542. doi:10.1093/jac/dku400

Collaboration. (1981). Effect of antenatal dexamethasone administration on the prevention of respiratory distress syndrome. *Am J Obstet Gynecol, 141*(3), 276-287.

Cressey, T. R., Urien, S., Capparelli, E. V., Best, B. M., Buranabanjasatean, S., Limtrakul, A., . . . Mirochnick, M. (2015). Impact of body weight and missed doses on lopinavir concentrations with standard and increased lopinavir/ritonavir doses during late pregnancy. *J Antimicrob Chemother, 70*(1), 217-224. doi:10.1093/jac/dku367

Crowe, A., & Tan, A. M. (2012). Oral and inhaled corticosteroids: differences in P-glycoprotein (ABCB1) mediated efflux. *Toxicol Appl Pharmacol, 260*(3), 294-302. doi:10.1016/j.taap.2012.03.008

Crowther, C. A., Doyle, L. W., Haslam, R. R., Hiller, J. E., Harding, J. E., Robinson, J. S., & Group, A. S. (2007). Outcomes at 2 years of age after repeat doses of antenatal corticosteroids. *N Engl J Med, 357*(12), 1179-1189. doi:10.1056/NEJMoa071152

Crowther, C. A., & Harding, J. E. (2007). Repeat doses of prenatal corticosteroids for women at risk of preterm birth for preventing neonatal respiratory disease. *Cochrane Database Syst Rev*(3), CD003935. doi:10.1002/14651858.CD003935.pub2

Dallmann, A., Ince, I., Coboeken, K., Eissing, T., & Hempel, G. (2018). A Physiologically Based Pharmacokinetic Model for Pregnant Women to Predict the Pharmacokinetics of Drugs Metabolized Via Several Enzymatic Pathways. *Clin Pharmacokinet, 57*(6), 749-768. doi:10.1007/s40262-017-0594-5

Dallmann, A., Pfister, M., van den Anker, J., & Eissing, T. (2018). Physiologically Based Pharmacokinetic Modeling in Pregnancy: A Systematic Review of Published Models. *Clin Pharmacol Ther*. doi:10.1002/cpt.1084

De Sousa Mendes, M., Hirt, D., Urien, S., Valade, E., Bouazza, N., Foissac, F., . . . Benaboud, S. (2015). Physiologically-based pharmacokinetic modeling of renally excreted antiretroviral drugs in pregnant women. *Br J Clin Pharmacol, 80*(5), 1031-1041. doi:10.1111/bcp.12685

De Sousa Mendes, M., Lui, G., Zheng, Y., Pressiat, C., Hirt, D., Valade, E., . . . Benaboud, S. (2017). A Physiologically-Based Pharmacokinetic Model to Predict Human Fetal Exposure for a Drug Metabolized by Several CYP450 Pathways. *Clin Pharmacokinet, 56*(5), 537-550. doi:10.1007/s40262-016-0457-5

Dyer, J. (2019). Neonatal Respiratory Distress Syndrome: Tackling A Worldwide Problem. *P T, 44*(1), 12-14.

Egawa, M., Kamata, H., Kushiyama, A., Sakoda, H., Fujishiro, M., Horike, N., . . . Asano, T. (2008). Long-term forskolin stimulation induces AMPK activation and thereby enhances tight junction formation in human placental trophoblast BeWo cells. *Placenta, 29*(12), 1003-1008. doi:10.1016/j.placenta.2008.09.008

Enders, A. C., & Blankenship, T. N. (1999). Comparative placental structure. *Adv Drug Deliv Rev, 38*(1), 3-15.

Eron, J. J., Feinberg, J., Kessler, H. A., Horowitz, H. W., Witt, M. D., Carpio, F. F., . . . Sun, E. (2004). Once-daily versus twice-daily lopinavir/ritonavir in antiretroviral-naive HIV-positive patients: a 48-week randomized clinical trial. *J Infect Dis, 189*(2), 265-272. doi:10.1086/380799

Fauchet, F., Treluyer, J. M., Illamola, S. M., Pressiat, C., Lui, G., Valade, E., . . . Hirt, D. (2015). Population approach to analyze the pharmacokinetics of free and total lopinavir in HIV-infected pregnant women and consequences for dose adjustment. *Antimicrob Agents Chemother, 59*(9), 5727-5735. doi:10.1128/AAC.00863-15

Foissac, F., Zheng, Y., Hirt, D., Lui, G., Bouazza, N., Ville, Y., . . . Treluyer, J. M. (2020). Maternal Betamethasone for Prevention of Respiratory Distress Syndrome in Neonates: Population Pharmacokinetic and Pharmacodynamic Approach. *Clin Pharmacol Ther, 108*(5), 1026-1035. doi:10.1002/cpt.1887

Gaohua, L., Abduljalil, K., Jamei, M., Johnson, T. N., & Rostami-Hodjegan, A. (2012). A pregnancy physiologically based pharmacokinetic (p-PBPK) model for disposition of drugs metabolized by CYP1A2, CYP2D6 and CYP3A4. *Br J Clin Pharmacol, 74*(5), 873-885. doi:10.1111/j.1365-2125.2012.04363.x

Gentile, D. M., Tomlinson, E. S., Maggs, J. L., Park, B. K., & Back, D. J. (1996). Dexamethasone metabolism by human liver in vitro. Metabolite identification and inhibition of 6-hydroxylation. *J Pharmacol Exp Ther, 277*(1), 105-112.

Gil, S., Saura, R., Forestier, F., & Farinotti, R. (2005). P-glycoprotein expression of the human placenta during pregnancy. *Placenta, 26*(2-3), 268-270. doi:10.1016/j.placenta.2004.05.013

Gimenez, F., Fernandez, C., & Mabondzo, A. (2004). Transport of HIV protease inhibitors through the blood-brain barrier and interactions with the efflux proteins, P-glycoprotein and multidrug resistance proteins. *J Acquir Immune Defic Syndr, 36*(2), 649-658. doi:10.1097/00126334-200406010-00001

Glavinas, H., Mehn, D., Jani, M., Oosterhuis, B., Heredi-Szabo, K., & Krajcsi, P. (2008). Utilization of membrane vesicle preparations to study drug-ABC transporter interactions. *Expert Opin Drug Metab Toxicol, 4*(6), 721-732. doi:10.1517/17425255.4.6.721

Grube, M., Reuther, S., Meyer Zu Schwabedissen, H., Kock, K., Draber, K., Ritter, C. A., . . . Kroemer, H. K. (2007). Organic anion transporting polypeptide 2B1 and breast cancer resistance protein interact in the transepithelial transport of steroid sulfates in human placenta. *Drug Metab Dispos, 35*(1), 30-35. doi:10.1124/dmd.106.011411

Gyamfi-Bannerman, C., & Thom, E. A. (2016). Antenatal Betamethasone for Women at Risk for Late Preterm Delivery. *N Engl J Med, 375*(5), 486-487. doi:10.1056/NEJMc1605902

Gyamfi, C., Mele, L., Wapner, R. J., Spong, C. Y., Peaceman, A., Sorokin, Y., . . . Human Development Maternal-Fetal Medicine Units, N. (2010). The effect of plurality and obesity on betamethasone concentrations in women at risk for preterm delivery. *Am J Obstet Gynecol, 203*(3), 219 e211-215. doi:10.1016/j.ajog.2010.04.047

Han, L. W., Gao, C., & Mao, Q. (2018). An update on expression and function of P-gp/ABCB1 and BCRP/ABCG2 in the placenta and fetus. *Expert Opin Drug Metab Toxicol, 14*(8), 817-829. doi:10.1080/17425255.2018.1499726

Hayer-Zillgen, M., Bruss, M., & Bonisch, H. (2002). Expression and pharmacological profile of the human organic cation transporters hOCT1, hOCT2 and hOCT3. *Br J Pharmacol, 136*(6), 829-836. doi:10.1038/sj.bjp.0704785

Hebert, M. F., Easterling, T. R., Kirby, B., Carr, D. B., Buchanan, M. L., Rutherford, T., . . . Unadkat, J. D. (2008). Effects of pregnancy on CYP3A and P-glycoprotein activities as measured by disposition of midazolam and digoxin: a University of Washington specialized center of research study. *Clin Pharmacol Ther, 84*(2), 248-253. doi:10.1038/clpt.2008.1

Huisman, M. T., Smit, J. W., Wiltshire, H. R., Hoetelmans, R. M., Beijnen, J. H., & Schinkel, A. H. (2001). P-glycoprotein limits oral availability, brain, and fetal penetration of saquinavir even with high doses of ritonavir. *Mol Pharmacol, 59*(4), 806-813.

Ikeda, K., Utoguchi, N., Tsutsui, H., Yamaue, S., Homemoto, M., Nakao, E., . . . Hirotani, Y. (2011). In vitro approaches to evaluate placental drug transport by using differentiating JEG-3 human choriocarcinoma cells. *Basic Clin Pharmacol Toxicol, 108*(2), 138-145. doi:10.1111/j.1742-7843.2010.00634.x

Illsley, N. P., Wang, Z. Q., Gray, A., Sellers, M. C., & Jacobs, M. M. (1990). Simultaneous preparation of paired, syncytial, microvillous and basal membranes from human placenta. *Biochim Biophys Acta, 1029*(2), 218-226.

Ishida, K., Ullah, M., Toth, B., Juhasz, V., & Unadkat, J. D. (2018). Successful Prediction of In Vivo Hepatobiliary Clearances and Hepatic Concentrations of Rosuvastatin Using Sandwich-Cultured Rat Hepatocytes, Transporter-Expressing Cell Lines, and Quantitative Proteomics. *Drug Metab Dispos, 46*(1), 66-74. doi:10.1124/dmd.117.076539

Jamei, M. (2016). Recent Advances in Development and Application of Physiologically-Based Pharmacokinetic (PBPK) Models: a Transition from Academic Curiosity to Regulatory Acceptance. *Curr Pharmacol Rep, 2*, 161-169. doi:10.1007/s40495-016-0059-9

Jamei, M., Dickinson, G. L., & Rostami-Hodjegan, A. (2009). A framework for assessing inter-individual variability in pharmacokinetics using virtual human populations and integrating general knowledge of physical chemistry, biology, anatomy, physiology and genetics: A tale of 'bottom-up' vs 'top-down' recognition of covariates. *Drug Metab Pharmacokinet, 24*(1), 53-75. doi:10.2133/dmpk.24.53

Jeffrey, P., & Summerfield, S. (2010). Assessment of the blood-brain barrier in CNS drug discovery. *Neurobiol Dis, 37*(1), 33-37. doi:10.1016/j.nbd.2009.07.033

Jimenez, V., Henriquez, M., Llanos, P., & Riquelme, G. (2004). Isolation and purification of human placental plasma membranes from normal and pre-eclamptic pregnancies. a comparative study. *Placenta, 25*(5), 422-437. doi:10.1016/j.placenta.2003.10.013

Jobe, A. H., Milad, M. A., Peppard, T., & Jusko, W. J. (2020). Pharmacokinetics and Pharmacodynamics of Intramuscular and Oral Betamethasone and Dexamethasone in

Reproductive Age Women in India. *Clin Transl Sci, 13*(2), 391-399. doi:10.1111/cts.12724

Joshi, A. A., Vaidya, S. S., St-Pierre, M. V., Mikheev, A. M., Desino, K. E., Nyandege, A. N., . . . Gerk, P. M. (2016). Placental ABC Transporters: Biological Impact and Pharmaceutical Significance. *Pharm Res, 33*(12), 2847-2878. doi:10.1007/s11095-016-2028-8

Ke, A. B., & Milad, M. A. (2019). Evaluation of Maternal Drug Exposure Following the Administration of Antenatal Corticosteroids During Late Pregnancy Using Physiologically-Based Pharmacokinetic Modeling. *Clin Pharmacol Ther, 106*(1), 164-173. doi:10.1002/cpt.1438

Ke, A. B., Nallani, S. C., Zhao, P., Rostami-Hodjegan, A., & Unadkat, J. D. (2012). A PBPK Model to Predict Disposition of CYP3A-Metabolized Drugs in Pregnant Women: Verification and Discerning the Site of CYP3A Induction. *CPT Pharmacometrics Syst Pharmacol, 1*, e3. doi:10.1038/psp.2012.2

Ke, A. B., Nallani, S. C., Zhao, P., Rostami-Hodjegan, A., & Unadkat, J. D. (2014). Expansion of a PBPK model to predict disposition in pregnant women of drugs cleared via multiple CYP enzymes, including CYP2B6, CYP2C9 and CYP2C19. *Br J Clin Pharmacol, 77*(3), 554-570. doi:10.1111/bcp.12207

Kelley, L. K., Smith, C. H., & King, B. F. (1983). Isolation and partial characterization of the basal cell membrane of human placental trophoblast. *Biochim Biophys Acta, 734*(1), 91-98.

Kemp, M. W., Saito, M., Usuda, H., Watanabe, S., Sato, S., Hanita, T., . . . Jobe, A. H. (2018). The efficacy of antenatal steroid therapy is dependent on the duration of low-concentration fetal exposure: evidence from a sheep model of pregnancy. *Am J Obstet Gynecol, 219*(3), 301 e301-301 e316. doi:10.1016/j.ajog.2018.05.007

Kirby, B. J., Collier, A. C., Kharasch, E. D., Whittington, D., Thummel, K. E., & Unadkat, J. D. (2011). Complex drug interactions of HIV protease inhibitors 1: inactivation, induction, and inhibition of cytochrome P450 3A by ritonavir or nelfinavir. *Drug Metab Dispos, 39*(6), 1070-1078. doi:10.1124/dmd.110.037523

Konig, S. K., Herzog, M., Theile, D., Zembruski, N., Haefeli, W. E., & Weiss, J. (2010). Impact of drug transporters on cellular resistance towards saquinavir and darunavir. *J Antimicrob Chemother, 65*(11), 2319-2328. doi:10.1093/jac/dkq324

Koren, G., & Ornoy, A. (2018). The role of the placenta in drug transport and fetal drug exposure. *Expert Rev Clin Pharmacol*, 1-13. doi:10.1080/17512433.2018.1425615

Kumar, A. R., Prasad, B., Bhatt, D. K., Mathialagan, S., Varma, M. V. S., & Unadkat, J. D. (2021). IVIVE of Transporter-Mediated Renal Clearance: Relative Expression Factor (REF) vs Relative Activity Factor (RAF) Approach. *Drug Metab Dispos*. doi:10.1124/dmd.121.000367

Kumar, V., Nguyen, T. B., Toth, B., Juhasz, V., & Unadkat, J. D. (2017). Optimization and Application of a Biotinylation Method for Quantification of Plasma Membrane Expression of Transporters in Cells. *AAPS J, 19*(5), 1377-1386. doi:10.1208/s12248-017-0121-5

Kumar, V., Yin, J., Billington, S., Prasad, B., Brown, C. D. A., Wang, J., & Unadkat, J. D. (2018). The Importance of Incorporating OCT2 Plasma Membrane Expression and Membrane Potential in IVIVE of Metformin Renal Secretory Clearance. *Drug Metab Dispos, 46*(10), 1441-1445. doi:10.1124/dmd.118.082313

Kummu, M., Sieppi, E., Koponen, J., Laatio, L., Vahakangas, K., Kiviranta, H., . . . Myllynen, P. (2015). Organic anion transporter 4 (OAT 4) modifies placental transfer of perfluorinated alkyl acids PFOS and PFOA in human placental ex vivo perfusion system. *Placenta, 36*(10), 1185-1191. doi:10.1016/j.placenta.2015.07.119

Lee, A. C., Katz, J., Blencowe, H., Cousens, S., Kozuki, N., Vogel, J. P., . . . Group, C. S.-P. B. W. (2013). National and regional estimates of term and preterm babies born small for gestational age in 138 low-income and middle-income countries in 2010. *Lancet Glob Health, 1*(1), e26-36. doi:10.1016/S2214-109X(13)70006-8

Lee, N., Hebert, M. F., Prasad, B., Easterling, T. R., Kelly, E. J., Unadkat, J. D., & Wang, J. (2013). Effect of gestational age on mRNA and protein expression of polyspecific organic cation transporters during pregnancy. *Drug Metab Dispos, 41*(12), 2225-2232. doi:10.1124/dmd.113.054072

Lee, N., Hebert, M. F., Wagner, D. J., Easterling, T. R., Liang, C. J., Rice, K., & Wang, J. (2018). Organic Cation Transporter 3 Facilitates Fetal Exposure to Metformin during Pregnancy. *Mol Pharmacol, 94*(4), 1125-1131. doi:10.1124/mol.118.112482

Levitz, M., Jansen, V., & Dancis, J. (1978). The transfer and metabolism of corticosteroids in the perfused human placenta. *Am J Obstet Gynecol, 132*(4), 363-366.

Liggins, G. C., & Howie, R. N. (1972). A controlled trial of antepartum glucocorticoid treatment for prevention of the respiratory distress syndrome in premature infants. *Pediatrics, 50*(4), 515-525.

Liu, X. I., Momper, J. D., Rakhmanina, N., van den Anker, J. N., Green, D. J., Burckart, G. J., . . . Dallmann, A. (2020). Physiologically Based Pharmacokinetic Models to Predict Maternal Pharmacokinetics and Fetal Exposure to Emtricitabine and Acyclovir. *J Clin Pharmacol, 60*(2), 240-255. doi:10.1002/jcph.1515

Lopez Quinones, A. J., Wagner, D. J., & Wang, J. (2020). Characterization of Meta-Iodobenzylguanidine (mIBG) Transport by Polyspecific Organic Cation Transporters: Implication for mIBG Therapy. *Mol Pharmacol, 98*(2), 109-119. doi:10.1124/mol.120.119495

Maliepaard, M., Scheffer, G. L., Faneyte, I. F., van Gastelen, M. A., Pijnenborg, A. C., Schinkel, A. H., . . . Schellens, J. H. (2001). Subcellular localization and distribution of the breast cancer resistance protein transporter in normal human tissues. *Cancer Res, 61*(8), 3458-3464.

Mandelbrot, L., Duro, D., Belissa, E., & Peytavin, G. (2014). Placental transfer of darunavir in an ex vivo human cotyledon perfusion model. *Antimicrob Agents Chemother, 58*(9), 5617-5620. doi:10.1128/AAC.03184-14

Mao, Q. (2008). BCRP/ABCG2 in the placenta: expression, function and regulation. *Pharm Res, 25*(6), 1244-1255. doi:10.1007/s11095-008-9537-z

Mao, Q., & Unadkat, J. D. (2015). Role of the breast cancer resistance protein (BCRP/ABCG2) in drug transport--an update. *AAPS J, 17*(1), 65-82. doi:10.1208/s12248-014-9668-6

Mathias, A. A., Hitti, J., & Unadkat, J. D. (2005). P-glycoprotein and breast cancer resistance protein expression in human placentae of various gestational ages. *Am J Physiol Regul Integr Comp Physiol, 289*(4), R963-969. doi:10.1152/ajpregu.00173.2005

McClure, E. M., Goldenberg, R. L., Jobe, A. H., Miodovnik, M., Koso-Thomas, M., Buekens, P., . . . Althabe, F. (2016). Reducing neonatal mortality associated with preterm birth: gaps in knowledge of the impact of antenatal corticosteroids on preterm birth outcomes in low-middle income countries. *Reprod Health, 13*(1), 61. doi:10.1186/s12978-016-0180-6

Memon, N., Bircsak, K. M., Archer, F., Gibson, C. J., Ohman-Strickland, P., Weinberger, B. I., . . . Aleksunes, L. M. (2014). Regional expression of the BCRP/ABCG2 transporter in term human placentas. *Reprod Toxicol, 43*, 72-77. doi:10.1016/j.reprotox.2013.11.003

Meyer zu Schwabedissen, H. E., Grube, M., Dreisbach, A., Jedlitschky, G., Meissner, K., Linnemann, K., . . . Kroemer, H. K. (2006). Epidermal growth factor-mediated activation of the map kinase cascade results in altered expression and function of ABCG2 (BCRP). *Drug Metab Dispos, 34*(4), 524-533. doi:10.1124/dmd.105.007591

Mitchell, A. A., Gilboa, S. M., Werler, M. M., Kelley, K. E., Louik, C., Hernandez-Diaz, S., & National Birth Defects Prevention, S. (2011). Medication use during pregnancy, with particular focus on prescription drugs: 1976-2008. *Am J Obstet Gynecol, 205*(1), 51 e51-58. doi:10.1016/j.ajog.2011.02.029

Muller, F., Konig, J., Hoier, E., Mandery, K., & Fromm, M. F. (2013). Role of organic cation transporter OCT2 and multidrug and toxin extrusion proteins MATE1 and MATE2-K for transport and drug interactions of the antiviral lamivudine. *Biochem Pharmacol, 86*(6), 808-815. doi:10.1016/j.bcp.2013.07.008

Murphy, V. E., Fittock, R. J., Zarzycki, P. K., Delahunty, M. M., Smith, R., & Clifton, V. L. (2007). Metabolism of synthetic steroids by the human placenta. *Placenta, 28*(1), 39-46. doi:10.1016/j.placenta.2005.12.010

Murtagh, R., Else, L. J., Kuan, K. B., Khoo, S. H., Jackson, V., Patel, A., . . . Lambert, J. S. (2019). Therapeutic drug monitoring of darunavir/ritonavir in pregnancy. *Antivir Ther*. doi:10.3851/IMP3291

Myllynen, P., Immonen, E., Kummu, M., & Vahakangas, K. (2009). Developmental expression of drug metabolizing enzymes and transporter proteins in human placenta and fetal tissues. *Expert Opin Drug Metab Toxicol, 5*(12), 1483-1499. doi:10.1517/17425250903304049

Myllynen, P., Pasanen, M., & Pelkonen, O. (2005). Human placenta: a human organ for developmental toxicology research and biomonitoring. *Placenta, 26*(5), 361-371. doi:10.1016/j.placenta.2004.09.006

Myllynen, P., Pasanen, M., & Vahakangas, K. (2007). The fate and effects of xenobiotics in human placenta. *Expert Opin Drug Metab Toxicol, 3*(3), 331-346. doi:10.1517/17425255.3.3.331

Nishimura, M., & Naito, S. (2005). Tissue-specific mRNA expression profiles of human ATP-binding cassette and solute carrier transporter superfamilies. *Drug Metab Pharmacokinet, 20*(6), 452-477.

Oladapo, O. T., Vogel, J. P., Piaggio, G., Nguyen, M. H., Althabe, F., Gulmezoglu, A. M., . . . Chellani, H. K. (2020). Antenatal Dexamethasone for Early Preterm Birth in Low-Resource Countries. *N Engl J Med, 383*(26), 2514-2525. doi:10.1056/NEJMoa2022398

Ornoy, A. (2009). Valproic acid in pregnancy: how much are we endangering the embryo and fetus? *Reprod Toxicol, 28*(1), 1-10. doi:10.1016/j.reprotox.2009.02.014

Pasanen, M. (1999). The expression and regulation of drug metabolism in human placenta. *Adv Drug Deliv Rev, 38*(1), 81-97. doi:10.1016/s0169-409x(99)00008-3

Patilea-Vrana, G., & Unadkat, J. D. (2016). Transport vs. Metabolism: What Determines the Pharmacokinetics and Pharmacodynamics of Drugs? Insights From the Extended Clearance Model. *Clin Pharmacol Ther, 100*(5), 413-418. doi:10.1002/cpt.437

Peets, E. A., Staub, M., & Symchowicz, S. (1969). Plasma binding of betamethasone-3H, dexamethasone-3H, and cortisol-14C--a comparative study. *Biochem Pharmacol, 18*(7), 1655-1663. doi:10.1016/0006-2952(69)90153-1

Peng, H. H., Kao, C. C., Chang, S. D., Chao, A. S., Chang, Y. L., Wang, C. N., . . . Wang, H. S. (2011). The effects of labor on differential gene expression in parturient women, placentas, and fetuses at term pregnancy. *Kaohsiung J Med Sci, 27*(11), 494-502. doi:10.1016/j.kjms.2011.06.012

Petersen, M. C., Collier, C. B., Ashley, J. J., McBride, W. G., & Nation, R. L. (1983). Disposition of betamethasone in parturient women after intravenous administration. *Eur J Clin Pharmacol, 25*(6), 803-810.

Petersen, M. C., Nation, R. L., Ashley, J. J., & McBride, W. G. (1980). The placental transfer of betamethasone. *Eur J Clin Pharmacol, 18*(3), 245-247.

Petersen, M. C., Nation, R. L., McBride, W. G., Ashley, J. J., & Moore, R. G. (1983). Pharmacokinetics of betamethasone in healthy adults after intravenous administration. *Eur J Clin Pharmacol, 25*(5), 643-650.

Pinto, L., Bapat, P., de Lima Moreira, F., Lubetsky, A., de Carvalho Cavalli, R., Berger, H., . . . Koren, G. (2021). Chiral Transplacental Pharmacokinetics of Fexofenadine: Impact of P-Glycoprotein Inhibitor Fluoxetine Using the Human Placental Perfusion Model. *Pharm Res, 38*(4), 647-655. doi:10.1007/s11095-021-03035-7

Poulsen, M. S., Rytting, E., Mose, T., & Knudsen, L. E. (2009). Modeling placental transport: correlation of in vitro BeWo cell permeability and ex vivo human placental perfusion. *Toxicol In Vitro, 23*(7), 1380-1386. doi:10.1016/j.tiv.2009.07.028

Prasad, B., Evers, R., Gupta, A., Hop, C. E., Salphati, L., Shukla, S., . . . Unadkat, J. D. (2014). Interindividual variability in hepatic organic anion-transporting polypeptides and P-glycoprotein (ABCB1) protein expression: quantification by liquid chromatography tandem mass spectroscopy and influence of genotype, age, and sex. *Drug Metab Dispos, 42*(1), 78-88. doi:10.1124/dmd.113.053819

Prasad, B., Gaedigk, A., Vrana, M., Gaedigk, R., Leeder, J. S., Salphati, L., . . . Unadkat, J. D. (2016). Ontogeny of Hepatic Drug Transporters as Quantified by LC-MS/MS Proteomics. *Clin Pharmacol Ther, 100*(4), 362-370. doi:10.1002/cpt.409

Prasad, B., Johnson, K., Billington, S., Lee, C., Chung, G. W., Brown, C. D., . . . Unadkat, J. D. (2016). Abundance of Drug Transporters in the Human Kidney Cortex as Quantified by Quantitative Targeted Proteomics. *Drug Metab Dispos, 44*(12), 1920-1924. doi:10.1124/dmd.116.072066

Prasad, B., & Unadkat, J. D. (2015). The concept of fraction of drug transported (ft) with special emphasis on BBB efflux of CNS and antiretroviral drugs. *Clin Pharmacol Ther, 97*(4), 320-323. doi:10.1002/cpt.72

Raikkonen, K., Gissler, M., & Kajantie, E. (2020). Maternal Antenatal Corticosteroid Treatment and Childhood Mental and Behavioral Disorders-Reply. *JAMA, 324*(15), 1570-1571. doi:10.1001/jama.2020.15449

Roberts, D., Brown, J., Medley, N., & Dalziel, S. R. (2017). Antenatal corticosteroids for accelerating fetal lung maturation for women at risk of preterm birth. *Cochrane Database Syst Rev, 3*, CD004454. doi:10.1002/14651858.CD004454.pub3

Rothbauer, M., Patel, N., Gondola, H., Siwetz, M., Huppertz, B., & Ertl, P. (2017). A comparative study of five physiological key parameters between four different human trophoblast-derived cell lines. *Sci Rep, 7*(1), 5892. doi:10.1038/s41598-017-06364-z

Rowland, M., Peck, C., & Tucker, G. (2011). Physiologically-based pharmacokinetics in drug development and regulatory science. *Annu Rev Pharmacol Toxicol, 51*, 45-73. doi:10.1146/annurev-pharmtox-010510-100540

Russell, M. A., Carpenter, M. W., Akhtar, M. S., Lagattuta, T. F., & Egorin, M. J. (2007). Imatinib mesylate and metabolite concentrations in maternal blood, umbilical cord blood, placenta and breast milk. *J Perinatol, 27*(4), 241-243. doi:10.1038/sj.jp.7211665

Sachar, M., Kumar, V., Gormsen, L. C., Munk, O. L., & Unadkat, J. D. (2020). Successful Prediction of Positron Emission Tomography-Imaged Metformin Hepatic Uptake Clearance in Humans Using the Quantitative Proteomics-Informed Relative Expression Factor Approach. *Drug Metab Dispos, 48*(11), 1210-1216. doi:10.1124/dmd.120.000156

Sager, J. E., Yu, J., Ragueneau-Majlessi, I., & Isoherranen, N. (2015). Physiologically Based Pharmacokinetic (PBPK) Modeling and Simulation Approaches: A Systematic Review of Published Models, Applications, and Model Verification. *Drug Metab Dispos, 43*(11), 1823-1837. doi:10.1124/dmd.115.065920

Salama, E., Eke, A. C., Best, B. M., Mirochnick, M., & Momper, J. D. (2020). Pharmacokinetic Enhancement of HIV Antiretroviral Therapy During Pregnancy. *J Clin Pharmacol, 60*(12), 1537-1550. doi:10.1002/jcph.1714

Samtani, M. N., Schwab, M., Nathanielsz, P. W., & Jusko, W. J. (2004). Stabilization and HPLC analysis of betamethasone sodium phosphate in plasma. *J Pharm Sci, 93*(3), 726-732. doi:10.1002/jps.10577

Sastry, B. V. (1999). Techniques to study human placental transport. *Adv Drug Deliv Rev, 38*(1), 17-39. doi:10.1016/s0169-409x(99)00004-6

Scaffidi, J., Mol, B. W., & Keelan, J. A. (2017). The pregnant women as a drug orphan: a global survey of registered clinical trials of pharmacological interventions in pregnancy. *BJOG, 124*(1), 132-140. doi:10.1111/1471-0528.14151

Schinkel, A. H., & Jonker, J. W. (2003). Mammalian drug efflux transporters of the ATP binding cassette (ABC) family: an overview. *Adv Drug Deliv Rev, 55*(1), 3-29. doi:10.1016/s0169-409x(02)00169-2

Schmidt, A. F., Kemp, M. W., Rittenschober-Bohm, J., Kannan, P. S., Usuda, H., Saito, M., . . . Jobe, A. H. (2018). Low-dose betamethasone-acetate for fetal lung maturation in preterm sheep. *Am J Obstet Gynecol, 218*(1), 132 e131-132 e139. doi:10.1016/j.ajog.2017.11.560

Schmitz, T., Alberti, C., Ursino, M., Baud, O., Aupiais, C., group, B. s., & the, G. (2019). Full versus half dose of antenatal betamethasone to prevent severe neonatal respiratory distress syndrome associated with preterm birth: study protocol for a randomised, multicenter, double blind, placebo-controlled, non-inferiority trial (BETADOSE). *BMC Pregnancy Childbirth, 19*(1), 67. doi:10.1186/s12884-019-2206-x

Sekar, V., Spinosa-Guzman, S., De Paepe, E., Stevens, T., Tomaka, F., De Pauw, M., & Hoetelmans, R. M. (2010). Pharmacokinetics of multiple-dose darunavir in combination with low-dose ritonavir in individuals with mild-to-moderate hepatic impairment. *Clin Pharmacokinet, 49*(5), 343-350. doi:10.2165/11530690-000000000-00000

Sekar, V. J., Lefebvre, E., De Pauw, M., Vangeneugden, T., & Hoetelmans, R. M. (2008). Pharmacokinetics of darunavir/ritonavir and ketoconazole following co-administration in HIV-healthy volunteers. *Br J Clin Pharmacol, 66*(2), 215-221. doi:10.1111/j.1365-2125.2008.03191.x

Sheffield, J. S., Siegel, D., Mirochnick, M., Heine, R. P., Nguyen, C., Bergman, K. L., . . . Nesin, M. (2014). Designing drug trials: considerations for pregnant women. *Clin Infect Dis, 59 Suppl 7*, S437-444. doi:10.1093/cid/ciu709

Shields, K. E., & Lyerly, A. D. (2013). Exclusion of pregnant women from industry-sponsored clinical trials. *Obstet Gynecol, 122*(5), 1077-1081. doi:10.1097/AOG.0b013e3182a9ca67

Shoop, J., Ruggiero, M., Zhang, Y., & Hagenbuch, B. (2015). Protein-Protein Interactions Between Organic Anion Transporting Polypeptide 1B3 (OATP1B3) and Organic Cation Transporter 1 (OCT1). *The FASEB Journal, 29*(1_supplement), 939.936. doi:10.1096/fasebj.29.1_supplement.939.6

Smith, M. A., Thomford, P. J., Mattison, D. R., & Slikker, W., Jr. (1988). Transport and metabolism of dexamethasone in the dually perfused human placenta. *Reprod Toxicol, 2*(1), 37-43.

Stek, A., Best, B. M., Wang, J., Capparelli, E. V., Burchett, S. K., Kreitchmann, R., . . . Mirochnick, M. (2015). Pharmacokinetics of Once Versus Twice Daily Darunavir in Pregnant HIV-Infected Women. *J Acquir Immune Defic Syndr, 70*(1), 33-41. doi:10.1097/QAI.0000000000000668

Stevens, J. C., Hines, R. N., Gu, C., Koukouritaki, S. B., Manro, J. R., Tandler, P. J., & Zaya, M. J. (2003). Developmental expression of the major human hepatic CYP3A enzymes. *J Pharmacol Exp Ther, 307*(2), 573-582. doi:10.1124/jpet.103.054841

Storelli, F., Anoshchenko, O., & Unadkat, J. D. (2021). Successful prediction of human brain Kp,uu of P-gp substrates using the proteomics-informed relative expression factor approach. *Clin Pharmacol Ther*. doi:10.1002/cpt.2227

Storelli, F., Billington, S., Kumar, A. R., & Unadkat, J. D. (2020). Abundance of P-Glycoprotein and Other Drug Transporters at the Human Blood-Brain Barrier in Alzheimer's Disease: A Quantitative Targeted Proteomic Study. *Clin Pharmacol Ther*. doi:10.1002/cpt.2035

Storelli, F., Billington, S., Kumar, A. R., & Unadkat, J. D. (2021). Abundance of P-Glycoprotein and Other Drug Transporters at the Human Blood-Brain Barrier in Alzheimer's Disease: A Quantitative Targeted Proteomic Study. *Clin Pharmacol Ther, 109*(3), 667-675. doi:10.1002/cpt.2035

Sun, M., Kingdom, J., Baczyk, D., Lye, S. J., Matthews, S. G., & Gibb, W. (2006). Expression of the multidrug resistance P-glycoprotein, (ABCB1 glycoprotein) in the human placenta decreases with advancing gestation. *Placenta, 27*(6-7), 602-609. doi:10.1016/j.placenta.2005.05.007

Tayrouz, Y., Ganssmann, B., Ding, R., Klingmann, A., Aderjan, R., Burhenne, J., . . . Mikus, G. (2001). Ritonavir increases loperamide plasma concentrations without evidence for P-glycoprotein involvement. *Clin Pharmacol Ther, 70*(5), 405-414. doi:10.1067/mcp.2001.119212

Thorpe, P. G., Gilboa, S. M., Hernandez-Diaz, S., Lind, J., Cragan, J. D., Briggs, G., . . . National Birth Defects Prevention, S. (2013). Medications in the first trimester of pregnancy: most common exposures and critical gaps in understanding fetal risk. *Pharmacoepidemiol Drug Saf, 22*(9), 1013-1018. doi:10.1002/pds.3495

Thygesen, S. K., Olsen, M., Pedersen, L., Henderson, V. W., Ostergaard, J. R., & Sorensen, H. T. (2018). Respiratory distress syndrome in preterm infants and risk of epilepsy in a Danish cohort. *Eur J Epidemiol, 33*(3), 313-321. doi:10.1007/s10654-017-0308-1

Trapa, P. E., Belova, E., Liras, J. L., Scott, D. O., & Steyn, S. J. (2016). Insights From an Integrated Physiologically Based Pharmacokinetic Model for Brain Penetration. *J Pharm Sci, 105*(2), 965-971. doi:10.1016/j.xphs.2015.12.005

Trapa, P. E., Troutman, M. D., Lau, T. Y., Wager, T. T., Maurer, T. S., Patel, N. C., . . . Liras, J. L. (2019). In vitro-In vivo extrapolation of key transporter activity at the blood-brain barrier. *Drug Metab Dispos*. doi:10.1124/dmd.118.083279

Tsuei, S. E., Moore, R. G., Ashley, J. J., & McBride, W. G. (1979). Disposition of synethetic glucocorticoids. I. Pharmacokinetics of dexamethasone in healthy adults. *J Pharmacokinet Biopharm, 7*(3), 249-264.

Tsuei, S. E., Petersen, M. C., Ashley, J. J., McBride, W. G., & Moore, R. G. (1980). Disporition of synthetic glucocorticoids. II. Dexamethasone in parturient women. *Clin Pharmacol Ther, 28*(1), 88-98.

Uchida, Y., Ohtsuki, S., Kamiie, J., & Terasaki, T. (2011). Blood-brain barrier (BBB) pharmacoproteomics: reconstruction of in vivo brain distribution of 11 P-glycoprotein substrates based on the BBB transporter protein concentration, in vitro intrinsic transport activity, and unbound fraction in plasma and brain in mice. *J Pharmacol Exp Ther, 339*(2), 579-588. doi:10.1124/jpet.111.184200

Uchida, Y., Ohtsuki, S., & Terasaki, T. (2014). Pharmacoproteomics-based reconstruction of in vivo P-glycoprotein function at blood-brain barrier and brain distribution of substrate verapamil in pentylenetetrazole-kindled epilepsy, spontaneous epilepsy, and phenytoin treatment models. *Drug Metab Dispos, 42*(10), 1719-1726. doi:10.1124/dmd.114.059055

Uchida, Y., Wakayama, K., Ohtsuki, S., Chiba, M., Ohe, T., Ishii, Y., & Terasaki, T. (2014). Blood-brain barrier pharmacoproteomics-based reconstruction of the in vivo brain distribution of P-glycoprotein substrates in cynomolgus monkeys. *J Pharmacol Exp Ther, 350*(3), 578-588. doi:10.1124/jpet.114.214536

Ueda, K., Okamura, N., Hirai, M., Tanigawara, Y., Saeki, T., Kioka, N., . . . Hori, R. (1992). Human P-glycoprotein transports cortisol, aldosterone, and dexamethasone, but not progesterone. *J Biol Chem, 267*(34), 24248-24252.

Ugele, B., Bahn, A., & Rex-Haffner, M. (2008). Functional differences in steroid sulfate uptake of organic anion transporter 4 (OAT4) and organic anion transporting polypeptide 2B1 (OATP2B1) in human placenta. *J Steroid Biochem Mol Biol, 111*(1-2), 1-6. doi:10.1016/j.jsbmb.2008.04.001

Vahakangas, K., & Myllynen, P. (2009). Drug transporters in the human blood-placental barrier. *Br J Pharmacol, 158*(3), 665-678. doi:10.1111/j.1476-5381.2009.00336.x

Vanky, E., Zahlsen, K., Spigset, O., & Carlsen, S. M. (2005). Placental passage of metformin in women with polycystic ovary syndrome. *Fertil Steril, 83*(5), 1575-1578. doi:10.1016/j.fertnstert.2004.11.051

Varis, T., Kivisto, K. T., Backman, J. T., & Neuvonen, P. J. (2000). The cytochrome P450 3A4 inhibitor itraconazole markedly increases the plasma concentrations of dexamethasone and enhances its adrenal-suppressant effect. *Clin Pharmacol Ther, 68*(5), 487-494. doi:10.1067/mcp.2000.110772

Velasquez, J. C., Goeden, N., & Bonnin, A. (2013). Placental serotonin: implications for the developmental effects of SSRIs and maternal depression. *Front Cell Neurosci, 7*, 47. doi:10.3389/fncel.2013.00047

Vermeer, L. M., Isringhausen, C. D., Ogilvie, B. W., & Buckley, D. B. (2016). Evaluation of Ketoconazole and Its Alternative Clinical CYP3A4/5 Inhibitors as Inhibitors of Drug

Transporters: The In Vitro Effects of Ketoconazole, Ritonavir, Clarithromycin, and Itraconazole on 13 Clinically-Relevant Drug Transporters. *Drug Metab Dispos, 44*(3), 453-459. doi:10.1124/dmd.115.067744

Vertommen, A., Panis, B., Swennen, R., & Carpentier, S. C. (2010). Evaluation of chloroform/methanol extraction to facilitate the study of membrane proteins of non-model plants. *Planta, 231*(5), 1113-1125. doi:10.1007/s00425-010-1121-1

Vogel, J. P., Oladapo, O. T., Manu, A., Gulmezoglu, A. M., & Bahl, R. (2015). New WHO recommendations to improve the outcomes of preterm birth. *Lancet Glob Health, 3*(10), e589-590. doi:10.1016/S2214-109X(15)00183-7

Vogel, J. P., Oladapo, O. T., Pileggi-Castro, C., Adejuyigbe, E. A., Althabe, F., Ariff, S., . . . Metin Gulmezoglu, A. (2017). Antenatal corticosteroids for women at risk of imminent preterm birth in low-resource countries: the case for equipoise and the need for efficacy trials. *BMJ Glob Health, 2*(3), e000398. doi:10.1136/bmjgh-2017-000398

Wagner, C., Zhao, P., Arya, V., Mullick, C., Struble, K., & Au, S. (2017). Physiologically Based Pharmacokinetic Modeling for Predicting the Effect of Intrinsic and Extrinsic Factors on Darunavir or Lopinavir Exposure Coadministered With Ritonavir. *J Clin Pharmacol, 57*(10), 1295-1304. doi:10.1002/jcph.936

Wang, H., Qian, W. J., Mottaz, H. M., Clauss, T. R., Anderson, D. J., Moore, R. J., . . . Smith, R. D. (2005). Development and evaluation of a micro- and nanoscale proteomic sample preparation method. *J Proteome Res, 4*(6), 2397-2403. doi:10.1021/pr050160f

Wang, L., Collins, C., Kelly, E. J., Chu, X., Ray, A. S., Salphati, L., . . . Unadkat, J. D. (2016). Transporter Expression in Liver Tissue from Subjects with Alcoholic or Hepatitis C Cirrhosis Quantified by Targeted Quantitative Proteomics. *Drug Metab Dispos, 44*(11), 1752-1758. doi:10.1124/dmd.116.071050

Wapner, R. J., Sorokin, Y., Thom, E. A., Johnson, F., Dudley, D. J., Spong, C. Y., . . . Human Development Maternal Fetal Medicine Units, N. (2006). Single versus weekly courses of antenatal corticosteroids: evaluation of safety and efficacy. *Am J Obstet Gynecol, 195*(3), 633-642. doi:10.1016/j.ajog.2006.03.087

Williams, J. A., Ring, B. J., Cantrell, V. E., Jones, D. R., Eckstein, J., Ruterbories, K., . . . Wrighton, S. A. (2002). Comparative metabolic capabilities of CYP3A4, CYP3A5, and CYP3A7. *Drug Metab Dispos, 30*(8), 883-891.

Xia, B., Heimbach, T., Gollen, R., Nanavati, C., & He, H. (2013). A simplified PBPK modeling approach for prediction of pharmacokinetics of four primarily renally excreted and CYP3A metabolized compounds during pregnancy. *AAPS J, 15*(4), 1012-1024. doi:10.1208/s12248-013-9505-3

Yates, C. R., Chang, C., Kearbey, J. D., Yasuda, K., Schuetz, E. G., Miller, D. D., . . . Swaan, P. W. (2003). Structural determinants of P-glycoprotein-mediated transport of glucocorticoids. *Pharm Res, 20*(11), 1794-1803.

Zhang, Z., Farooq, M., Prasad, B., Grepper, S., & Unadkat, J. D. (2015). Prediction of gestational age-dependent induction of in vivo hepatic CYP3A activity based on HepaRG cells and human hepatocytes. *Drug Metab Dispos, 43*(6), 836-842. doi:10.1124/dmd.114.062984

Zhang, Z., Imperial, M. Z., Patilea-Vrana, G. I., Wedagedera, J., Gaohua, L., & Unadkat, J. D. (2017). Development of a Novel Maternal-Fetal Physiologically Based Pharmacokinetic Model I: Insights into Factors that Determine Fetal Drug Exposure through Simulations

and Sensitivity Analyses. *Drug Metab Dispos, 45*(8), 920-938. doi:10.1124/dmd.117.075192

Zhang, Z., & Unadkat, J. D. (2017). Development of a Novel Maternal-Fetal Physiologically Based Pharmacokinetic Model II: Verification of the model for passive placental permeability drugs. *Drug Metab Dispos, 45*(8), 939-946. doi:10.1124/dmd.116.073957

Zhao, P., Rowland, M., & Huang, S. M. (2012). Best practice in the use of physiologically based pharmacokinetic modeling and simulation to address clinical pharmacology regulatory questions. *Clin Pharmacol Ther, 92*(1), 17-20. doi:10.1038/clpt.2012.68

VITA

Olena Anoshchenko was an international Ph.D student at the University of Washington. Originally from Ukraine, she received education at Lester B. Pearson United World College of the Pacific (Victoria, BC, Canada) and at Lewis & Clark College (Portland, OR).